Technical Report

WIND DRAG WITHIN A

SIMULATED FOREST CANOPY FIELD
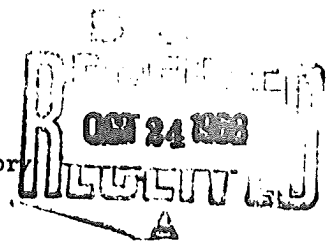
by

G. Hsi and J. H. Nath

Prepared for

Fluid Dynamics and Diffusion Laboratory
College of Engineering
Colorado State University
Fort Collins, Colorado

ABSTRACT

        This report presents an experimental and analysis study of wind

drag within simulated forest canopy fields. The drag coefficients,

aerodynamic roughness and wind velocity profiles are studied for vari-

ous types of forest canopies. Furthermore, a brushy canopy field was

studied which simulated the leafy portion of a forest without the tree

trunks present. The wind drag force on a single experimental tree was

also studied. This information is useful to those who are concerned

with diffusion within a canopy in an atmospheric boundary layer.

        In the course of this study a shear plate was developed which

reliably measures a drag force from 0.1 gram to 2000 grams. The func-

tion of this plate was successfully validated by testing it in a tur-

bulent flow over a smooth surface.

        The drag coefficient of a single model tree, which was the same

as those used in the simulated forest canopy fields, was compared with

prototype conifers. The work found that a plastic model tree has drag

coefficients between those for spruce and Douglas fir trees. The varia-

tion of the tree drag coefficient among trees of the same type is con-

cluded by a statistical study on a number of plastic trees which have

the same amount of foliage but which are different in the arrangement

of the tree branches and the tree leaves.

ACKNOWLEDGEMENTS

TABLE OF CONTENTS

TABLE OF CONTENTS - Continued

TABLE OF CONTENTS - Continued

LIST OF TABLES

LIST OF FIGURES

x

LIST OF FIGURES - Continued

LIST OF FIGURES - Continued

LIST OF FIGURES - Continued

LIST OF SYMBOLS

Symbol	Definition
A	The largest frontal area of the roughness element, or a tree, perpendicular to the direction of flow
b	The width of the fence
B	Roughness function in equation 2.1.18
c	Specific heat
C_a	Concentration of mass a
C_a'	The fluctuation of mass concentration a
C_D	Tree drag coefficient
c_p	Friction factor of the plate in disturbed boundary layer
c_f'	Local drag coefficient
c_{f_1}'	Local drag coefficient from analytic solution
c_{f_2}'	Local drag coefficient from direct measurement
d	Zero-point displacement
D	Coefficient of diffusion
Δf_D	Drag force of the roughness element, in equation 2.3.1
f_D	Total drag force of a tree
f_f	The fence drag
f_m	The increase in drag caused by the fence
f_p	The plate drag
f_{po}	The plate drag under undisturbed boundary layer
f_w	Total wall skin friction in equation 2.2.1
h	Physical height of a roughness, or canopy height
H	Shape factor
k	The universal Karman constant, 0.4

Symbol	Definition
k'	The thermal conductivity
k_s	Equivalent sand roughness
l	The length of the heat element in equation 2.1.22
n	Constant in equation 1.1.4
N	A characteristic length
q	Heat flux
$\bar{q}$	The stagnation pressure averaged over the height of the roughness element
T	Temperature
T'	The temperature fluctuation
u	The local wind velocity in x direction
v	The local wind velocity in y direction
u',v'	The velocity fluctuation in x and y directions respectively
x	The longitudinal distance in flow direction
y	The vertical distance
z	The lateral distance
U_a	Ambient wind velocity
z_o	Aerodynamic roughness
$\frac{W_a}{A}$	Mass flux a
θ	Momentum thickness
τ_o	Surface shear stress
τ_{o_s}	Wall shear stress of a smooth boundary
τ_{o_r}	Wall shear stress of a rough boundary
ρ	Mass density of the fluid

LIST OF SYMBOLS - Continued

Symbol	Definition
δ	Boundary layer thickness
δ^*	Displacement thickness
μ	Absolute viscosity
ν	Kinematic viscosity
α	Thermal diffusivity
ϵ_m, ϵ_h, ϵ_D	Eddy diffusivity of momentum, heat and mass
Re	Reynolds number
Re_x	Reynolds number based on the effective starting length x
Re_ℓ	Reynolds number based on the total length of a plate
Nu	Nusselt number, $\frac{hN}{k}$
Pr	Prandtl number, $\frac{\nu}{\alpha}$
Sh	Sherwood number, $\frac{h_D N}{D}$
Sc	Schmidt number, $\frac{\nu}{D}$

Chapter 1

INTRODUCTION

1.1 General Background

The surface of the earth is composed of sea and land. Like the vivid and unpredictable variation of the sea, the appearance of land presents complex features, such as mountains, rivers and plains. Some of the land is shaded with vegetation covers which are vitally related to human life and are thus interesting to many scientists and engineers in various fields.

This work is concerned with relatively high vegetative coverings of the land. A single tree, orchard-type canopies, forest-type canopies and brushy canopies are the objects of main interest. The research was conducted on:

  a. Single model tree and prototype tree drag coefficients, in which tree flexibility and standard deviation of the single tree drag force are included.

  b. Construction and verification of a shear plate which was used to measure smooth boundary shear and the local surface drag forces within canopies.

  c. The local drag coefficient of a simulated orchard canopy.

  d. The local drag coefficient of a simulated forest canopy, in which velocity profiles over and within the canopy were studied. The aerodynamic roughness for the forest canopy was also studied.

e. The local drag coefficient of a simulated brushy canopy, in which velocity profiles of the canopy and the aerodynamic roughness were studied.

f. The simulation of prototype canopy fields with models in low velocity wind tunnels.

The work "canopy" will be used frequently in this work and is defined as a vegetative field which has large geometric roughness, flexible or non-flexible, about which there is either two-dimensional or three-dimensional flow conditions. A single tree, a row of trees, a corn field, a paddy field, an orchard, brush, and a forest belong to this category.

The following literature review is intended to present an introduction to existing knowledge of canopy fields. Some of the references cited below are reviewed in detail in Chapter 2 within subsections, and some precise mathematical definitions for the terminology will also be included there.

Lettau (1961) studied a vegetative surface roughness which dealt with regional and seasonal variations. Because of the lack of pertinent information, he suggested that his results should be considered as tentative. Lettau's study on the vegetative covers of the state of Wisconsin was, nevertheless, valuable. He grouped vegetation type into grains such as corn, oats and hay, and trees such as oak, maple and aspen. Field crops other than grains were studied such as idle and non-cropped land, pastured woodland and bare land. He used an empirical equation by Kung (1961) to find the weighted averages of $\log z_o$.

$$\log \ z_0 = - 1.24 + 1.19 \ \log \ h \qquad\qquad (1.1.1)$$

Here, the aerodynamic roughness, z_0 , and plant height h are in cm.
The use of z_0 will be illustrated below in Equation 1.1.2. The aver-
age aerodynamic roughnesses, obtained from the vegetation height, of
the state of Wisconsin are tabulated below:

Table 1.1.1 The average aerodynamic roughnesses
of the state of Wisconsin

	z_0		z_0
northeast	64.96	east	5.24
north	44.62	southwest	3.19
northwest	38.85	south	4.29
west	8.12	southeast	6.82
central	12.71		

Deacon (1953) conducted research on various natural surfaces.
He found the aerodynamic roughness of natural surfaces by using the
logarithmic velocity distribution equation:

$$\frac{u}{u_*} = \frac{1}{k} \ \ell n \left(\frac{y}{z_0} \right) \qquad\qquad (1.1.2)$$

where:

u = wind velocity as a function of y above the ground

u_* = shear velocity, $\sqrt{\dfrac{\tau_0}{\rho}}$

τ_0 = surface shear stress

ρ = mass density of the fluid

k = the universal Karman constant, 0.4

z_o = aerodynamic roughness.

Deacon's studies were mainly conducted on two surface conditions, i.e., a surface without natural vegetation and a surface of low vegetation. The result of his study was widely recognized and used by many researchers in fluid mechanics and meteorology. Deacon indicated that the aerodynamic roughness decreases with an increase of wind velocity for both cases of 45 cm and 65 cm height mown grass surface. His study showed that Kung's empirical equation for estimated aerodynamic roughness was good in the study of rather stiff vegetative coverings.

For large crops such as a forest canopy and a brushy canopy, however, the description of the velocity distribution by Equation 1.1.2 was not satisfactory because no meaningful logarithmic curve could be found within and above the canopy. Thus, Rossby and Montgomery (1935) suggested the following equation:

$$\frac{u}{u_*} = \frac{1}{k} \ln \left(\frac{y-d}{z_o} \right) . \tag{1.1.3}$$

The zero point displacement, d , is the vertical distance where the logarithmic velocity profile has u=0 . Thus, d was the third parameter which was determined experimentally and which had to be scaled properly if the distribution of wind above large crops was to be simulated in a wind tunnel.

Stoller and Lemon (1963) did a study on wheat fields and obtained wind velocity data in dimensionless form versus y/h within the wheat field. Tan and Ling (1961) did the same kind of study on corn fields and wheat fields, as did Paeschke (1937). Their results

are limited to the wind velocity profiles within their studied fields and are shown in Fig. 4.3.1.5.

Plate and Quraishi (1965) did a thorough study on canopies of wood pegs and of plastic strips. The wood peg was 5.08 cm high and 0.475 cm in diameter, arranged in a pattern of squares, 2.54 cm spacing in both longitudinal and lateral directions. The flexible strip was 0.635 cm wide, 0.019 cm thick and 10.2 cm high. Strips were fastened to wooden strips. The plastic strips were arranged to face the direction of the wind with their broad side, with a spacing in the direction normal to the flow of one element per 2.54 cm, and a spacing in the direction of flow of one row every 5.08 cm. Their canopies were uniformly and regularly arranged on a wind tunnel floor of 183 cm by 610 cm area and velocity distributions were studied under various ambient wind speeds. They found that the velocity distribution in the flow above the plant cover could be represented by

$$\frac{u}{U_a} = \left(\frac{y-h}{\delta-h}\right)^{\frac{1}{n}} \qquad (1.1.4)$$

where:

n = a constant

U_a = the ambient wind velocity

δ = the boundary layer thickness

h = plant height, or height of element.

The exponent $n = 3$ agrees remarkably well with Moore (1951) and Bhaduri (1963) for roughness elements consisting of wooden strips fastened to the wind tunnel floor at equal intervals of 30.48 cm. Each wooden strip had a cross-section of 0.635 cm by 0.635 cm and a

length of 183 cm. The axis was perpendicular to the wind flow direction. The exponent n = 3 also agrees well with the forest canopy study in this research.

Plate and Quraishi adopted Equation 1.1.3 and used the physical height of roughness h instead of the zero-point displacement d originated by Rossby and Montgomery.

$$\frac{u}{u_*} = \frac{1}{k} \ln \left(\frac{y-h}{z_o} \right) .$$ (1.1.5)

Considering the above mentioned works, it is seen that more data are available in the measurement of velocity distributions than in aerodynamic roughness and shear velocity. Furthermore, none of them elaborated upon the influence of the boundary layer thickness on the surface stress and on the aerodynamic roughness of the canopy field. Neither did they study the initial flow region and the end region of the canopy fields, nor any direct measurement of the surface stress within the canopy fields. Therefore, it is the purpose of this work to study these topics extensively. The velocity profiles and aerodynamic roughness of the center region of the canopies will be studied and compared, when possible, with the data available from the above mentioned researchers.

1.2 Purpose and Scope

The general purpose of this work is to present experimental determinations of the drag coefficient for various types of canopies by using artificial plastic trees in a wind tunnel where the study of the canopy field can be regulated in a careful fashion by controlling the physical height of the canopy, the density of the canopy, the

arrangement of the canopy, the boundary layer thickness and the ambient wind velocities, according to the purpose of study. More specifically the following topics are studied thoroughly in this research, details of which will be discussed in Chapters 2 and 4.

1.2.1 Surface Shear on a Smooth Boundary

The surface shear stress on a smooth boundary under incompressible, turbulent flow conditions was studied in a wind tunnel. The purpose was to test the use of a drag measuring device developed by Nath and called a shear plate. The smooth boundary condition created a testing situation where the value of the boundary shear stress has been well established. Thus confidence was gained in the sue of the shear plate for measuring wall shear under other surface conditions. The description of the shear plate will be presented in Chapter 3. The shear plate was, in consequence, used for measuring the local surface shear of the model forest-type canopy and the model brushy canopy in this work.

1.2.2 Drag Coefficient of a Single Experimental Tree

In this work, a single artificial tree was studied in a free stream and in a well submerged boundary layer condtiion. It was felt that by defining the characteristic velocity as the root mean square velocity on the tree frontal area, the tree drag coefficient would be the same for the artificial tree in a free stream as for the artificial tree in a thick boundary layer. Definition of the tree drag coefficient will be seen in Chapter 2.

By comparing the tree drag coefficient of the artificial plastic tree with prototype trees, it was felt that confidence would

be gained in determining the tree drag coefficient of a real tree under various flow conditions. The tree drag coefficient of an artificial plastic tree was found to be between that of Douglas fir and spruce. This revealed that the experimental forest studied in this work may be considered as a simulated Douglas fir forest or a spruce forest. Moreover, the information of a single tree drag coefficient can be useful to the study of wind breaks.

The tree flexibility and the statistical variation of drag force on an artificial tree were studied. This information can be used to estimate the tree drag coefficient and the stiffness of a single tree.

1.2.3 Drag Coefficient of Various Canopies

The standardized local skin friction drag coefficients for flow in pipes and along plates are used successfully in engineering applications. However, the drag coefficients for various vegetative canopies are scarce. Therefore, this work intends to do a thorough study on this subject regarding experimental tree canopies in the hope that the canopies may be generalized and a laboratory study of canopies may simulate prototype canopies. It will be shown how this information is useful for diffusion studies.

In this work, the local drag coefficient was found for various types of canopies. The experimental results compared favorably with the analytical results. The simulated forest-type canopies studied here were composed of artificial trees which were described in previous subsection 1.2.2. A close-up photo, Figure 3.4.1.1, and the dimensions of an artificial plastic tree will be seen in Chapter 3.

9

The total drag coefficients for flow in pipes and along flat plates are used by engineers in estimating over-all drag force of the problem. For this reason, the total drag coefficient of experimental forest-type canopies were studied. Moreover, two different thicknesses of boundary layer were applied to the same experimental brushy canopy in order to find some relation between the thickness of the boundary layer and the total drag coefficient of the experimental canopies. This information will provide at least a qualitative clue when the information of the total drag coefficient of an experimental canopy is applied to a prototype canopy which is under a certain thickness of an atmospheric boundary layer.

1.2.4 The Velocity Profiles Over and Within the Simulated Forest Canopy

The velocity profiles of the simulated forest canopy have an interesting phenomenon. The flow above the top of a forest canopy is expected to possess a logarithmic velocity profile towards the center portion of the canopy field, and the profile below becomes approximately uniform flow.

The study of the wind velocity profiles over and within the simulated forest canopies has two purposes: one is rather for research interest. There are no forest wind profile data which cover from the beginning to the end of a forest canopy, and only by simulating a forest canopy in a wind tunnel was such a study possible and meaningful. The other is for practical applications. By knowing the wind character, that is the local wind velocity, over and within the forest canopy the de-foliaging or fertilizing operation can be performed more

efficiently when considering the characteristics of the wind. The forest fire, snow pack, desease control, etc., are problems which are closely related to the wind character of a forest.

In this work, the wind velocity profiles over the center region of a simulated forest canopy were fitted to the logarithmic velocity distribution Equation 1.1.3 and to the power velocity distribution Equation 1.1.4 for the purpose of comparing with others' work. The wind velocity profiles within the center portion of the simulated forest canopy were uniform up to 0.6 tree height from the flow, that is, no velocity gradient existed in the vertical direction. These data are presented in Chapter 4, together with the wind profiles at the initial and the end regions of the simulated forest canopy.

1.2.5 The Aerodynamic Roughness of Canopies

The aerodynamic roughness, z_0 , is one of the parameters in Equation 1.1.5 which was used to interpret the velocity profiles at the center region of the simulated forest and brushy canopies. It was felt that the magnitude of the aerodynamic roughness is not only proportional to the physical height of the studied canopies but also a function of the drag force for flow over a transition region or over a completely rough region of a canopy. The terminology of "transition region" and "completely rough region" were adopted from Schlichting (1968).

The purpose of studying the aerodynamic roughness in this work was to find out whether Equation 1.1.1 worked also for the simulated forest and brushy canopies. Thus, the local shear stress of canopies could be approximated through Equations 1.1.1 and 1.1.5 by just measuring

the local velocity u . This knowledge is particularly important
to the study of the prototype forest canopies, because then the local
shear stress, or the local drag coefficient, of the prototype forest
canopy can be calculated from Equations 1.1.1 and 1.1.5.

The results of the aerodynamic roughness of the simulated
forest and brushy canopies were compared with those of Deacon, Lettau,
and Kung.

Chapter 2

THEORETICAL CONSIDERATIONS

2.1 The Resistance Formula for a Smooth Plate and a Uniform Rough Plate in Turbulent Flow

The turbulent boundary layer on a flat plate at zero incidence with and without zero pressure gradient is of great practical importance. However, like the case with laminar flow, the skin friction coefficients in a mild pressure gradient are not materially different from those for zero pressure gradient, provided there is no separation. The only methods available at the present time for the mathematical treatment of turbulent boundary layers are approximate methods.

A method for the smooth plate is based on the momentum integral equation for a two-dimensional incompressible boundary layer which is presented in Schlichting (1968) as:

$$\frac{\tau_o}{\rho} = \frac{d}{dx} (U_a^2 \theta) + \delta^* U_a \frac{dU_a}{dx} \qquad (2.1.1)$$

where the momentum thickness θ is

$$\theta = \int_0^\infty \frac{u}{U_a} \left(1 - \frac{u}{U_a}\right) dy \qquad (2.1.2)$$

and the displacement thickness δ^* is

$$\delta^* = \int_0^\infty \left(1 - \frac{u}{U_a}\right) dy \quad . \qquad (2.1.3)$$

The ambient wind velocity U_a is a function of x because the Equation 2.1.1 is derived for the flow with pressure gradient, and

U_a varies according to the magnitude of the pressure gradient. By introducing the shape factor H which is the ratio of the displacement thickness and the momentum thickness,

$$H = \frac{\delta^*}{\theta} .$$ (2.1.4)

The Equation 2.1.1 can be expressed in another form:

$$\frac{\tau_o}{\rho U_a^2} = \frac{d\theta}{dx} + (H + 2) \frac{\theta}{U_a} \frac{dU_a}{dx} .$$ (2.1.5)

These equations express the wall shear stress in terms of the boundary layer thickness and the ambient velocity which is influenced by the pressure gradient. If no pressure gradient is presented, the second term on the right side of Equation 2.1.5 will drop, and it becomes

$$\frac{\tau_o}{\rho U_a^2} = \frac{d\theta}{dx}$$ (2.1.6)

The derivative of θ with respect to x is very sensitive, and in most cases the wall shear stress cannot be found accurately by Equation 2.1.6. Therefore, other analytic approaches to find the wall shear stress are needed.

There are two ways, which are based on velocity profile distribution, to find the wall shear stress on a smooth plate in a turbulent flow: one is based on the power velocity distribution and the other is based on the logarithmic velocity distribution. The power velocity distribution is shown as:

$$\frac{u}{U_a} = \left(\frac{y}{\delta}\right)^{\frac{1}{7}}$$ (2.1.7)

for Reynolds numbers, Re_ℓ , between 5×10^5 and 10^7. And the following relation for a circular pipe, by Nikuradse, when modified for the smooth surface in a turbulent flow case, is

$$\frac{\tau_o}{\rho U_a^2} = 0.0225 \left(\frac{\nu}{U_a \delta}\right)^{\frac{1}{4}} \qquad (2.1.8)$$

where ν is the kinematic viscosity, $\frac{\mu}{\rho}$. By using Equations 2.1.2 and 2.1.6, Equation 2.1.8 can be written as

$$\frac{7}{72} \frac{d\delta}{dx} = 0.0225 \left(\frac{\nu}{U_a \delta}\right)^{\frac{1}{4}} . \qquad (2.1.9)$$

The deriving procedures are omitted here and can be found from Schlichting (1968) that

$$\theta(x) = 0.036 \ x \left(\frac{U_a x}{\nu}\right)^{-\frac{1}{5}} \qquad (2.1.10)$$

and

$$c_f' = 0.0576 \left(\frac{U_a x}{\nu}\right)^{-\frac{1}{5}} \qquad (2.1.11)$$

where the c_f' is the local drag coefficient which is defined as

$$c_f' = \frac{\tau_o}{\frac{1}{2}\rho U_a^2} . \qquad (2.1.12)$$

Equations 2.1.10 and 2.1.11 apply only for a smooth plate in a turbulent boundary layer and are valid on the assumption that the boundary layer is turbulent from the leading edge onward.

The local drag coefficient equation based on the power velocity distribution is restricted to $U_a \delta/\nu < 10^5$. The local drag

coefficient deduced from the logarithmic velocity distribution leads to a fairly cumbersome set of equations. However, H. Schlichting found an empirical equation which fits well with laboratory experimentation, i.e.,

$$c_f' = (2 \log Re_x - 0.65)^{-2.3} \qquad (2.1.13)$$

where $U_a x/\nu$, the Reynolds number, is based on the longitudinal distance x . No restriction is posed on Equation 2.1.13.

The following are a number of recognized local drag coefficient equations for a smooth plate in a turbulent boundary layer. F. Schultz-Granow (1941) found that the resistance formula from his experiments was

$$c_f' = 0.370 (\log Re_x)^{-2.584} \qquad (2.1.14)$$

Nikuradse (1942) also conducted a very comprehensive series of experiments on flat plates. He found the local drag coefficient formula as

$$c_f' = 0.02296 (Re_x)^{-0.139} \qquad (2.1.15)$$

Ludwieg and Tillman (1950) proposed an analytic method for the calculation of local drag coefficient of a flat plate, with or without pressure gradient on it, i.e.,

$$c_f' = 0.246 \times 10^{-0.678H} \left(\frac{U_a \theta}{\nu} \right)^{0.268} \qquad (2.1.16)$$

Throughout the study of a smooth boundary in this work, the virtual origin was estimated for the calculation of Re_x by the method of Rubesin (1951). Physically, the turbulent boundary cannot start with zero boundary layer thickness, and the effective starting point is called the virtual origin. The method of estimating the virtual origin

together with the experimental results will be discussed in detail in Chapter 4. The local drag coefficient Equations 2.1.6, 2.1.12, 2.1.14, and 2.1.16 were used in this work. Particularly, Equation 2.1.6 will be discussed at further length in Chapter 4.

The rough plate is more common in engineering problems than the smooth plate and deserves more attention. If the relative roughness $\frac{h}{\delta}$ is considered, the relative roughness will decrease along the plate. The h is the roughness height which remains constant for uniform rough plate, while the boundary layer thickness increases downstream. This circumstance causes the front of the plate to behave differently from the rearward portion as far as the influence of roughness on drag is concerned. The completely rough flow is over the forward portion, followed by the transition region and, eventually, the rough plate may become hydraulically smooth if it is sufficiently long. The forest and brushy canopies did not have a hydraulically smooth region in this work.

The dimensionless roughness parameter $\frac{u_* k_s}{\nu}$ is used to define the limit between character categories as follows:

completely rough: $\quad \frac{u_* k_s}{\nu} > 70$

transition: $\quad 5 < \frac{u_* k_s}{\nu} < 70$ $\hfill$ (2.1.17)

hydraulically smooth: $\quad \frac{u_* k_s}{\nu} < 5$

where

$\qquad k_s$ = the equivalent sand roughness.

Based on the logarithmic velocity distribution, Prandtl and Schlichting presented the following equation:

$$\frac{u}{u_*} = \frac{1}{k} \ln\left(\frac{y}{k_s}\right) + B_1 \tag{2.1.18}$$

where B_1 is called the roughness function and is a constant 8.5 under completely rough conditions. In order to find the relation between the equivalent sand roughness, k_s , and the physical height of the roughness, h , Schlichting performed experiments for a large number of roughnesses arranged on a flat plate and determined the constant B_2 in the universal equation,

$$\frac{u}{u_*} = \frac{1}{k} \ln\left(\frac{y}{h}\right) + B_2 \quad . \tag{2.1.19}$$

On comparing Equations 2.1.18 and 2.1.19, the equivalent sand roughness can be obtained from the resulting equation:

$$\frac{1}{k} \ln\left(\frac{k_s}{h}\right) = 8.5 - B_2 \quad . \tag{2.1.20}$$

Paeshke (1937) demonstrated from experiment that Equation 2.1.19 can be applied to the motion of a natural wind over surfaces which were covered with different kinds of vegetation. He found that $B = 5$ when the physical height of the vegetable growth h is used. In accordance with Equation 2.1.20 this is the same as taking the equivalent sand roughness to be $k_s = 4 h$.

The equivalent sand roughness is useful for the rough plate study, for there are charts based on c_f' , k_s , Re_x existing in Schlichting (1968). The c_f' of the experimental canopies in this work can also be approximated by the method mentioned above. However, for a detailed inside look into the roughness and the local drag coefficient of the experimental canopies, the following method is recommended.

Many investigators used the logarithmic velocity distribution and omitted the roughness function , B , to find their aerodynamic roughness z_o and shear velocity u_* from the equation

$$\frac{u}{u_*} = \frac{1}{k} \ell n \left(\frac{y}{z_o} \right) \tag{1.1.2}$$

where u_* and z_o are two unknowns. Two sets of u and y data from the same experimental velocity profile have to be used to solve Equation 2.1.2 for u_* and z_o . The value of u and y , however, should be taken at a certain distance away from the rough surface for the logarithmic velocity distribution is not present adjacent to the rough wurface. Deacon (1953) did a study by using Equation 1.1.2 for natural surfaces without vegetation such as sea, deserts and snow surface, and for natural surfaces with low vegetation such as mown grass surfaces. Plate and Hidy (1967) used Equation 1.1.2 as well to find the aerodynamic roughness of small water waves.

One of the difficulties in the use of Equation 1.1.2 is that as $z_o \to 0$, it does not approach the smooth surface condition, which is:

$$\frac{u}{u_*} = \frac{1}{k} \ell n \left(\frac{u_* y}{\nu} \right) + \text{constant} \tag{2.1.21}$$

which is the law of the wall proposed by L. Prandtl. Another problem is that the local wind velocity has to become zero at the elevation of $y = z_o$ in order to have Equation 1.1.2 valid mathematically, i.e., the no slip condition at the surface of a boundary is subject to question. However, Equation 1.1.2 has its merit. For one thing, u_* and z_o in a turbulent flow are the counterpart characteristic velocity and length U_a and δ in a laminar flow. With these two parameters,

the velocity profile in turbulent flow does show the logarithmic distribution character. For the other, the aerodynamic roughness is correlated with the height of the roughness. Although the aerodynamic roughness reflects only a qualitative measure of the height of the roughness, the z_0 is also influenced by u_* , which is related to the local surface stress, and hence the density of the roughness and the flow condition.

In this work, the height of studied canopies being rather large, the flow character can hardly be shown by using Equation 1.1.2. Rossby and Montgomery (1935) suggested that for high crops, the equation should be

$$\frac{u}{u_*} = \frac{1}{k} \ln \left(\frac{y-d}{z_0} \right) .$$

$$(1.1.3)$$

This equation shows the logarithmic velocity distribution started from the elevation of zero-point displacement d upward and avoids the variation of flow condition below d . Again, mathematically the local velocity is zero at $y = d + z_0$, which cannot be true in nature. The zero-point displacement is found from experiment for the different roughnesses present.

For simplicity, the physical height of the roughness h replaces the zero-point displacement d in Equation 1.1.3. It then reads:

$$\frac{u}{u_*} = \frac{1}{k} \ln \left(\frac{y-d}{z_0} \right) .$$

$$(1.1.5)$$

Equation 1.1.5 was used to study the experimental forest and brushy canopies in this work.

The following is a citation of existing surface shear stress measuring devices innovated by various researchers.

Schultz-Grunow (1940) succeeded in direct measurement by means of a mechanical balance, see Figure 2.1.1, but the balance was not easy to use for it needs a large amount of instrumental accessories. Fage and Falkner (1930) used the pressure orifice at the point of the wall where the shearing stress is to be measured. Approximately 1/20 mm above the orifice was a sharp knife edge, also called a Stanton tube. The portion of the velocity near the wall is then dammed up between knife edge and wall. The pressure rises below the knife edge with respect to the undisturbed static pressure gave Fago and Falkner a measure for the wall shearing stress, since the velocity distribution in the wall proximity is definitely correlated to the shearing stress. However, because of the difficulty in handling and of the extremely sensitive test probe, the method was not easy to use.

H. Ludwieg (1950) used a small heat transfer element which was built into the wall and had a higher temperature than the flow. He found a definite relationship between surface shear stress and heat transfer as follows:

$$Nu = 0.807 \left(\frac{\ell^2}{\mu \alpha} \right) \tau_o^{\frac{1}{3}} \qquad\qquad (2.1.22)$$

where

    Nu = Nusselt number

    ℓ = the length of the heat element

    α = the thermal diffusivity, $\frac{k'}{c\rho}$.

The derivation steps are omitted here but can be found in his paper.

The heat transfer element is heated by a small electric heater. A warm boundary layer, starting from the forward edge of the element, is formed. The heat volume Q of the element can be calculated from

the heat input to the element after the warm boundary layer reaches the steady state. The temperatures at the wall and at the edge of the warm boundary layer can be detected by a thermocouple. By knowing θ and $(T_0 - T_\infty)$, the Nusselt number can be obtained from

$$Nu = \frac{\bar{\alpha}\ell}{k'} = \frac{Q}{bk'(T_0 - T_\infty)} \qquad (2.1.23)$$

where

$$\bar{\alpha} = \frac{Q}{b\ell(T_0 - T_\infty)} \qquad (2.1.24)$$

b = the width of the heat element.

The thermal diffusivity, α , can also be obtained with the information $(T_0 - T_\infty)$. Thus, the surface shear stress can be calculated from Equation 2.1.22. Another use of Equation 2.1.22 is to determine a relationship between τ_0 , Nu and α by a calibration measurement where surface shear stresses are known.

With the success of Ludwieg's surface shear measuring device, Ludwieg and Tillman (1950) had the contribution of the analytic Equation 2.1.16 for the calculation of the local drag coefficient, with or without pressure gradient on a smooth boundary in a turbulent flow.

Smith and Walker (1959) used a floating element skin-friction balance to measure the local surface-shear for a turbulent flow on a flat smooth plate having zero-pressure gradient. Their data, verified by using a calibrated total head tube located on the surface of the test wall, agreed well with the measurements of Schultz-Grunow.

In this work, a shear plate was used to measure the surface shear stress of a smooth boundary and of experimental canopies. Semiconductor strain gages were used to sense the surface shear stress

of the object on the shear plate. Details of the plate are given in Chapter 3.

2.2 The Momentum Integral for Approximate Tree Drag Calculation

In Figure 2.2.1 by taking a control volume around a tree and considering the law of conservation of momentum, the sum of the force acting is equal to the change in momentum through the boundaries. Since the pressure is constant, the momentum equation, as applied to the control volume shown in Figure 2.2.1, can be stated as:

$$-F_D - f_W = \rho \int_0^z \int_0^Y u_{i+1}^2 \, dy \, dz + \rho \, U_a \left[\int_0^z \int_0^Y u_i \, dy \, dz \right.$$

$$\left. - \int_0^z \int_0^Y u_{i+1} \, dy \, dz \right] - \rho \int_0^z \int_0^Y u_i^2 \, dy \, dz$$

$$(2.2.1)$$
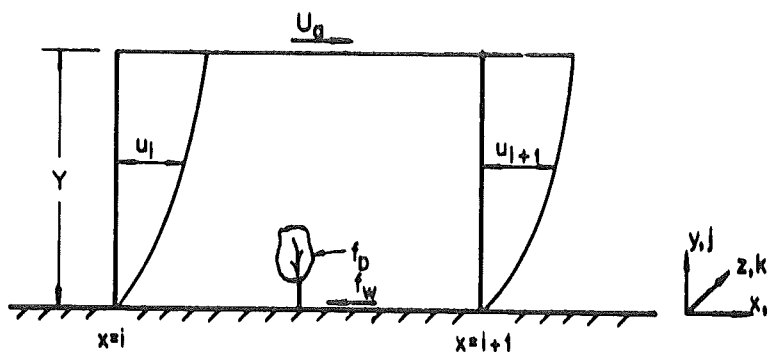
Figure 2.2.1 Control volume around a tree

where

Y = the vertical distance which is larger than the boundary layer thickness at $x = 1$ and $x = i+1$

Z = the lateral distance which covers the tree wake influence zone at $x = i+1$

u_i = the local wind velocity at $x = i$

u_{i+1} = the local wind velocity at $x = i+1$

f_D = the total drag force acting on the tree

f_W = the total surface shear for $i \leq x \leq i+1$ and $0 \leq z \leq z$.

The drag force on the tree is far larger than the surface shear on the wall. The f_W is thus neglected and the tree drag is, using the numerical representation:

$$f_D = \rho \left\{ \sum_{k=1}^{m} \sum_{j=1}^{m} \left[U_a(u_{i+1} - u_i) + (u_i - u_{i+1}) \right]_{k,j} \Delta y \Delta z \right\} .$$

$$(2.2.2)$$

The above method can be used to find the total drag force of a number of trees, provided that the control volume is large enough to cover all trees in it. This method was used on one of the orchard canopy cases. The name of the orchard canopy used here indicates that trees are equally spaced in both longitudinal and lateral directions. The tree array in the longitudinal direction is called a "column" and in the lateral direction is called a "row," where the longitudinal direction is parallel to the centerline of the wind tunnel. The case computed here was a one column, twenty row orchard canopy with 25.4 cm tree spacing. The ambient wind velocity was 915 cm/sec. A CDC 6400 was used for the calculations.

2.3 Single Roughness Element

The problem of determining the drag force on a single roughness
element, which is mounted on a flat plate, is complicated. The drag
depends on the characteristics of the boundary-layer flow as well as
on the geometry of the roughness element. A theoretical solution to
the problem is not feasible at present; therefore, analyses must be
based on experimental data.

K. Wieghardt (1953) and W. Tillmann (1953) carried out a large
number of measurements on roughness in Goettingen Laboratory. The wall
friction drag was measured on a 50 cm by 30 cm rectangular test plate
with a balance. The drag on the test plate with a single roughness
element on it gave an increase in drag. After subtracting the drag of
the test plate without the roughness element, the difference was then
presumed to be the drag force of the roughness element, denoted by Δf_D.
Wieghardt used the following definition for the drag coefficient of
the roughness elements:

$$C_D = \frac{\Delta f_D}{\bar{q}A} \qquad\qquad (2.3.1)$$

where

C_D = the drag coefficient of the roughness element

Δf_D = the drag force of the roughness element

A   = the largest frontal area of the roughness element
        perpendicular to the direction of flow

$\bar{q}$ = the stagnation pressure averaged over the height of
        the roughness element which is

$$\overline{q} = \frac{1}{k} \int_0^h \frac{1}{2} \rho u^2 (y) \, dy \quad . \tag{2.3.2}$$

Here, a question is raised because the flow pattern behind the roughness element changes the drag measurement of the flat plate, and hence the drag force difference Δf_D is not the real drag of the roughness element.

According to Plate (1964) the total drag on the plate will increase because the turbulent boundary flow is disturbed by the roughness element. He did a two-dimensional fence study in a wind tunnel and used the following method to determine the drag force:

$$f_n = f_f + f_p - f_{po} \tag{2.3.3}$$

where

f_n = the increase in drag caused by the fence

f_f = the fence drag

f_p = the plate drag

f_{po} = the plate drag under undisturbed boundary layer.

The f_{po} can be calculated from well-established techniques by Schlichting (1960) and by such methods as previously mentioned in sub-section 2.1 for turbulent flow over a smooth boundary or be measured, such as with a shear plate.

The fence drag f_f is obtained by measuring the pressure in front of the fence p_f and the pressure on the rear of the fence p_b experimentally. The equation in calculating f_f reads

$$f_f = b \int_0^h (p_f - p_b) \, dy = (p_{fav} - p_{bav}) \cdot b \cdot h \tag{2.3.4}$$

where the p_{fav} and p_{bav} are the averaged values of p_f and p_b , and b the width of the fence.

The f_p is from

$$f_p(x) = b \int_{x_1}^{x} c_p \, dx \cdot \frac{1}{2} \rho U_a^2 \qquad (2.3.5)$$

where

$\quad c_p$ = friction factor of the plate in disturbed boundary layer,

$\quad\quad c_p = f\left(\frac{x}{h}\right)$, see Plate (1965).

Equations 2.3.4 and 2.3.5 can also be expressed as

$$f_f + f_p(x) = \rho U_a^2 \left[\theta(x) - \theta(x_1) \right] \quad . \qquad (2.3.6)$$

Equation 2.3.6 is the friction drag on the plate between points x_1 and x , and $\theta(x)$ and $\theta(x_1)$ are the momentum thickness at x and x_1 , respectively. See Figure 2.3.1. Hence it was considered advisable to measure single tree alone with a special strain gage dynamometer independent of wall shear.

In this work the drag force and the drag coefficient of a single model tree are studied. The tree drag was obtained by using a strain gage force dynamometer which was built on a portal gage principle, Hsi and Nath (1968). Thus, the drag force on a single tree element was measured directly. The drag coefficient was defined as follows:

$$C_D = \frac{f_D}{\frac{1}{2}\rho \overline{u^2} A} \qquad (2.3.7)$$

where

$\quad A$ = the frontal area od the model tree, and

$$\overline{u^2} = \frac{1}{A} \int_A u^2 \, dA \quad .$$

The Reynolds number was defined as:

$$Re = \frac{\sqrt{\overline{u^2}}\ \sqrt{A}}{\nu} \ .$$

(2.3.8)

It was found experimentally that the root mean square wind speed of the tree frontal area was approximately equal to the wind speed measured at the geometric center of the tree frontal area.

2.4 Transition from a Smooth to a Rough Surface, or from a Rough to a Smooth Surface

When a wind approaches or leaves a canopy field, the flow is subject to a sudden change of the surface roughness, and hence varies abruptly. The difference of the boundary roughnesses creates a unique flow problem. This topic will be discussed below. Results of wind approaching and leaving the experimental forest and brushy canopies are presented in Chapter 4.

W. Jacobs (1940) investigated the flow pattern near a boundary which consisted of a smooth section followed immediately by a rough one He proposed an empirical equation to interpolate the shearing stress for the smooth to rough surface case. It reads:

$$\tau(x,y) = \left\{ \tau_{o_s} - (\tau_{o_s} - \tau_{o_r})\, e^{-11.6\frac{y}{x}} \right\} \left(\frac{h-y}{h} \right)$$

(2.4.1)

where

x = the longitudinal distance, started from the leading edge of the rough surface downstream

y = the vertical distance from the rough surface upward

τ_{o_s} = wall shear stress of the smooth surface

τ_{o_r} = wall shear stress of the rough surface.

28

For the reverse order of transition (rough to smooth) Equation 2.4.1 may be used, according to Jacobs, by interchanging τ_{o_s} and τ_{o_r} in the Equation 2.4.1. This equation can be used to find the turbulent shear stress if the wall shear stress of the rough and smooth surfaces are known.

Clauser (1956) obtained velocity profiles downstream from a sudden change in roughness on a flat plate in a constant pressure turbulent boundary layer. He concluded that the inner portion of the layer (the logarithmic velocity profile based on the aerodynamic roughness and shear velocity after change) responds to the change within a few boundary layer thicknesses downstream from the change, while the outer portion (the logarithmic velocity profile based on the aerodynamic roughness and shear velocity before the change) takes tens of boundary layer thicknesses for the response to be detected. The phenomena can be seen in a qualitative manner in Figure 4.3.1.6 in Chapter 4. The lower 40 percent of the velocity profile changed right after leaving the experimental forest canopy, but the upper part of the velocity profile still possessed the character of the velocity profile of the forest canopy and remained unchanged. Figure 4.3.1.6 did not show the velocity profile in logarithmic manner, and hence Clauser's statement is noted but not verified in this work.

Glaser, Elliott and Druce (1957) studied the case for a thermally neutral flow (flow neither heated nor cooled) from rough to smooth surface. They found that the logarithmic velocity profile can encounter a sudden change in surface roughness without losing the character of the logarithmic distribution of wind profile. Form this point of view, they claimed, an "internal boundary layer" is supposed

to develop having a clearly defined top across which the wind velocity
is continuous and the stress discontinuous. Aobve and upwind of the
internal boundary layer, the parameters of the original velocity distri-
bution apply. Inside it, the developing logarithmic profile is defined
by the new aerodynamic roughness and a new shearing stress which is
allowed to vary with downstream distance in such a way as to maintain
the required continuity at the top of the layer. Their study is some-
what a step further, compared to the work of Clauser.

The problem of the transition from a smooth to a rough surface
attracts much attention from those who are interested in the disturbed
boundary layer problem. Theoretical works have been elaborated upon
by Townsend (1965, 1966) and Taylor (1962), and experimental works by
Jones (1963) and Plate and Quraishi (1965).

2.5 Simulation of Model and Prototype Canopy Fields

The simulation between model and prototype canopy fields has
two purposes: the simulation of the flow condition and the structural
simulation of the canopy field. Each involves a large number of fac-
tors. For modeling trees or canopy fields, much research has been
conducted in the Fluid Dynamics and Diffusion Laboratory, Colorado
State University.

Ostrowski (1967) did a study on single conifer trees in a wind
tunnel. He did not observe the geometric similarity between model and
prototype tree branches cannot be obtained, nor the vibrations of
needles. The major modeling factors are the density of foliage struc-
ture, the tree shape, the wake similarity, the drag force on the tree,
and the turbulence level.

Plate and Quraishi (1965) successfully simulated corn and
wheat fields in a wind tunnel with the substitution of a wood pegs
canopy and a plastic strips canopy. In their work, they concentrated
on the modified logarithmic wind distribution:

$$\frac{u}{u_*} = \frac{1}{k} \ln \left(\frac{Y-h}{z_o} \right) .$$ (1.1.5)

The arrays of flexible plastic strips and wooden pegs simulated the
crop geometry and roughness characteristics. They were able to closely
fit the model crops to Equation 1.1.5 and to find remarkable corre-
spondence to field data for wind profiles within the model canopy.

It is felt that in this research the following conditions for
modeling a canopy field should be met:

a. The velocity distribution in the undisturbed boundary layer
should be similar for model and prototype canopy fields, i.e., modeling
upstream flow condition such as boundary layer thickness, surface rough-
ness, turbulence level, flow temperature, dimensionless velocity pro-
file, etc.

b. The local drag coefficient of the model canopy should be
the same as that of the prototype canopy. (c_f') model = (c_f') proto-
type. The artificial tree in this work has a drag coefficient between
Douglas fir and spruce. Thus, the experiment forest canopy can be
termed as a Douglas fir forest or a spruce forest.

c. The disturbed velocity profiles of the canopies should be
similar. At least, the disturbed velocity profiles should be similar
at the center region of the canopies. The logarithmic velocity distri-
bution should be as follows

$$\frac{u}{u_*} = \frac{1}{k} \ln \left(\frac{y-h}{z_o} \right) \qquad (1.1.5)$$

The shear velocity u_* and the aerodynamic roughness z_o can be adjusted by the arrangement of the density, or the height, of the studied model canopy, so that the model and prototype canopy can have similar disturbed velocity profiles.

      d. The boundary layer thickness is one of the factors that influences the local drag coefficient, or shear velocity. Therefore, the follow relation should be held:

$$\left(\frac{\delta}{h} \right)_{model} = \left(\frac{\delta}{h} \right)_{prototype} . \qquad (2.5.1)$$

But this relation is difficult to achieve in a wind tunnel for

$$\left(\frac{\delta}{h} \right)_{prototype} \approx 50 \text{ to } 100$$

and

$$\left(\frac{\delta}{h} \right)_{model} \approx 5 \text{ to } 10 .$$

If the physical height of the model is scaled one order smaller to achieve the above relation, the detail of the studied canopy will disappear and the canopy field will become a uniform rough surface. A large cross-section wind tunnel with artificially thickened boundary layer can meet the above requirement better.

      e. The tree flexibility similarity must be valid. According to the definition in Chapter 4, the tree flexibility is

$$\text{Tree Flexibility} = \frac{\text{Actual Tree Frontal Area in Wind}}{\text{Tree Frontal Area in Still Air}} \qquad (2.5.2)$$

For a single tree case, the tree flexibility is very important.
The frontal area of a real tree does shrink under strong wind, and thus,
the tree drag force is a function of the strength of the wind and the
actual tree frontal area. However, tree flexibility is less critical
in canopy fields. For instance, the forest canopy does not vary its
frontal area under strong wind. Hence, the local drag coefficient
similarity is more important to a canopy field study.

Some of the conditions mentioned above are hard to accomplish.
At the present time, the result in this work can be used to fit some of
the existing prototype canopies. More research work is needed in order
to study a particular existing forest or orchard type canopy.

2.6 The Analogy between the Local Drag Coefficient and the Diffusion Coefficient

This subsection is a summary of existent knowledge on the
momentum, heat and mass transfers which might be useful in further de-
velopment of this research. In momentum, heat, and mass transfer prob-
lems, the rate of transfer is the flux and the intensity of the driving
force is the potential gradient. The rate equations, in general form,
will have both laminar and turbulent properties which characterize the
behavior of the transfer process.

The rate equations for momentum, heat, and mass transfer are

$$\tau = \mu \frac{du}{dy} - \rho \overline{v'u'} \tag{2.6.1}$$

$$q = - k' \left(\frac{dT}{dy}\right) + c_\rho \overline{v'T'} \tag{2.6.2}$$

$$\frac{W_a}{A} = - D\frac{dC_a}{dy} + \overline{v'C_a'} \tag{2.6.3}$$

where

Bar = time average

c = specific heat

C_a = concentration of mass a

C_a' = the fluctuation of the mass concentration, a

D = coefficient of diffusion

k' = the thermal conductivity

q = the heat flux

T = temperature

T' = the temperature fluctuation

$\dfrac{W_a}{A}$ = the mass flux, a

u',v' = the turbulent velocity fluctuations in the x and

y directions, respectively.

The first terms on the right side of the rate equations are the laminar terms, and the second terms are the turbulent terms which relate directly to turbulent intensity. For instance, in the neighborhood of a wall the turbulent fluctuation dies off and the laminar terms outweigh the turbulent terms in the rate equations. On the other hand, the turbulent terms outweigh the laminar terms where the turbulent fluctuation is strong, such as at a distance from the wall. These three equations can be simplified by introducing the following eddy diffusivity terms:

$$- \overline{v'u'} = \varepsilon_m \frac{du}{dy} \qquad (2.6.4)$$

$$- \overline{v'T'} = \varepsilon_h \frac{dT}{dy} \qquad (2.6.5)$$

$$- \overline{v'C_a'} = \epsilon_D \frac{dC_a}{dy} \qquad (2.6.6)$$

where

ϵ_m = eddy diffusivity of momentum

ϵ_h = eddy diffusivity of heat

ϵ_D = eddy diffusivity of mass

The simplified equations are

$$\frac{\tau}{f} = (\nu + \epsilon_m) \frac{du}{dy} \qquad (2.6.7)$$

$$\frac{q}{c\rho} = - (\alpha + \epsilon_h) \frac{dT}{dy} \qquad (2.6.8)$$

$$\frac{W_a}{A} = - (D + \epsilon_D) \frac{dC_a}{dy} \qquad (2.6.9)$$

where

$\alpha = \frac{k}{c\rho}$, called thermal diffusivity.

The diffusivities ϵ_m and ϵ_h can be found experimentally by the hot-wire anemometer technique. However, existing mass fluctuation detection instrumentation can sense for humidity fluctuation frequency only up to 100 cps. Therefore, the reliability of the eddy diffusivity of mass ϵ_D in turbulent flow is subject to question. However, ϵ_D can be obtained from Equation 2.6.9 by knowing W_a/A and dC_a/dy which are obtained experimentally.

The analogy concept has been used with success in many engineering problems, such as by Kreith et al., (1959), Sherwood (1950), Tien and Campbell (1963), etc.

In highly turbulent flow, in which $\nu << \epsilon_m$ and $\alpha << \epsilon_h$, Equations 2.6.7 and 2.6.8 can be put in non-dimensional form as

$$\frac{-\dfrac{q}{\rho c \, (u-u_e)(T-T_e)}}{\dfrac{\tau}{\rho(u-u_e)^2}} = \frac{\epsilon_h}{\epsilon_m} \qquad (2.6.10)$$

where the subscript e indicates values at a reference plane. If the case studied here is for the heat and momentum transfer at the wall, Equation 2.6.10 will be written as

$$\frac{\dfrac{q_o}{\rho c u_e \, (T - T_e)}}{\dfrac{\tau_o}{\rho u_e^2}} = \frac{\epsilon_h}{\epsilon_m} \qquad (2.6.11)$$

where the subscript o indicated the values at wall for

$$h = \frac{q_o}{(T_o - T_m)} \qquad (2.6.12)$$

and

$$\tau_o = c_f' \frac{\rho u_e^2}{2} . \qquad (2.6.13)$$

Equation 2.6.11 becomes

$$\frac{h}{\rho c u_e} = \left(\frac{\epsilon_h}{\epsilon_m}\right) \frac{c_f'}{2} \qquad (2.6.14)$$

or

$$\frac{Nu}{Re_N Pr} = \left(\frac{\epsilon_h}{\epsilon_m}\right) \frac{c_f'}{2} \qquad (2.6.15)$$

where

Nu = Nusselt number, $\frac{hN}{k'}$

R_{e_N} = Reynolds number based on N , $\frac{u_e N}{\nu}$

N = the characteristic length

Pr = Prandtl number, $\frac{\mu}{ck'}$

Equation 2.6.15 can be expressed by the Stanton number, St ,

$$St = \frac{Nu}{R_{e_N} P_r} = \left(\frac{\epsilon_h}{\epsilon_m} \right) \frac{c_f'}{2} \qquad (2.6.16)$$

by a change of notation from heat transfer to mass transfer, i.e.,

$T \rightarrow C_a$

$Pr \rightarrow Sc$

$Nu \rightarrow Sh$

$\epsilon_h \rightarrow \epsilon_D$

Equation 2.6.16 can be written as

$$\frac{Sh}{R_{e_N} Sc} = \left(\frac{\epsilon_D}{\epsilon_m} \right) \frac{c_f'}{2} \qquad (2.6.17)$$

where

Sh = the Sherwood number, $\frac{hDN}{D}$

Sc = Schmidt number, $\frac{\nu}{D}$

and

$$h_D = \frac{W_a}{A} \frac{1}{(C_{a_o} - C_{a_\infty})} \qquad (2.6.18)$$

The ratio $\frac{\epsilon_m}{\epsilon_h}$ is also called the turbulent Prandtl number. It is unity from the prediction of Prandtl's mixing length theory. However, the turbulent Prandtl number varies between 0.7 to 0.9, from

experiments, and increases with decreasing Reynolds number. The ε_D
has to be found from Equation 2.6.9.

Chapter 3

EXPERIMENTAL EQUIPMENT AND PROCEDURES

Experiments were performed in the U.S. Army meteorological wind tunnel and the Colorado State University wind tunnel. Both tunnels are located in the Fluid Dynamics and Diffusion Laboratory at the Engineering Researhc Center, Colorado State University. The experiments and procedures performed for this study will be discussed in the following sections.

3.1 Wind Tunnel

The Army meteorological wind tunnel was constructed by Colorado State University for the U.S. Army under Contract DA-36-039-SC-80371. The tunnel features a test section of 2700 cm length and a nominal cross-sectional area of 18" cm by 180 cm with a movable ceiling which can be adjusted for establishing negative and positive longitudinal pressure gradients or a zero pressure gradient. A large contraction ratio of 9 to 1 in conjunction with a set of four damping screens yields an ambient turbulence level of about 0.1 percent.

Test-section air velocities range from about 0 to 3700 cm/sec and the ambient temperature of the air can be varied from $0^\circ C$ to $85^\circ C$ at medium speeds.

The tunnel has a 1220 cm section of the test-section which can be heated or cooled to permit temperature differences between the cold plate and hot air of $65^\circ C$, and the hot plate and cold air of more than $105^\circ C$.

A carriage system is available which permits remote placement of probes.

The Colorado State University wind tunnel has a test section of 900 cm length and a nominal cross-sectional area of 180 cm by 180 cm. This tunnel complements the longer tunnel in that it allows the pursuit of less complex programs in an economical manner. Drawings of the U.S. Army meteorological wind tunnel and the Colorado State University wind tunnel are presented in Figures 3.1.1 and 3.1.2, respectively.

The performance characteristics of these two tunnels are summarized in Table 3.1.1.

3.2 Instrumentation

3.2.1 Drag force measurement - For direct measurements of drag force on a single artificial tree and the drag force of canopy fields, a strain gage force dynamometer and a shear plate were designed by J. H. Nath from Colorado State University.

The strain gage force dynamometer was used for single tree drag measurement. It was made of brass and was set on a metal plate as shown in Figure 3.2.1.1. This transducer measures accurately the total drag force on an artificial tree regardless of where the resultant of the drag force is applied, see Hsi and Nath (1968). The function of this transducer was verified experimentally for force ranging from 1 gram to 50 grams and for one ranging from 5 cm to 14 cm. The calibration curve shown in Figure 3.2.1.2 was obtained by applying various loads at one position on the stiff rod. The response did not change when the load was shifted to another position on the rod. The natural frequency of this transducer is 30 cycles per second. The electric bridge

arrangement of the strain gages and the dynamometer placed in the model orchard canopy are shown in Figures 3.2.1.3 and 3.2.1.4, respectively.

Instruments used for the study are shown in Figure 3.2.1.5. The eight-volt D.C. power supply for the strain gages is shown on the far left and next to it is the circuit which adds the response of four strain gages electronically. The D.C. Micro-ammeter Model 425 A type by Hewlett-Packard, is at the far right of Figure 3.2.1.5. The strain gages used for this force dynamometer were made by Micro-Measurements Co., Type EA-125BB-120, which has resistance 120 ±0.15% ohms and gage factor tolerance ±0.5%.

The shear plate was made of aluminum plate which had the dimensions 0.635 cm x 59.6 cm x 59.0 cm. This plate was separated from the foundation plate by three chrome-steel balls. The ball diameter was 0.635 cm. Two stainless restoring arms, 0.317 cm x 1.27 cm x 45.6 cm each, were used. One end of the arm was attached to the shear plate and the other to the foundation plate. Four semi-conductor strain gages, one to each side of the restoring arm, were installed at 1.27 cm from the end of the restoring arm which was attached to the foundation plate. The semi-conductor strain gages used for this shear plate were made by Electro-Optical System, Inc., Model No. P01-05-500, type P, which has a resistance of 500 ohms.

For frictionless purpose, the balls were set on hardened-finished tungsten cobalt disks which were imbedded in the shear plate and the foundation plate. The shear plate was able to move back and forth horizontally only, and it had a natural frequency 6 cycles per

second. The construction of the plate is shown in Figure 3.2.1.6 and
and a photograph of the shear plate in Figure 3.2.1.7.

When a given horizontal force is applied on the shear plate,
the plate will have a displacement according to the spring constant of
the restoring arms and the magnitude of the applied force. It was ex-
perimentally proven that the shear plate will return to its original
position after the applied force is removed. The read-out of these
four semi-conductor strain gages is added together by a circuit bridge
arrangement, as shown in Figure 3.2.1.3. The eight-volt D.C. power
supply and D.C. micro-ammeter used for the shear plate read-out are the
same as used for the strain gage force dynamometer. The method of the
shear plate calibration and the calibration curve are shown in Figure
3.2.1.8. This shear plate could measure a drag force ranging from 0.1
to 2000 grams.

3.2.2 Velocity profile measurement - The wind velocity profile
was measured with a Prandtl tube which was mounted on a carriage with
transverse and vertical movement mechanism. The position of the Prandtl
tube was sensed by an attached potentiometer. The difference between
static and dynamic pressure of the flow was read from a Trans-sonic Type
120 B Equibar pressure meter. This pressure meter operates over a total
pressure range of 0-30 mm Hg in eight full-scale range. For vertical
or horizontal velocity profiles, the position of the Prandtl tube and
the velocity signal from the equibar pressure meter were recorded in-
stantaneously on an x-y plot. The arrangement of the Prandtl tube, the
carriage, the pressure meter, and the x-y plotter is shown in Figure
3.2.2.1.

3.2.3 <u>Pressure gradient measurement</u> - Two Prandtl tubes were connected to the same equibar pressure meter with both the total head tubes disconnected from the pressure meter. In doing this, the read-out from the pressure meter is the static pressure difference between these two Prandtl tubes.

First, both tubes were set at the same height, side by side in the free stream, well above the wind tunnel floor and upstream of the studied boundary condition. At this point, the pressure difference between these tubes is zero in any flow speed. One of the Prandtl tubes is then used as a reference static pressure and the other Prandtl tube is moved downstream. The longitudinal pressure gradient, if any, of the boundary layer condition is thus obtained.

The ceiling of the U.S. Army meteorological wind tunnel can be adjusted so that a pre-determined pressure gradient can be obtained. For this study a zero pressure gradient is desired for the work in the Army facility.

It was assumed that a zero pressure gradient existed whenever the static pressure difference between the reference tube and the measured tube was within 0.003 mm Hg.

3.3 Smooth Boundary Surface

The smooth boundary surface covered a wind tunnel area of 183 cm in width and 731 cm in length. The surface arrangement is shown in Figure 3.3.1. The whole surface structure was composed of twenty-four particle boards. Each board had the dimensions 90 cm x 61 cm x 1.9 cm. The board thickness was so chosen that the surface of the board was

43

just flush with the surface of the shear plate. The shear plate could
be shifted from one position to the other by taking out two pieces of
particle boards. The space at both sides of the shear plate was also
filled with particle boards. See also Figure 3.3.1. Therefore, thir-
teen drag force measuring positions were available for the 731 cm smooth
boundary surface.

Upstream of the smooth surface, a gravel layer of 1.27 cm
diameter was paved and covered a length of 183 cm. The gravel layer
provided a transition slope from the wind tunnel floor to the smooth
boundary surface, and moved the point of transition toward the leading
edge of the smooth surface so that an early turbulent flow can be
assumed.

From the measured and analytic local drag coefficient of the
smooth surface, and the Reynolds number based on the effective longitu-
dinal distance x , this smooth surface is proved to be truly hydrauli-
cally smooth from Schlichting's data (1968).

Two dimensionality of the flow condition was checked by taking
a few transverse velocity profiles at various locations over the smooth
boundary surface, see Figure 3.3.2. Vertical velocity profiles were
taken along the centerline of the wind tunnel floor; the first station
was 30.4 cm upstream of the smooth boundary and hence was over the
gravel layer. Stations were at 60.8 cm intervals. Fifteen stations
of the vertical velocity profiles were recorded. The last station was
30.4 cm behind the smooth boundary.

3.4 Canopy Fields

In this work, four types of canopy are studied, namely a single
tree, orchard-type canopy, forest-type canopy and brushy canopy. A

single tree was investigated both in the free stream and in a boundary

layer. The orchard-type canopy and the brushy canopy were studied in

a thin boundary layer as well as in a thick boundary layer. As for the

forest-type canopy, only thick boundary layer was applied to it. Com-

plete descriptions of the various experimental canopies are given in

the following sections.

3.4.1 Single tree - The artificial tree was made of plastic and

is ordinarily used for decoration. The dimension of the tree was about

16.5 cm in height and 10.8 cm in the largest horizontal direction. The

tree trunk was 0.47 cm in diameter and the distance from the floor to

the lower branches was about 3.5 cm. A close-up photograph of the tree

is shown in Figure 3.4.1.1. The drag force measurement of the artifi-

cial tree was obtained by using the strain gage force dynamometer.

Due to the different arrangement of tree branches, the drag

force varied from tree to tree. For this reason, four tree orientations

with respect to the approaching wind direction were tested on the same

artificial tree, and twelve such trees were used to find out the stand-

ard deviation of the tree drag among artificial trees with the same

amount of foliage. The drag force data on the same artificial tree are

reproducible if the tree orientation with respect to wind direction is

fixed.

3.4.2 Orchard-type canopies - The orchard-type canopy was

constructed on plywood plates. The dimensions of the plate were 1.25 cm

x 91.5 cm x 61.0 cm. Holes were drilled in the plate 12.7 cm apart in

both the longitudinal and lateral directions. The tree trunks were

taped to pegs which fitted snugly into the holes. Hence, for the 12.7

cm tree spacing, the trees were placed according to the holes on the

plate, while the 25.4 cm tree spacing case was obtained by placing
trees in every second hole.

The artificial trees used for the orchard-type canopy were the
same as used for the single tree study. The arrangement of the orchard-
type canopy varied quite widely. Trees were arranged in one and three
columns parallel to the flows, with from one to several trees in each
column. The term "row" refers to the alignment perpendicular to the
flow. The largest orchard-type canopy studied here was seven columns
and forty-three rows with 25.4 cm tree spacing; it covered an area of
183 cm x 1092 cm.

The strain gage force dynamometer was used for the individual
tree drag force measurement. The artificial trees were under a thick
boundary layer about three times the artificial tree height, or under
a thin boundary layer which was about three-fourths of the tree height
at the first row tree position, while the drag force data were taken.

The seven column, forty-three row orchard-type canopy is shown
in Figure 3.4.2.1.

3.4.3 Forest-type canopies - A forest-type canopy was
constructed on aluminum plates which covered a wind tunnel floor area
of 183 cm x 1100 cm. Holes were drilled, in the aluminum plates,
1.27 cm apart in both the longitudinal and lateral directions. The
dimensions of each aluminum plate were 0.635 cm x 91.5 cm x 122.0 cm.
Artificial trees used to construct the forest-type canopy were the
same type as mentioned in Section 3.4.1. Trees were placed such that
the tree density was above 177 trees per square meter.

The shear plate was used to measure the local drag of the
forest-type canopy. In order to have the same structure of the

forest-type canopy over the shear plate, a plastic plate of 0.635 cm
thickness was mounted on the top of the shear plate. This plastic
plate was the same size as the shear plate and had the same hole arrange-
ment as the aluminum plate. Tree density for the plastic plate was kept
the same as the field. This shear plate, together with the plastic
plate and trees on top of it, were moved from station to station for
measuring the local forest drag data. Due to the fixed length of the
aluminum plate, there were ten positions in the longitudinal direction
that could be used for the local drag force measurement.

The forest-type canopy is shown in Figure 3.4.3.1. In this
Figure, the shear plate is under the cover of artificial trees. The
tree-top was flush at the same height throughout the entire field by
placing 2.54 cm thick wood pieces under aluminum plates.

Two dimensional flow condition was checked by taking transverse
velocity profiles at various positions over the canopy, shown in Figure
3.4.3.2. Vertical wind velocity profiles, within and above the canopy,
will be illustrated in Chapter 4.

3.4.4 Brushy canopy - The brushy canopy was obtained by stapling
the artificial trees flat on the plywood plate. The trees used were
the same type as mentioned in Section 3.4.1; however, the wood peg
which was used as the tree trunk was taken away for the brushy canopy
case. The arrangement of trees on a piece of plywood is shown in Fig-
ure 3.4.4.1. The brushy canopy had an average fuzzy surface thickness
of 2.8 cm.

The brushy canopy covered a wind tunnel floor area of 183 cm
x 732 cm. Each plywood plate had the dimensions of 1.27 cm x 61 cm x
89 cm; the whole canopy was composed of twenty-four plywood plates.

Wood pieces of 0.635 cm thickness were placed under the plywood plates in order to have a flush surface with the shear plate, which was used for the local brushy canopy drag measurement. Artificial trees were taped on top of the shear plate so that the shear plate had the same brushy canopy as the rest of the field.

A smooth surface of 183 cm in length was placed upstream of the brushy canopy field, and a transition slope was used at the leading edge of the smooth surface, see Figure 3.4.4.2. The smooth surface was made of particle boards. When two-dimensionality flow condition was checked for the brushy canopy field, it prevailed for both thick and thin boundary layers. Figure 3.4.4.3 illustrates the thick boundary layer case.

Chapter 4

RESULTS OF LABORATORY EXPERIMENTS

This chapter will display the results of the laboratory

experiments. Some topics will be presented here because they did not

fit logically into Chapter 2, such as the hypothesis of tree flexibility,

the standard deviation of tree drag force and the relation between $\frac{d\theta}{dx}$

and τ_o .

The experimental results presented in this chapter are under

titles: single tree data, verification of the shear plate measurement,

forest canopy data, orchard canopy data, and brushy canopy data. A

major effort was devoted to collecting the local drag coefficient and

velocity profiles for the forest and brushy canopies.

4.1 Single Tree Data

Real trees are always in the atmosphere boundary layer which

is about 50 to 100 times the height of trees. For this reason, an arti-

ficial tree was used for the experiment in the wind tunnel and the arti-

ficial tree was well submerged in the boundary layer. Data were also

obtained for the artificial tree in a uniform, or constant, velocity

field. Comparisons were made between the artificial tree and four coni-

fers, i.e., spruce, Douglas fir, western hemlock and scots pine. Con-

sidering the similarity of tree drag coefficient and tree structure,

the spruce and Douglas fir were approximated by the artificial tree.

The artificial tree drag coefficient and Reynolds number are

49

$$C_D = \frac{f_D}{\frac{1}{2}A\rho\overline{u^2}} \qquad\qquad (2.3.7)$$

and

$$R_e = \frac{\sqrt{\overline{u^2}}\,\sqrt{A}}{2} \qquad\qquad (2.3.8)$$

Results are shown in Figure 4.1.1 and summarized in the following tabulated form

Table 4.1.1 Artificial tree drag coefficient

Artificial Tree Drag Coefficient C = 0.74	
Flow Condition subject to the Tree	Reynolds Number Range
free stream	7.4×10^3 to 8.0×10^4
submerged in a boundary layer	1.3×10^4 to 7.3×10^4

For real trees, the tree frontal area tends to shrink under a strong wind. Based on W. B. Raymer's data (1962), this work estimated the actual spruce frontal area under different wind velocities. This was done by assuming that the real tree had a 21 percent reduction in tree frontal area from 915 cm/sec. Then from Raymer's data for the tree frontal area in still air and tree drag force at 915 cm/sec, the actual tree drag coefficient can be found. For spruce, the tree drag coefficient is 0.91, see Figure 4.1.2. Again, the $C_{D_{spruce}}$ = 0.91 was kept constant under various wind velocities, and using the measured spruce drag forces under various wind velocities by Raymer and equation 2.3.7 the actual spruce frontal area under various wind velocities can be found. The tree sample used for test in a wind tunnel by Raymer

and equation 2.3.7 the actual spruce frontal area under various wind

velocities can be found. The tree sample used for test in a wind tunnel

by Raymer had approximately, 130,000 cm^2 frontal area. His tree drag

coefficient data are summarized in Figure 4.1.3, in which the measured

deviation was calculated from the same kind of trees but different tree

samples. The real conifers used by Raymer, and the artificial tree com-

pared with the sample spruce tree are shown in Figures 4.1.4 and 4.1.5,

respectively.

      4.1.1 Tree Flexibility - Tree flexibility is known to exist

but difficult to estimate; however, a hypothesis is used in this work

to find the tree flexibility. See equation 2.5.2 for the definition

of tree flexibility. From the experiments of a single model plastic

tree, the drag coefficient was found to be constant under moderate wind

velocities, and the frontal area of the model tree did not change with

wind velocity. Therefore, a conclusion can be drawn that the drag

force of the tree is the function of the wind velocity only, and that

two trees with exactly the same frontal area will have the same drag

force provided under the same wind velocity. Later it will be shown

how the drag force varies statistically from tree to tree due to the

somewhat random nature of the model tree construction.

      Raymer used a tree frontal area in still air to interpret his

tree drag coefficients from wind velocities which varied from 915 cm/sec

to 2600 cm/sec. This work assumed that the real tree had a 21 percent

reduction in tree frontal area at 915 cm/sec in comparison with the

tree frontal area in still air. The 21 percent reduction in tree

frontal area at 915 cm/sec was deduced from Figure 4.1.1.1 and the drag

force data of Douglas fir under various wind velocities. By assuming

the 21 percent reduction in tree frontal area at 915 cm/sec, the actual

drag coefficient was obtained, which was 0.57. Then, keeping the actual

drag coefficient as a constant and using the drag force at 1750 cm/sec,

the actual tree frontal area could be found at that wind velocity. The

calculated tree flexibility was 0.51 which was again verified by the

estimated tree frontal areas under these two wind velocities from photo-

graphs in Figure 4.1.1.1. In the same fashion, the drag coefficient of

spruce is 0.72 when the tree frontal area in still air is used; by

taking into account the change in frontal area at 915 cm/sec, the drag

coefficient of spruce is 0.91. This compares with $C_D = 0.74$ for the

model trees in this work.

Based on the tree drag and tree drag coefficient data from

Raymer's work, and on equation 4.1.1 and on the above hypothesis, the

actual tree frontal area can be calculated under each wind velocity.

The tree flexibility is defined as follows

$$\text{Tree Flexibility} = \frac{\text{Actual Tree Frontal Area in Wind}}{\text{Tree Frontal Area in Still Air}} \qquad . \qquad (4.1.1.1)$$

Tree flexibility of spruce and Douglas fir is shown plotted in

Figure 4.1.2.

More work is required in order to establish the above hypothesis

beyond doubt.

4.1.2 Standard deviation of single tree drag force - Real

trees of the same kind and of the same growing conditions may possibly

have similar shapes although they are most likely different in the

arrangement of tree branches and foliage. Therefore, the tree drag

force under the same wind flow conditions may vary from tree to tree.

Again, the tree shape and tree foliage are hardly symmetric; therefore,

the tree drag force may also vary from different approach wind
directions for the same tree. To understand this kind of tree drag
force variation, as applied to the small, plastic laboratory trees,
experiments were conducted on nine randomly picked artificial trees
and each tree was tested under four orientations with respect to the
approaching wind direction. Two wind velocities, 610 cm/sec and 1220
cm/sec, were used, under the thin boundary layer condition.

Tree drag force data, under one wind velocity, were put into
eight different drag force ranges and then averaged. The cumulative
percentage was plotted on abscissa and ordinate respectively on normal
probability paper. A straight line was fitted to the points by eye.
This straight line on the plot indicated approximately a normal distri-
bution existed. Then, the mean (the tree drag force readings at
$p = 0.50$) and the standard deviation (the difference in tree drag force
readings from $p = 0.50$ to $p = 0.84$ or $p = 0.16$) of the plots was
determined. This straight line on the plots was determined. The stand-
ard deviation was 1.14 gram and the mean was 10.7 grams for 610 cm/sec
ambient wind velocity, and the standard deviation 4.94 grams and the
mean 44.97 grams for 1220 cm/sec ambient wind velocity. See Figures
4.1.2.1 and 4.1.2.2.

4.2 Verification of the Shear Plate Measurement

For verifying the accuracy of the shear plate measurement,
experiments were conducted in incompressible flow with negligible
pressure gradient to measure the local surface-shear stress on a smooth
flat plate under turbulent boundary layer conditions.

Physically, the turbulent boundary layer cannot start at the leading edge of the plate with zero boundary thickness. The estimation of the virtual origin, and hence the effective starting length of the turbulent boundary layer, becomes necessary. The method of finding the virtual origin used here is proposed by Rubesin et al., (1951). The momentum thickness, θ , of experimental data were multiplied by two and plotted on a logarithmic graph paper against the distance from the leading edge of the plate x. The slope of $d(\log 2\theta)/d(\log x)$ can be found. According to Rubesin, the magnitude of the slope should be 0.818, which was proved from his experiment that any turbulent boundary layer should have such a slope. If not, all experimental data points have to move horizontally an equal distance on the logaritymic paper until new data points form a slope that has the magnitude of 0.818. The moved distance is then called the effective starting length and is added to the front of the tested plate for calculating the effective Reynolds number. The effective Reynolds number represents real character of the turbulent flow over a smooth boundary.

In this work, experiments were performed in the Colorado State University wind tunnel which provided a thin boundary layer over the smooth boundary surface. The effective starting lengths were found to be 675 cm, 915 cm, and 1140 cm for 610 cm/sec, 1220 cm/sec, and 1675 cm/sec ambient wind velocities, respectively.

The velocity profiles were measured at stations 30.48 cm, 91.50 cm, 152.50 cm, and so on to station 762 cm, as shown on Figure 4.2.1. The distance between stations was 60.96 cm. The most forward measurement station (40.48 cm aft of the leading edge) was not used

since the velocity profile was very distorted there. Shear plate

measurements coincided with the velocity profile stations.

The longitudinal static-pressure gradient measured on the test

surface of the boundary-layer channel was 0.000057 mm Hg/cm. The two

dimensionality of the flow was checked as described in Chapter 3. The

effects from the longitudinal pressure gradient were determined to be

negligible and were not included in this paper.

The principal results are summarized in Figures 4.2.2 and 4.2.3.

In Figure 4.2.2, the surface shear stress measured by the shear plate

was converted to the measured local skin-friction coefficient c'_{f_2} and

is plotted against the effective Reynolds number. The shear plate was

tested under the ambient wind velocities 610, 1220, and 1675 cm/sec.

Data were compared with the works of Smith and Walker (1959), of Kemf-

Ponton (1932), and of Schultz-Grunow (1940). For the 610 cm/sec ambient

wind velocity, the shear plate measurements agree well with the other's

results. However, for ambient wind velocities 1220 cm/sec and 1675

cm/sec, the shear plate measurements showed a relatively high local

skin-friction coefficient which was about 7.5 percent average deviation

in comparison with the experimental and analytical data of Smith and

Walker's for $7.5 \times 10^6 \leq Re \leq 1.85 \times 10^7$. The direct measured local

skin-friction coefficient is usually higher than the analytical result;

however, the measured data of the shear plate showed higher than the

measured data of Smith and Walker.

In Figure 4.2.3, the local skin-friction coefficient of shear

plate measurement was compared with the analytic skin-friction coeffi-

cient. The effective Reynolds number is again used. The equation for

the calculation of analytic skin friction is from Ludwieg and Tillman (1950)

$$c'_{f_1} = 0.246 \times 10^{-0.678\,H} \left(\frac{U_a \theta}{\nu} \right)^{-0.268} .$$ (2.1.16)

All of the measured velocity profiles have been mechanically integrated to obtain both the boundary-layer displacement thickness, δ^* and the momentum thickness, θ . The ratio of these two parameters, known as the shape parameter, H , has been computed. The analytic local skin-friction coefficient c'_{f_1} , is then obtained for each station by equation 2.1.16. The local skin-friction coefficients of the shear plate measurement and the analytic local skin-friction coefficient agree well and they extend from $Re = 2.2 \times 10^6$ to 1.85×10^7 .

4.3 Forest Canopy Data

The forest canopy was studied in thick turbulent boundary layer flow. Tree density was about 0.016 tree/cm^2 . The following phenomena of flow were observed. The approaching turbulent velocity profile had a power distribution as

$$\frac{u}{U_a} = \left(\frac{y}{\delta} \right)^{\frac{1}{7}} .$$ (4.3.1)

Because high drag existed within the forest canopy, the flow was slowed down to a certain extent at the leading edge portion, and then, the uniform flow velocity and high turbulence intensity flow passed through a main portion of the forest until the flow reached the end region. The flow accelerated in the end region. Therefore, the flow accelerated and air jetted into the canopy from above. After the

canopy field, the velocity profile started to recover from the disturbed condition of the canopy as shown in Figure 4.3.1.6.

From the experimental vertical velocity profile, at various stations along the model forest canopy, the moemntum thickness variation at each station was calculated according to equation 2.1.2. The momentum thickness increased from the leading edge of the canopy to its maximum value at station 700 cm; then the momentum thickness started to decrease. From this point downstream, $\frac{d\theta}{dx} = \frac{c_f'}{2}$ was no longer valid since the relation $p + \frac{1}{2}\rho U_a^2 =$ constant could not be satisfied at the end region of the forest canopy, i.e., the vertical variation of pressure in the end region was significant. The method of verifying the analytic and directly measured momentum thickness is demonstrated in Figure 4.3.1. The momentum thickness is defined as

$$\theta = \int_0^\infty \frac{u}{U_a} \left(1 - \frac{u}{U_a}\right) dy \quad . \qquad (2.1.2)$$

The analytic momentum thickness was found from equation 2.1.2 and plotted in the upper part of Figure 4.3.1. The direct measured local drag coefficient c_{f_2}' was from the shear plate, and from the equation 2.1.6. The only thing that can be known from equation 2.1.6 is the slope $\frac{d\theta}{dx} \approx \frac{\Delta\theta}{\Delta x}$. By using the known c_{f_2}' at station 100 cm, the slope was 0.0075 under 610 cm/sec wind speed, the increment Δx here was 100 cm, the slope started at θ equal to zero at $x = 50$ cm and ended at θ equal to 0.75 cm at $x = 150$ cm, and the second slope continued at where the first slope ended. Following this fashion, the lower part of Figure 4.3.1 was constructed.

4.3.1 <u>Velocity profiles over and within the forest canopy</u>

<u>Field, and the Aerodynamic Roughness</u> - The approaching wind velocity

profile to the forest canopy, at 100 cm upstream of the leading edge of

the canopy displayed a power distribution character. The $\frac{1}{7}$th power

distribution of the velocity profile is shown in Figure 4.3.1.1 i.e.,

$$\frac{u}{U_a} = \left(\frac{y}{\delta}\right)^{\frac{1}{7}} \tag{4.3.1}$$

As soon as the wind encountered the forest canopy, the velocity

profile was disturbed by trees and separated into two parts. The pro-

file above the canopy started to go over a uniform fuzzy surface, and

some air flow jetted into the tree trunk region from below at the

leading edge portion of the canopy. The velocity profile within the

canopy was slowed down due to the high drag of tree leaves and tree

trunks. Therefore, at 15.2 cm from the leading edge, the profile within

the canopy was distorted but air still fed into the profile from above

and a jet form existed at a level above the tree trunks. This is illus-

trated in Figure 4.3.1.2. As the wind profile moved further downstream,

the jet form smoothed out and disappeared at 200 cm downstream. From

200 cm onward uniform flow prevailed within the canopy. The wind pro-

file had some slight variation until it reached the end region of the

canopy. However, the wind profile above the canopy tended to have a

logarithmic distribution as it moved farther downstream. The varia-

tions of wind flow after encountering the canopy as described above are

termed the initial region of the forest canopy and are shown in Figure

4.3.1.2.

For the center region of the forest canopy, the velocity

profile above the canopy was plotted in two ways: the logarithmic

form as suggested by Rossby and Montgomery (1935) and the power

distribution form of Plate and Quraishi (1965).

The equation of the logarithmic form is:

$$\frac{u}{u_*} = \frac{1}{k} \ln\left(\frac{y-d}{z_o}\right) \quad . \tag{1.1.3}$$

The zero plane displacement d was replaced by the tree height h in

this work and the shear velocity u_* was from the direct measurement

of the shear plate. The Karman constant k was 0.4. Data at stations

400, 500, 600, 700, 800 cm are plotted in Figure 4.3.1.3 which shows

that the data follows equation 1.1.3 fairly well. In Figure 4.3.1.3

the maximum deviation of data points was 11 percent throughout the ve-

locity profile except at the level barely above the top of the forest

where the velocity profile has been somewhat disturbed and the data is

considerably off the line of equation 1.1.3. This equation shows that

the aerodynamic roughness was 0.045 h . For the average forest height

of 16.50 cm, the aerodynamic roughness was equal to 0.74 cm for the

center region of the forest canopy.

Plate and Quraishi (1965) suggested a power distribution

velocity profile above the canopy field which has the form:

$$\frac{u}{U_a} = \left(\frac{y-h}{\delta-h}\right)^{\frac{1}{n}} \tag{4.3.1.4}$$

where U_a is the ambient wind velocity, δ is the boundary layer

thickness, and h is the height of the canopy. To their plastic strip

canopy and wooden pegs canopy, they found that n was 3. This phe-

nomenon existed also in Bhaduri's (1963) wood strip study, and in the

model forest tree canopy in this work. Comparisons of these three are

shown in Figure 4.3.1.4.

Both field data for wheat and corn, and experimental data for model canopies are available within the canopy in the center region. They are plotted in Figure 4.3.1.5. The model forest canopy was rather uniform in velocity from the floor up to the 0.6 height of the trees. This was due to the stiffness of the model trees. Nevertheless, the prototype trees have this kind of stiffness with respect to the tree height. The height of Douglas fir under 1750 cm/sec strong wind speed is 0.85 of the original height in still air as shown in Figure 4.1.1.1.

At the end region of the forest canopy, the wind speed within the canopy increased. It is because of accelerating flow due to less drag downstream. Two velocity profiles, one barely inside the canopy, and one at 29 cm behind the canopy, are compared in Figure 4.3.1.6. The velocity profiles showed some recovery at the lower part after passing through the canopy field. The upper part of the velocity profile, however, had less influence and maintained the same shape. From these two velocity profiles, it was checked that

$$\left(\int_0^\delta udy \right)_{\text{at forest canopy end}} = \left(\int_0^\delta udy \right)_{\substack{\text{29 cm downstream of} \\ \text{forest canopy.}}}$$

In Figure 4.3.1.6, the velocity profile at 29 cm downstream, i.e., above the smooth wind tunnel floor, had θ larger than that at the forest canopy end. Hence, $\frac{d\theta}{dx} > 0$ and (τ_o) smooth surface $< (\tau_o)$ forest canopy were true. This demonstrated also the reason why the flow accelerated near the end of the forest canopy. For the flow was from a large resistance surface to a small resistance surface.

4.3.2 The variation of drag coefficient within a forest

canopy field - It was determined that the local drag coefficient of the

forest canopy was not a function of Reynolds number but a function of

$\frac{x}{h}$. Plots are shown in Figure 4.3.2.1. The shear plate was used for

the local surface drag measurements. For these wind speeds 305, 610, and

910 cm/sec, the maximum deviation 28 percent happened at station 152 cm.

Otherwise, the drag forces, or the local drag coefficient, under these

three wind speeds agreed quite closely at each station.

The local drag coefficient increased from $\frac{x}{h}$ = !8 to the end

of the forest canopy. This end region phenomenon was verified by experi-

ments on two shortened forest canopies; one had a length of 850 cm and

the other 610 cm. Both showed an increase in surface drag toward the

end of the canopy field. These two cases are not included in this

paper.

4.4 Orchard Canopy Data

The orchard canopy field was composed of artificial trees that

were equally spaced and regularly arranged both in rows and columns.

Two cases are discussed below.

By using the momentum integral method mentioned in Section 2.2,

one column and twenty rows of model trees with tree spacing 25.4 cm were

studied under a thick boundary layer. Twelve transverse wind speed

profiles were taken at each wind tunnel nominal cross section. The

first cross section was at 12.7 cm upstream of the first tree and the

rest had the 25.4 cm interval in between. The drag force of the indi-

vidual trees was then calculated from equation 2.2.4.

Here the increment Δy as well as Δz was 1.27 cm, j was 55.88 cm, and k , 76.20 cm. The wind speed data were punched into computer data cards and fed together with the computer program to the CDC 6400 computer.

The result is plotted in the cumulative drag force fashion, shown in Figure 4.4.1. The computer data had a good agreement with the directly measured data which were measured by the strain gage force dynamometer on each individual artificial tree under the above condition. The maximum deviation amounted to 20 percent for the first three cumulative tree drag forces. The rest of the data was within 10 percent. These deviations mainly resulted from the gross error of the instrumentation.

Another orchard canopy field of 7 columns and 43 rows with trees spaced 25.4 cm both in longitudinal and lateral directions was studied under a thick boundary layer. The following significant information was determined. Two zones of the tree drag phenomena were found as shown in Figure 4.4.2. These were termed the initial zone and the steady decay zone. The initial zone extended from the first row of trees to the fourth row of trees. In this zone, the drag force decreased steeply from the first row of trees to the second row of trees, and then tended to be constant to the fifth row. The steady decay zone started from the fifth row of trees and extended to the end of the canopy field. The dimensionless tree drag coefficient vs x/L was fairly linear on the log-log plot. The local drag force vs longitudinal distance in dimensionless form for the 610, 915, and 1370 cm/sec ambient wind speeds are shown in Figure 4.4.3. However, the local drag force did show an amount of increase at the end of this orchard

canopy. These are among many other orchard canopy data which can be
found in Hsi and Nath (1968).

4.5 Brushy Canopy Data

The brushy canopy was studied in a turbulent flow. Two
boundary layer thicknesses, thin and thick, were applied to the same
canopy in the hope that the different thicknesses of boundary layer
would reveal some relation between the drag coefficient of the brushy
canopy and the thickness of the boundary layer. This is presented later
in subsection 4.5.2.

4.5.1 The velocity profiles of the brushy canopy - The approach-
ing wind velocity profile for the thin boundary layer had the power dis-
tribution of

$$\frac{u}{U_a} = \left(\frac{y}{\delta}\right)^{\frac{1}{9}} . \tag{4.5.1.1}$$

For the thick boundary layer, the power was $\frac{1}{7}$. See Figures 4.5.1.1
and 4.5.1.2.

At the center region of the brushy canopy, the logarithmic wind
velocity profile for the thin boundary layer case was

$$\frac{u}{u_{*_2}} = \frac{1}{k} \ln \left(\frac{y-h}{0.11\ h}\right) \tag{4.5.1.2}$$

where u_{*_2} is the direct measured shear velocity from the shear plate,
and h the physical height of the brushy canopy, h = 2.8 cm. From
the equation 4.5.1.2 the aerodynamic roughness was 0.307 cm as shown
in Figure 4.5.1.3. The logarithmic wind velocity profile appears to
be universal; the data of 915 cm/sec and 1675 cm/sec fitted the equation
well.

For the thick boundary layer, the logarithmic wind velocity profile was

$$\frac{u}{u_{*_2}} = \frac{1}{k} \ln \left(\frac{y-h}{0.08\ h} \right) \qquad\qquad (4.5.1.3)$$

as shown in Figure 4.5.1.4. The aerodynamic roughness was 0.224 cm and was smaller for the thicker boundary layer.

4.5.2 The variation of drag coefficient in the brushy canopy, and aerodynamic roughness - For the thin boundary layer, the local drag coefficient of the brushy canopy was a function of the position in the canopy. Three ambient wind velocities 305, 915, and 1675 cm/sec were applied on the brushy canopy, and the surface shear stress was directly measured by the shear plate. The local drag coefficient was plotted against x/h in Figure 4.5.2.1. Under these three ambient wind velocities, data points were matched well with one another for the same x/h . The local drag coefficient was about 1.7×10^{-2} for $99 \leq x/h \leq 253$ which is the same as the other canopies where the local drag coefficient c'_{f_2} was maximum near the leading edge of the canopy and dropped steeply at a short distance downstream at x/h = 33. The difference between x/h = 11 and x/h = 33 of drag coefficient was about six times. At x/h = 100 the local drag coefficient recovered to 1.6×10^{-2} and kept almost constant to the end of the canopy.

For the thick boundary layer, the difference between x/h = 11 and x/h = 33 of local drag coefficient was about two times and from s/h = 99 onward the local drag coefficient was about 1.1×10^{-2} as shown in Figure 4.5.2.2.

However, the brushy canopy under a thick boundary layer showed an end effect from x/h = 207 to the end of the canopy. Based upon

only two boundary layer thicknesses applied to the brushy canopy, the decisive relation between drag coefficient and the boundary layer thickness could not be drawn. But it appeared that the brushy canopy under the thinner boundary layer had the larger drag coefficient. In conclusion, however, the studied canopies showed that c_f' for brushy canopy under thin boundary layer $\approx c_f'$ for brushy canopy under thick boundary layer $= c_f'$ forest canopy under thick boundary layer; all were in the established region.

The following are two tables in which the aerodynamic roughnesses of the simulated brushy and forest canopies are tabulated in terms of their physical height h . The second table is for comparative purpose. Deacon's results on aerodynamic roughness were also converted into the physical height h .

In Figure 4.5.2.3, the aerodynamic roughnesses of the simulated brushy and forest canopies under a thick boundary layer were plotted against their physical height to verify Kung's empirical formula, equation 1.1.1. The result agrees remarkably well with that empirical formula.

Table 4.5.2.1 The aerodynamic roughnesses
of simulated canopies

Experimental Canopies

Canopy	Aerodynamic Roughness z_o in terms of h	Boundary Layer Condition	Physical Height h (cm)
Plastic strips	0.150 h		10.1
Forest	0.045 h	δ/h = 5.5	16.5
Brushy	0.080 h	δ/h = 14.5	2.8
Brushy	0.110 h	δ/h = 7.2	2.8

Table 4.5.2.2 The aerodynamic roughnesses of low
vegetative surfaces, after Deacon

The Prototype Low Vegetative Surfaces

Surface Condition	Aerodynamic Roughness z_o in terms of h	Wind Speed (cm/sec)	Physical Height , h (cm)
Mown grass surface (lawn)	0.133 h		1.5
Mown grass surface (lawn)	0.234 h		3.0
Mown grass surface (high grass)	0.0534 h	200	45.0
Mown grass surface (high grass)	0.0378 h	700	45.0
Long grass	0.138 h	150	65.0
Long grass	0.094 h	310	65.0
Long grass	0.057 h	620	65.0

4.5.3 The comparison of velocity profiles in and above the

forest canopy with those of the brushy canopy - In Figure 4.5.3.1 the

comparison of the velocity profile in and above the forest canopy with

that of the brushy canopy was made in dimensionless form; the velocity

gradient was larger for the forest canopy than for the brushy canopy.

This was also true for the velocity profiles shown in Figure 4.5.3.2.

In this figure the velocity profiles were plotted in such a way that

$(y-h)/(\delta-h)$ was used for dimensionless vertical distance; the velocity

profiles and the boundary layer thickness hence started from the fuzzy

surface of the forest and brushy canopies upward. No velocity profile

similarity was apparent between the forest canopy and the brushy canopy.

66

Chapter 5

CONCLUSIONS

The general character of flow in and above vegetative canopies
may be satisfactorily simulated in a meteorological wind tunnel. In
particular, the drag coefficient of prototype forest and brushy canopies
can be evaluated from the results of this study. The drag coefficient
of a single conifer tree was obtained satisfactorily by studying a
plastic model tree in a wind tunnel. The conclusions are itemized as
follows:

1.   In a thick boundary layer a simulated forest canopy and a
simulated brushy canopy possess the same drag coefficient in the region
of established flow, in spite of a six-fold difference in physical
height. Hence, the drag-coefficient similarity concept is valid and
implies that the laboratory data can be applied to the prototype
forest canopies. The drag coefficients of simulated forest and brushy
canopies are shown in Figure 5.1.

2.   It was found in this study that the simulated forest and brushy
canopies have the surface stress proportional to 1.9 the power of the
ambient wind velocity in their center region. This is shown in
Figure 5.2. It is expected that the prototype forest and brushy cano-
pies may have the same relation between the surface stress and the
wind velocity.

3.   The Kung empirical equation for finding the aerodynamic
roughness of vegetative canopies, i.e., Equation 1.1.1, can be used
for the simulated forest and brushy canopies in this study. See
Figure 4.5.2.3.

4.   The logarithmic velocity profiles in the center region of
vegetative canopies are:

(i)   Simulated forest canopy, thick boundary layer

$$\frac{u}{u_*} = \frac{1}{k} \ln \left(\frac{y - h}{0.045h} \right) \quad , \quad h = 16.5 \text{ cm}$$

(ii)   Simulated brushy canopy, thick boundary layer

$$\frac{u}{u_*} = \frac{1}{k} \ln \left(\frac{y - h}{0.08h} \right) \quad , \quad h = 2.8 \text{ cm}$$

(iii)   Simulated brushy canopy, thin boundary layer

$$\frac{u}{u_*} = \frac{1}{k} \ln \left(\frac{y - h}{0.11h} \right) \quad , \quad h = 2.8 \text{ cm}$$

(iv)   Simulated peg and plastic strip canopies, Plate and
         Quraishi (1965)

$$\frac{u}{u_*} = \ln \left(\frac{y - h}{0.15h} \right)$$

         h wooden peg canopy = 5.1 cm

         h plastic strip canopy = 10.2 cm

The aerodynamic roughness from the simulated velocity profiles,
as found by Plate and Quraishi, is larger than that in this study.
The aerodynamic roughness found in this study was based on the shear
plate measurement for u_* and simulated velocity profile for u and
y .

5.   The single plastic model tree in this study had its tree drag
coefficient between the Douglas fir and the spruce. Therefore, the
simulation of a single tree is possible and can be carried out in a
wind tunnel.

6.   The shear plate used to measure the surface stress of various
canopies can also be used to study the horizontal force component pro-
duced by air flow over modeled irregular topography.

7.   With the existent model forest canopy used in this work, future research related to forest fire behavior, snow pack, soil erosion, wind breaks, watershed management, or other aspects of silviculture can be developed.

69

Chapter 6

REFERENCES

Bradshaw, P. A., (1959), "A Simple Method for Determining Turbulent
Skin Friction from Velocity Profiles," J. Aero Space Sci.,
26, 841.

Bidwell, J. M., (1951), "Application of the von Karman Momentum
Theorem to Turbulent Boundary Layer," NACA-TN 2571.

Clauser, F. H., (1956), "The Turbulent Boundary Layer," Advanced Appl.
Mech. 4, 1-51, New York.

Coles, D., (1955), "The Law of the Wall in Turbulent Shear Flow,"
50 Jahre Grenschichtforschung, 153-163, Braunschweig.

Cermak, J. E., et al, (1966), "Simulation of Atmospheric Motion by
Wind-Tunnel Flows," Tech. Report, Colorado State University,
CER66JEC-VAS-EJP-GJB-HC-RNM-SI17, May.

Deacon, E. L., (1953), "Vertical Profile of Mean Wind in the Surface
Layer of the Atmosphere," Geophysical Memoirs 2, No. 91.

Dhawan, S., (1953), "Direct Measurements of Skin Friction,"
NACA-TN 2567.

Elliott, W. P., (1958), "The Growth of the Atmospheric Internal
Boundary Layer," Trans. Am. Geophys, Union 39, 1048.

Ellison, T. H., (1957), "Turbulent Transport of Heat and Momentum from
an Infinite Rough Plane," J. Fluid Mech. 2, 456.

Elrod, H. G., Jr., (1957), "Note on the Turbulent Shear Stress near a
Wall," J. Aero. Sci. 24, 468-469.

Fons, W. L., (1940), "Influence of Forest Cover on Wind Velocity,"
J. of Forest 38, No. 6.

Glaser, A. H., Elliott, W. P. and Druce, A. J., (1957), "Final Report
on Internal Boundary Layer," A. and M. College of Texas,
Project No. 85, Ref. 57-8F.

Goldschmied, F. R., (1951), "Skin Friction of Incompressible Turbulent
Boundary Layers under Adverse Pressure Gradients," NACA-TN
2431.

Hama, F. R., (1954), "Boundary Layer Characteristics for Smooth and
Rough Surfaces," Trans. Soc. Naval Arch. Marine Engrs. 62,
333-358.

REFERENCES - Continued

Hartnett, J., et al, (1962), "A Comparison of Predicted and Measured
        Friction Factors for Turbulent Flow through Rectangular Ducts,"
        J. Heat Transfer, ser. C, Vol. 84.

Hoerner, S., (1958), "Fluid Dynamic Drag," 148 Bustead Drive, Midland
        Park, N. J.

Hsi, G., Binder, G. J. and Cermak, J. E., (1968), "Topographic Influence
        on Wind near Green River, Utah," Tech. Rep., CER67-68GH-GJB-JEC,
        Colorado State University, April.

Hsi, G. and Nath, J. H., (1968), "A Laboratory Study on the Drag Force
        Distribution within Model Forest Canopies in Turbulent Shear
        Flow," Tech. Report, CER67-68GH-JHN50, Colorado State University,
        March.

Jacob, W., (1940), "Variation in Velocity Profile with Change in Surface
        Roughness of Boundary," NACA-TM 951.

Jones, J. B., (1963), "Flow in a Pipe Following an Abrupt Increase in
        Surface Roughness," Trans. ASME 85, D, 35.

Klebanoff, P. S., (1954), "Characteristics of Turbulence Layer with
        Zero Pressure Gradient," NACA-TN 3178.

Klebanoff, P. S. and Diehl, Z. W., (1952), "Some Features of Artificial
        Thickened Fully Developed Turbulent Boundary Layer with Zero
        Pressure Gradient," NACA-Rep 1110.

Lai, W., (1955), "Aerodynamic Crown Drag of Several Broad-Leaf Tree
        Species," Interim Tech. Report, AFSWP 63.

Lettau, H. H., (1959), "Studies of the Three-Dimensional Structure of
        the Planetary Boundary Layer," Annual Report, DA-36-039-SC-
        80282, U.S. Army Electronic Proving Ground.

Ludwieg, H. and Tillman, W., (1950), "Investigation of the Wall Shearing
        Stress in Turbulent Boundary Layer," NACA-TM 1285.

Meroney, R. N., (1968), "Characteristics of Wind and Turbulence in and
        Above Model Forests," to be printed in J. Applied Meteorology,
        October.

Meroney, R. N. and Cermak, J. E., (1967), "Characteristics of Diffusion
        within Model Canopies," Paper presented at Symposium on Atmos-
        pheric Turbulence and Diffusion in the Planetary Boundary Layer.

Miyake, M., (1961), "Transformation of Atmospheric Boundary Layer
        Induced by Inhomogeneous Surface," M.S. Thesis, University of
        Washington, Seattle.

REFERENCES - Continued

Ostrowski, J., (19??), "Single Tree Data," Unpublished, Colorado State
        University, Fort Collins, Colorado.

Panofsky, H. A. and Townsend, A. A., (1964), "Change of Terrain
        Roughness and the Wind Profile," Quart. J. Roy. Meteorol. Soc.,
        90, 147.

Perry, C. C. and Lissner, H. R., (1955), "The Strain Gage Primer,"
        McGraw Hill, New York.

Plate, E. J. and Hidy, G. M., (1967), "Laboratory Study of Air Flowing
        over a Smooth Surface onto Water Waves," J. of Geophysical
        Research, Vol. 72, No. 18, September.

Plate, E. J. and Quraishi, A. A., (1965), "Modeling of Velocity
        Distribution inside and above Tall Crops," J. of Applied
        Meteorology, Vol. 4, No. 3, June.

Raymer, W. G., (1962), "Wind Resistance of Conifers," NPL Aero Report
        1008, April.

Roshko, A., (1955), "On the Wake and Drag of Bluff Bodies," J. of
        Aero. Sci. 22, 124-132.

Ross, D. and Robertson, J. M., (1951), "A Superposition Analysis of
        the Turbulent Boundary Layer in an Adverse Pressure Gradient,"
        J. Appl. Mech. 18, 95-100.

Rotta, J. C., (1962), "Turbulent Boundary Layers in Incompressible
        Flows," Progress in Aeronautical Science, Vol. 2, McMillan Co.,
        New York.

Rubesin, M. W., (1951), "An Analytical and Experimental Investigation
        of the Skin Friction of the Turbulent Boundary Layer on a Flat
        Plate at Supersonic Speeds," NACA-TN 2305.

Sauer, F. M., et al, (1951), "Experimental Investigation of Aerodynamic
        Drag in Tree Crowns Exposed to Steady Wind Conifers," Division
        of Forest Fire Research, USDA, For. Ser., Washington, D. C.

Schlichting, H., (1968), "Boundary Layer Theory," McGraw Hill, New York.

Schubauer, G. B. and Tchen, C. M., (1959), "Turbulent Flow," High
        Speed Aerodynamics and Jet Propulsion 5, 75-195, Princeton
        University Press, N. J.

Schultz-Grunow, F., (1941), "New Frictional Resistance Law for Smooth
        Plates," NACA-TM 986.

Smith, D. W., (1957), "Turbulent Skin-Friction Measurements on a
        Smooth Flat Plate in Incompressible Flow," Proc. Fifth Mid-
        Western Conf. Fluid Mech. 108-121, Univ., Michigan.

REFERENCES - Continued

Smith, D. W. and Walder, J. H., (1959), "Skin-Friction Measurements in Incompressible Flow," NASA-Rep R-26 .

Sutton, O. G., (1953), "Micrometeorology," McGraw Hill, New York.

Townsend, A. A., (1965), "Self-Preserving Flow inside a Turbulent Boundary Layer," J. Fluid Mech. 22, Part 4.

Townsend, A. A., (1965), "The Response of a Turbulent Boundary Layer to Abrupt Changes in Surface Conditions," J. Fluid Mech. 22, Part 4.

Townsend, A. A., (1966), "The Flow in a Turbulent Boundary Layer after a Change in Surface Roughness," J. Fluid Mech. 26, Part 2.

Uram, E. M., (1960), "Skin-Friction Calculation for Turbulent Layer in Adverse Pressure Distribution," J. Aero Space Science 27, 75-76.

van Le, N., (1952), "The von Karman Integral Method as Applied to a Turbulent Boundary Layer," J. Aero Sci. 19, 647-648.

von Karman, T., (1946), "On Laminar and Turbulent Friction," NACA-TM 1092.

Walshe, D. E. and Fraser, A. I., (1963), "Wind-Tunnel Tests on a Model Forest," NPL Aero Report 1078, October.

Worley, F. L., (1965), "A Study of Roughness Effects in Turbulent Flow," Ph.D. Dissertation, University of Houston, Houston, Texas.

Yano, M., (1966), "Turbulent Diffusion in a Simulated Vegetative Cover," Ph.D. Thesis, Colorado State University, Fort Collins, Colorado.

Chapter 7

APPENDIX

Table 3.1.1 Performance characteristics of the Army Meteorological
and the Colorado State University Wind Tunnels

Characteristic	Army Meteorological Wind Tunnel	Colorado State University Wind Tunnel
1. Dimensions		
Test-section length	27 m	9.2 m
Test-section area	3.4 m^2	3.4 m^2
Contraction ratio	9.1	9.1
Length of temperature controlled boundary	12 m	3.1 m
2. Wind-tunnel drive		
Total power	200 kw	75 hp
Type of drive	4-blade propeller	16-blade axial fan
Speed control: coarse	Ward-Leonard DC control	single-speed induction motor
Speed control: fine	pitch control	pitch control
3. Temperatures		
Ambient air temperature	5°C to 95°C	not controlled
Temp. of controlled boundary	5°C to 205°C	ambient to 95°C
4. Velocities		
Mean velocities	approx. 0 mps to 37 mps	approx. 1 mps to 27 mps
Boundary layers	up to 50 cm	up to 20 cm
Turbulence level	low (about 0.1 percent)	low (about 0.5 percent)
5. Pressures	adjustable gradients	not controlled
6. Humidity	controlled from approx. 20% to 80% relative humidity under average ambient conditions.	not controlled

74

2 mm   12 mm

H = Hand Wheel
D = Wire
F = Spring Hinge
S = Float

H

D

Test Plate

F

S

S
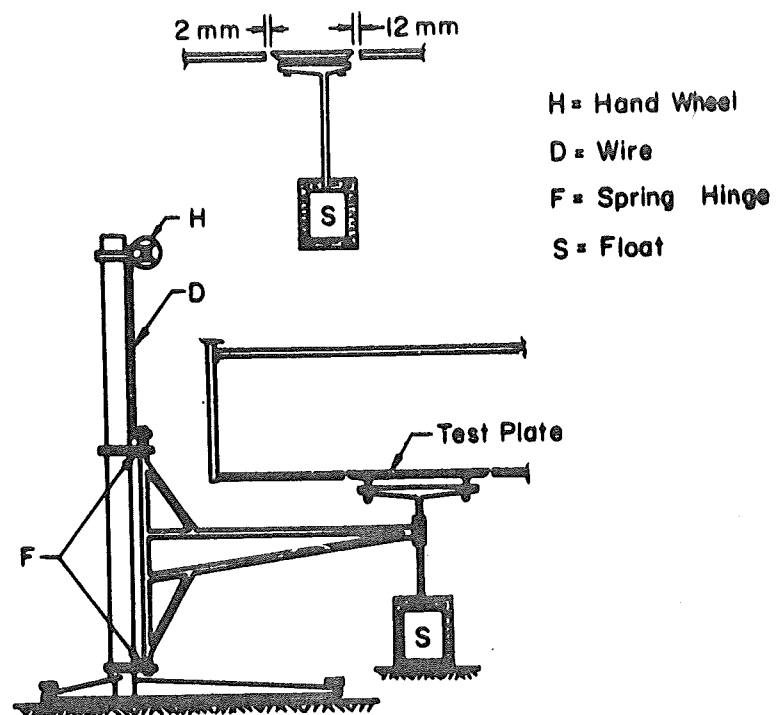
Fig. 2.1.1   Arrangement of test plate and balance,
             Schultz-Grunow (1940)
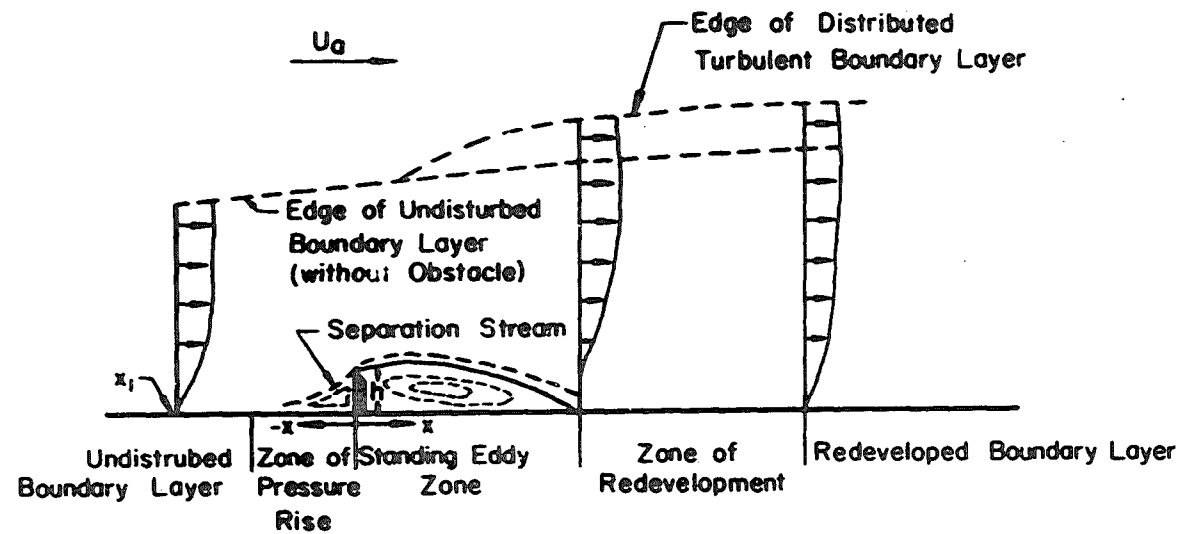
Fig. 2.3.1 Zones of disturbed boundary layer, after Plate (1965)
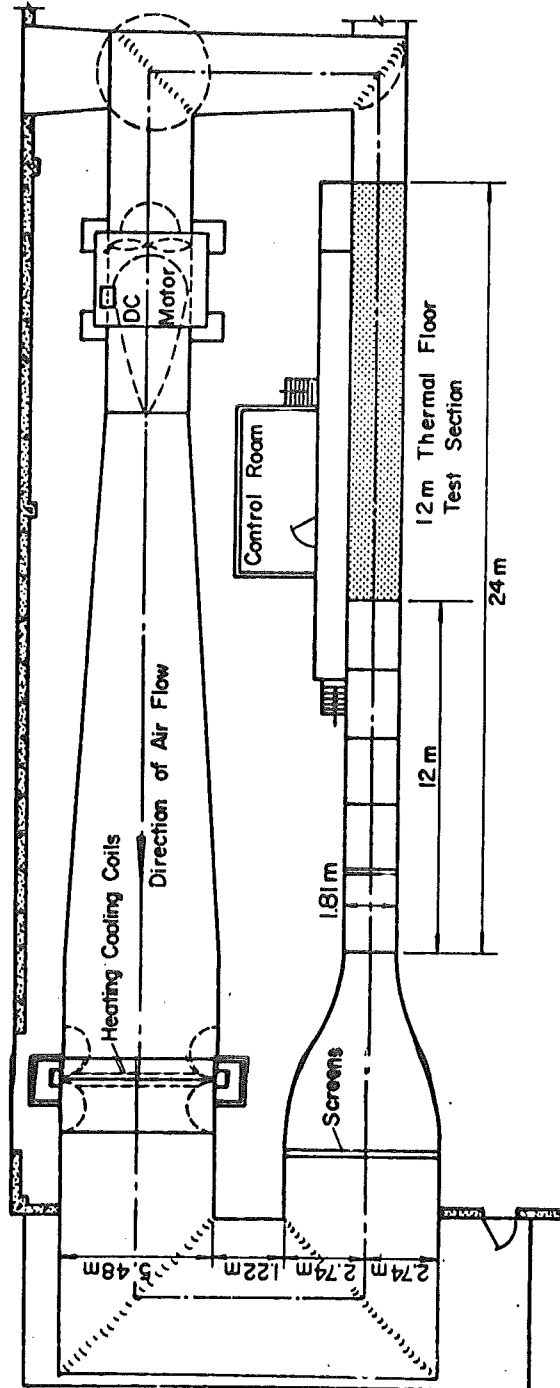
PLAN VIEW

Figure 3.1.1 The U. S. Army meteorological wind tunnel
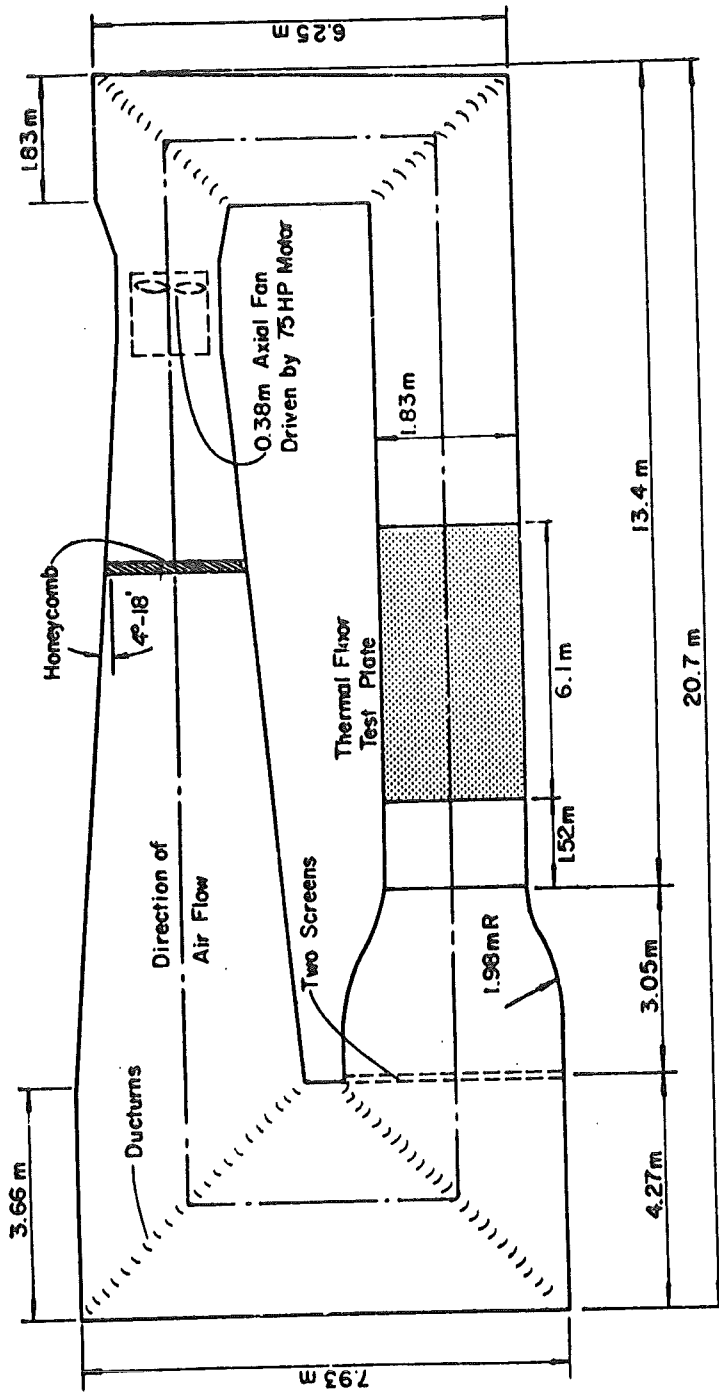
Fig. 3.1.2 Colorado State University wind tunnel
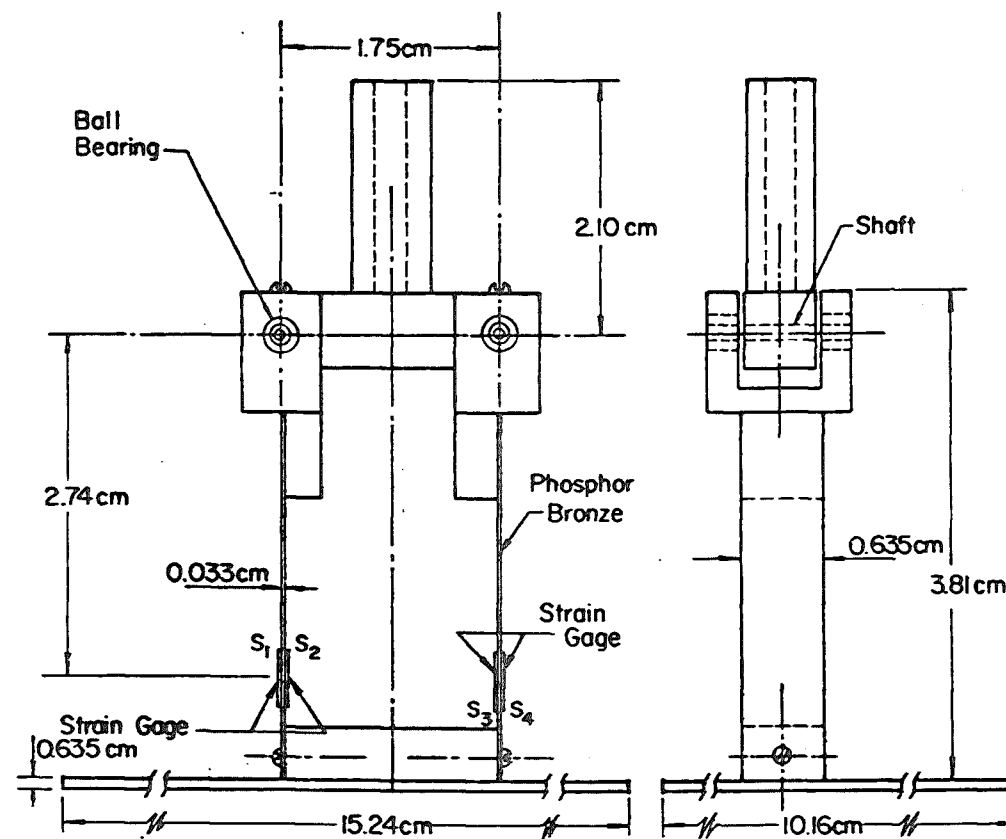
Fig. 3.2.1.1 The strain gage force dynamometer
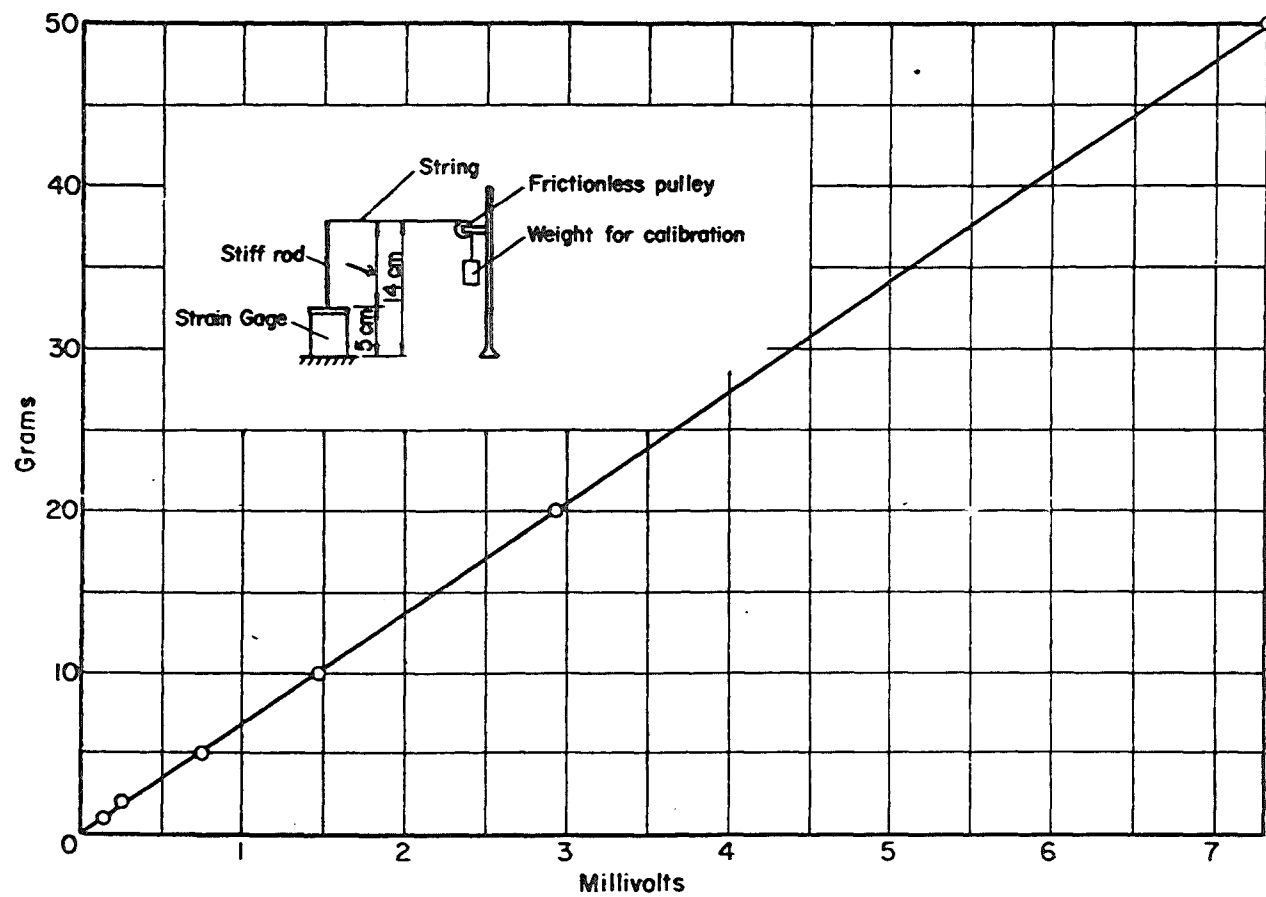
Fig. 3.2.1.2 The calibration curve of the strain gage force dynamometer

See figure 2.3 for the
position of the strain gages

S_1^+ S_2^-

8 v. DC   5 KΩ

E_{in}

S_4^- S_3^+

1 MΩ

E_{out}
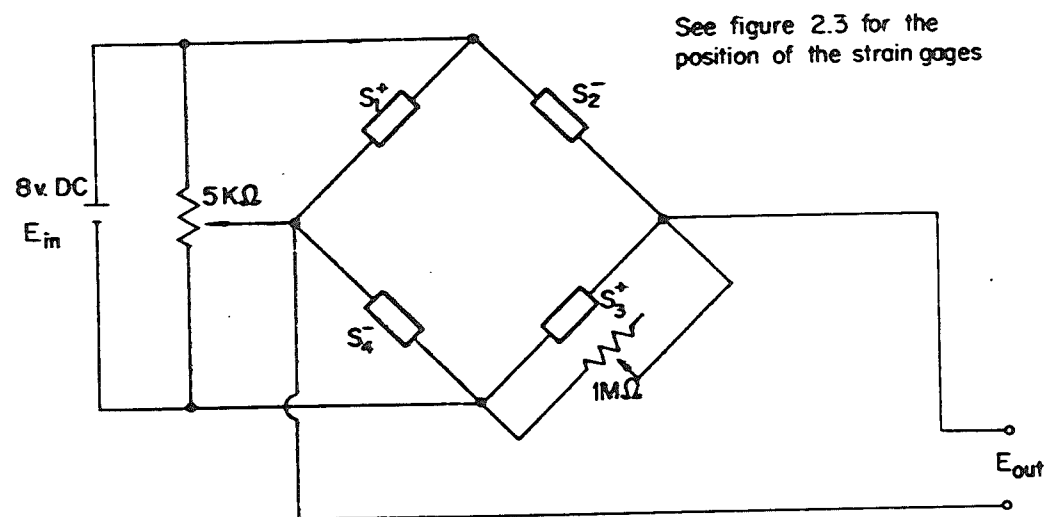
Fig. 3.2.1.3 The electric bridge arrangement for the strain gage force dynamometer
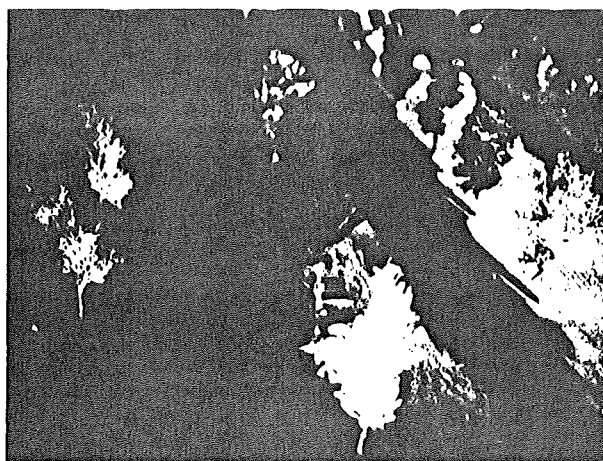
Figure 3.2.1.4 The strain gage force dynamometer
in a model orchard canopy field
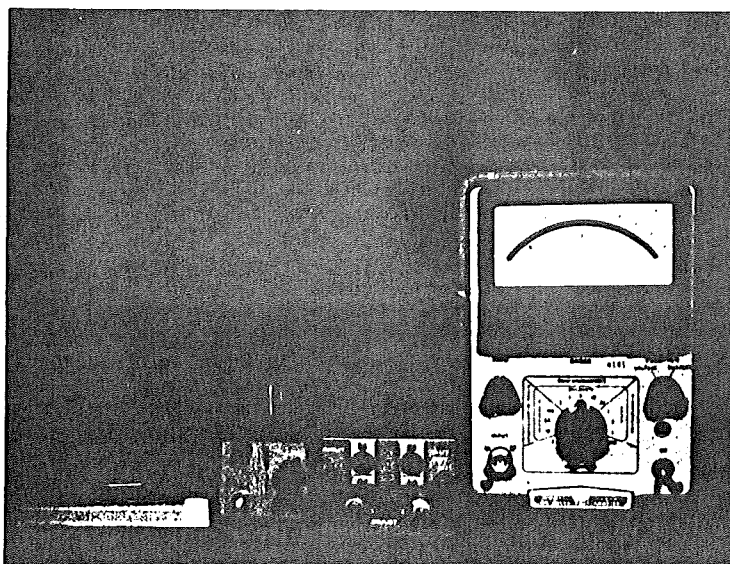
Fig. 3.2.1.5 Instruments for the strain gage force dynamometer
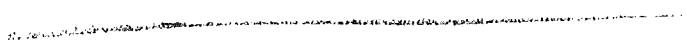
Fig. 3.2.1.6 The schematic diagram of the shear plate
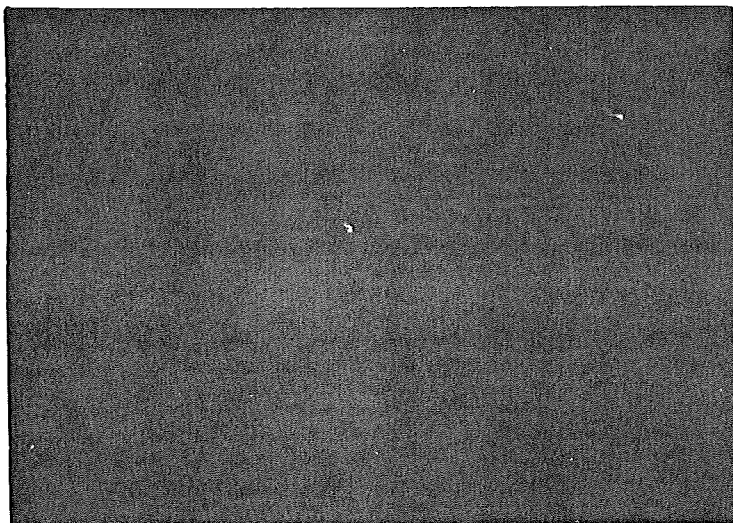
Figure 3.2.1.7 The shear plate
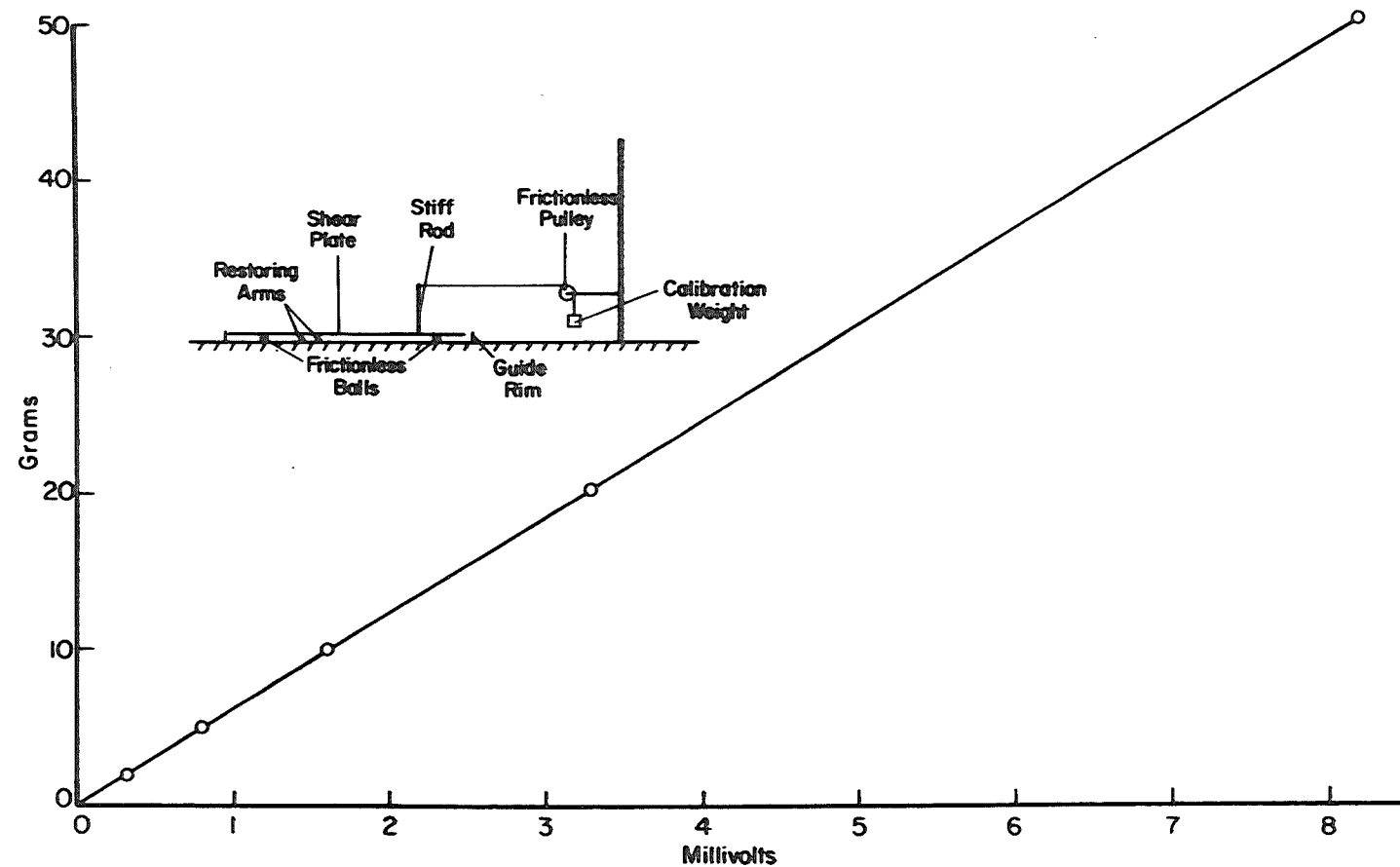
Figure 3.2.1.8 The calibration curve of the shear plate
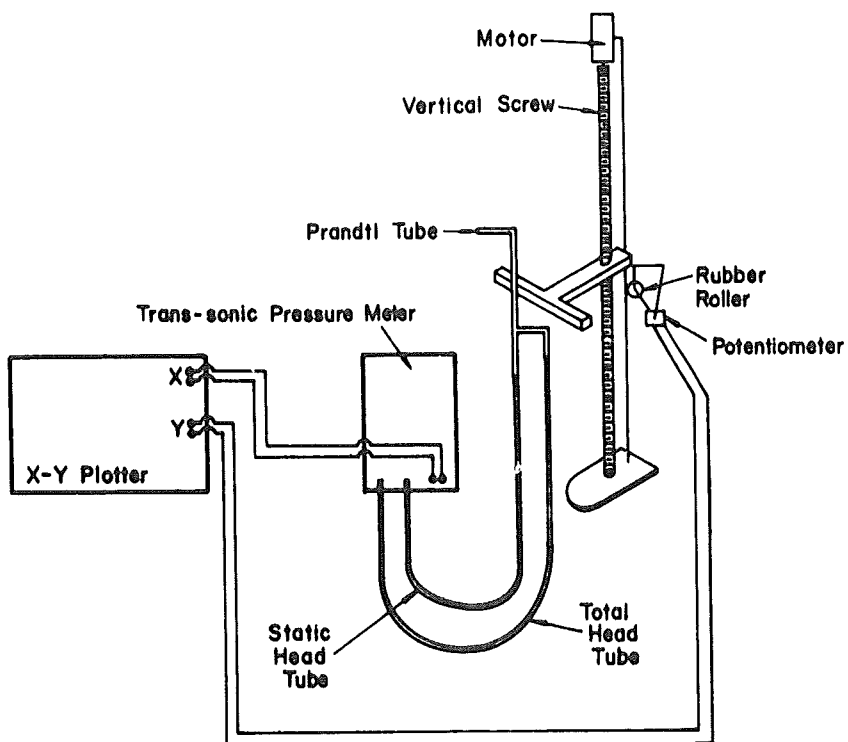
Figure 3.2.2.1 Schematic diagram of vertical velocity
profile measurement
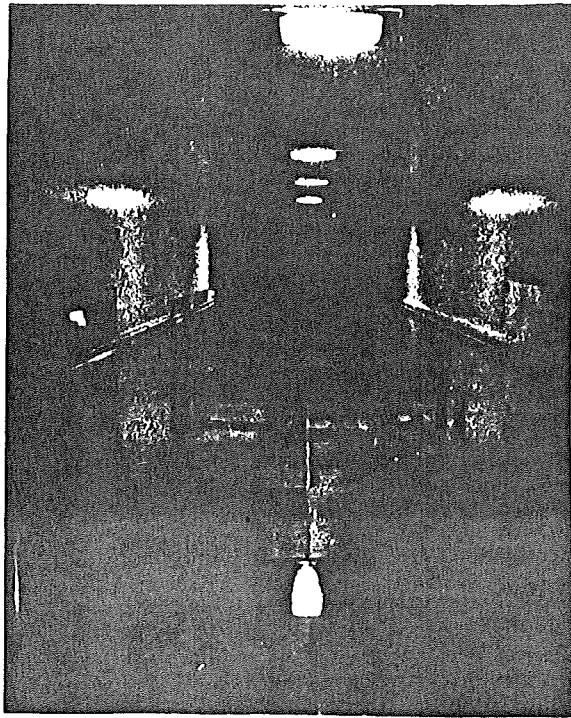
Fig. 3.3.1 The smooth boundary, with the shear plate, in a wind tunnel
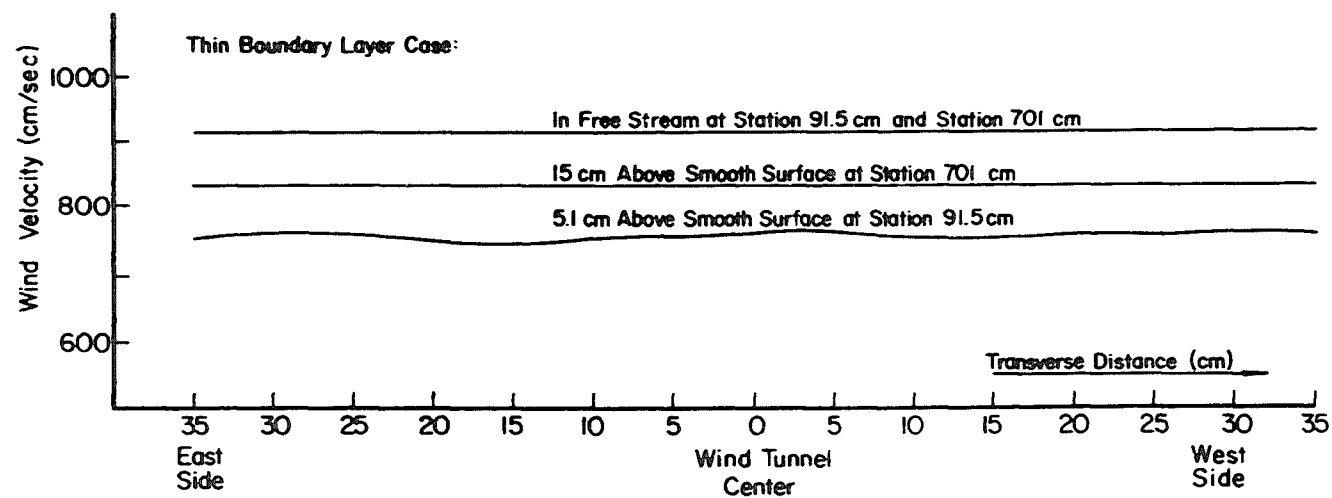
Fig. 3.3.2 Two dimensionality of flow condition over the smooth boundary
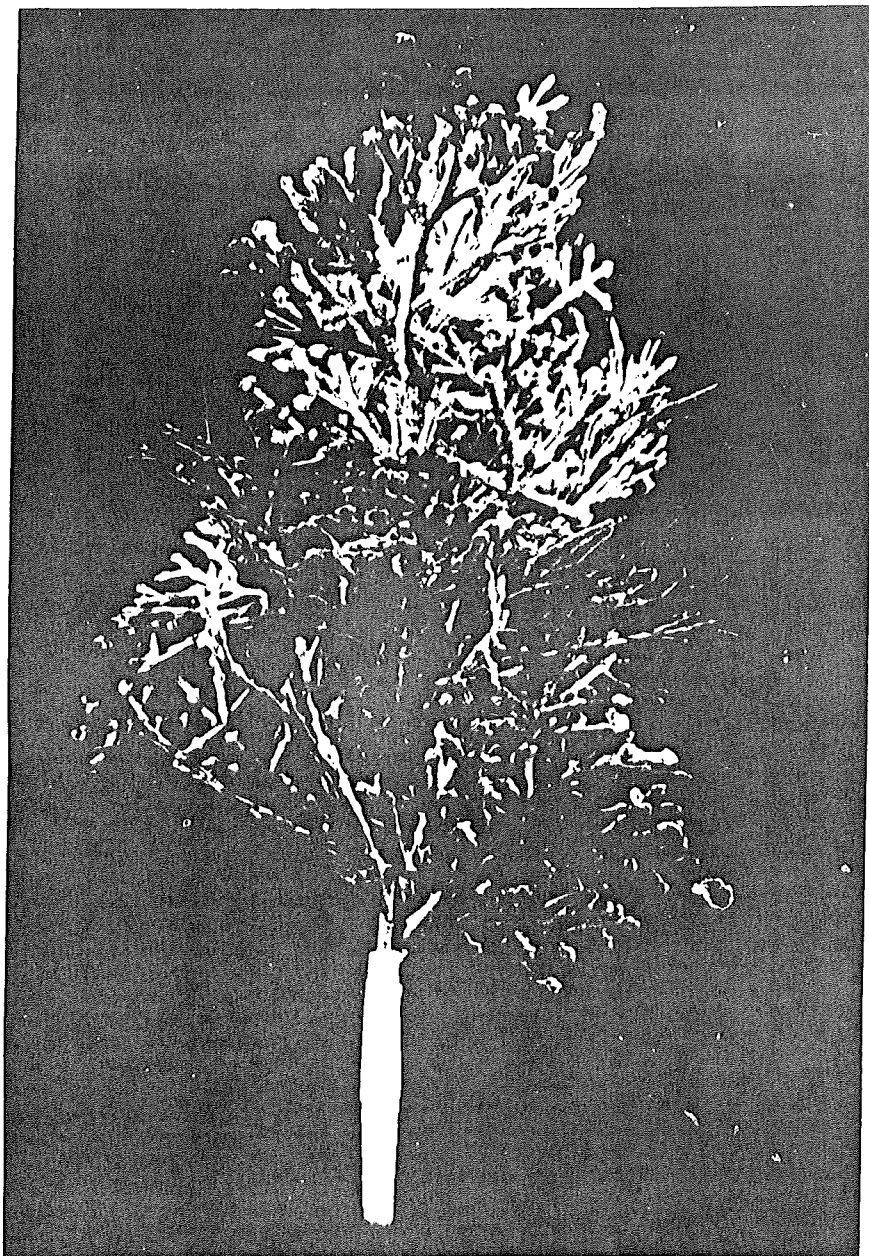
Figure 3.4.1.1 Close-up photograph of an artificial tree
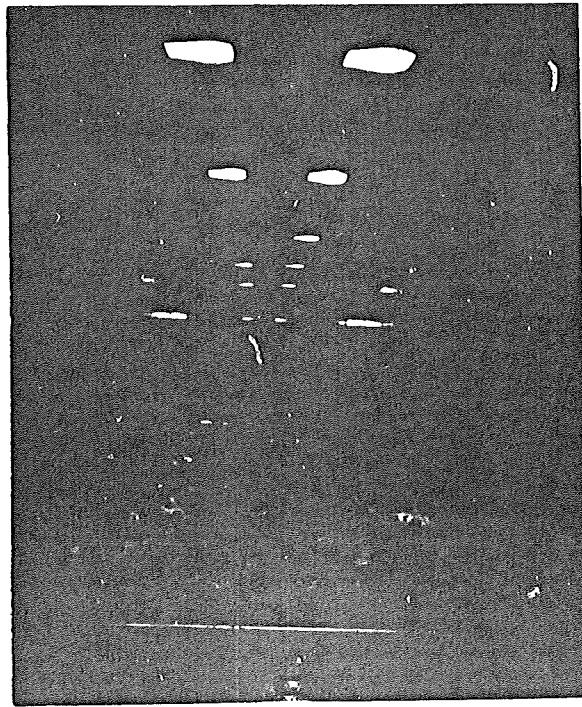
Figure 3.4.3.1   The forest-type canopy field

700

Thick Boundary Layer Case:

In Free Stream at Station 300 cm and Station 800 cm

600

Wind Velocity (cm/sec)

53 cm Above Tree Top at Station 300 cm

±4% Deviation in Two-dimensionality

500

53 cm Above Tree Top at Station 800 cm

±2.5% Deviation in Two-dimensionality

Transverse Distance (cm)

400

| 35 | 30 | 25 | 20 | 15 | 10 | 5 | 0 | 5 | 10 | 15 | 20 | 25 | 30 | 35 |

East
Side

Wind Tunnel
Center

West
Side
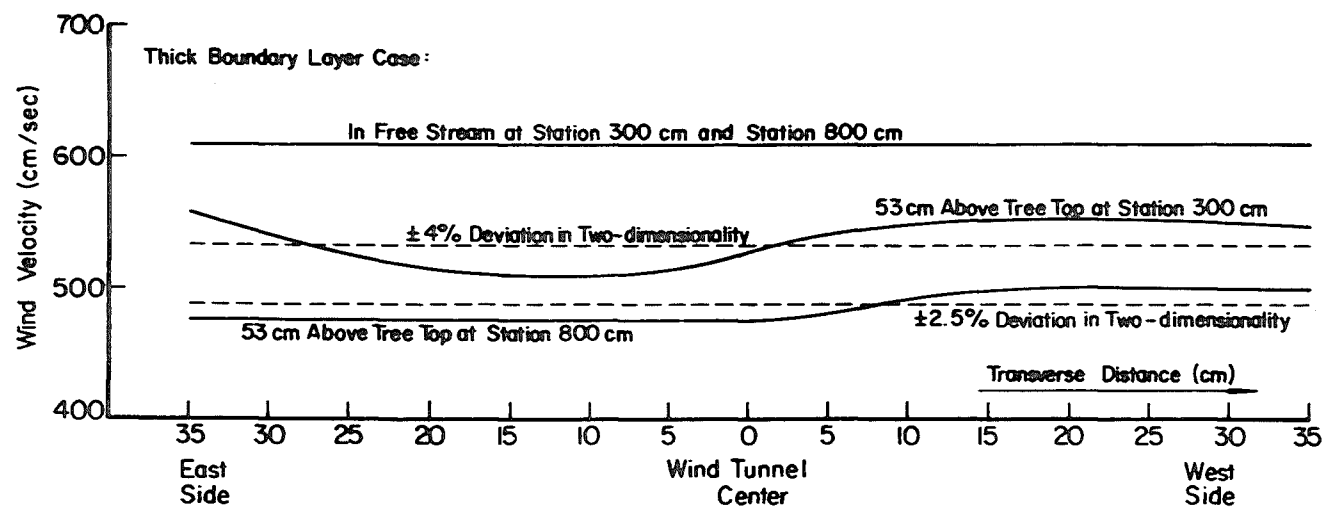
Fig. 3.4.3.2 Two dimensionality of flow condition over the forest-type canopy field

92
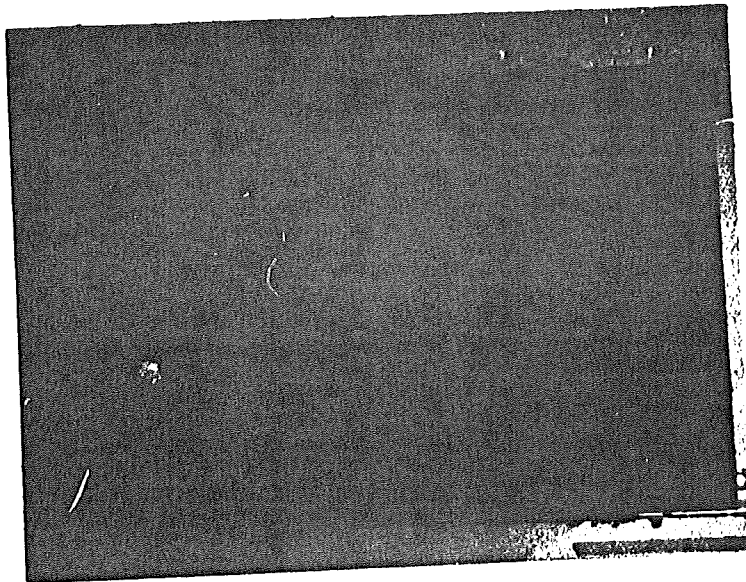
Figure 3.4.4.1 The arrangement of brushy canopy on a piece of plywood
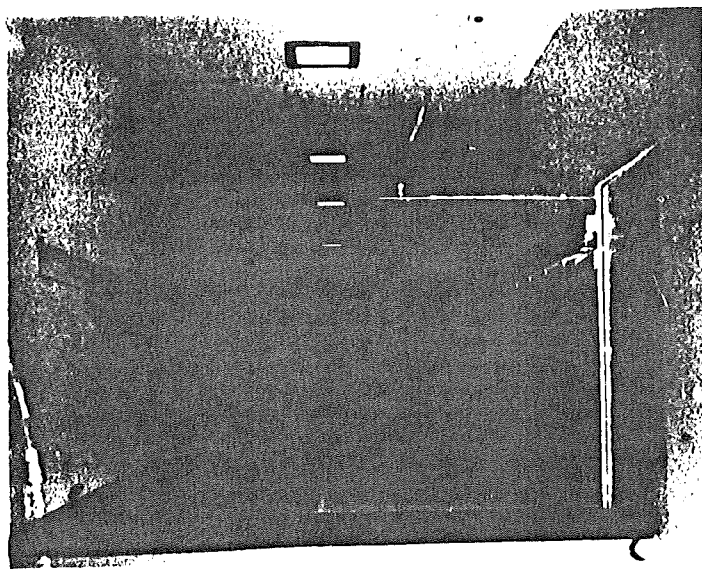
Fig. 3.4.4.2 The brushy canopy field in a wind tunnel
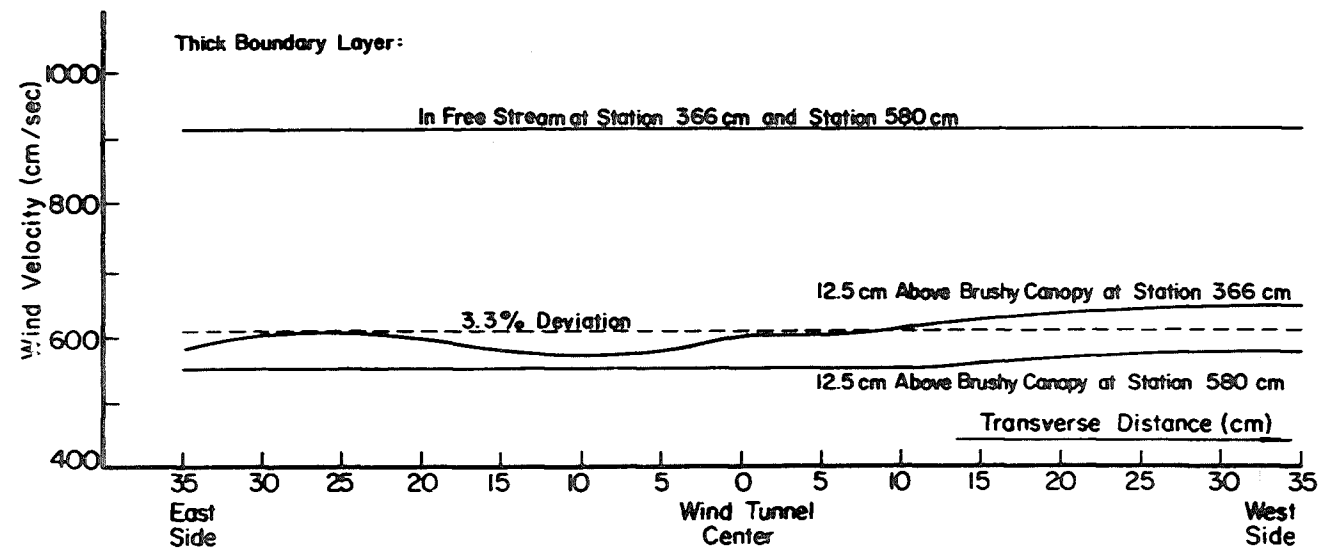
Figure 3.4.4.3 Two dimensionality of flow condition over the brushy canopy field
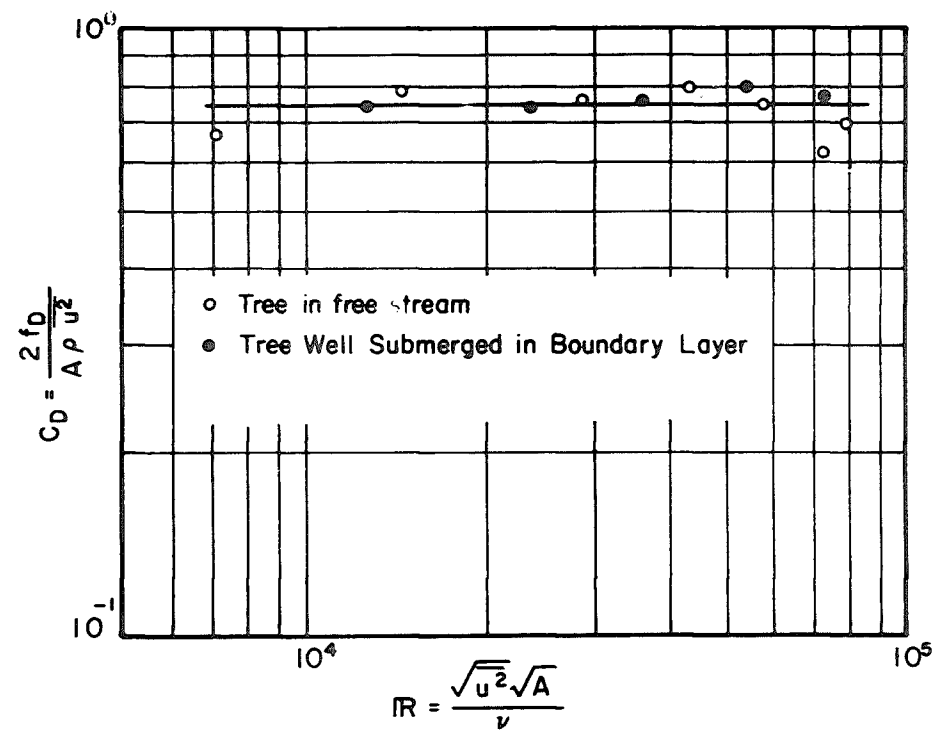
Figure 4.1.1 Drag coefficient of a single model tree
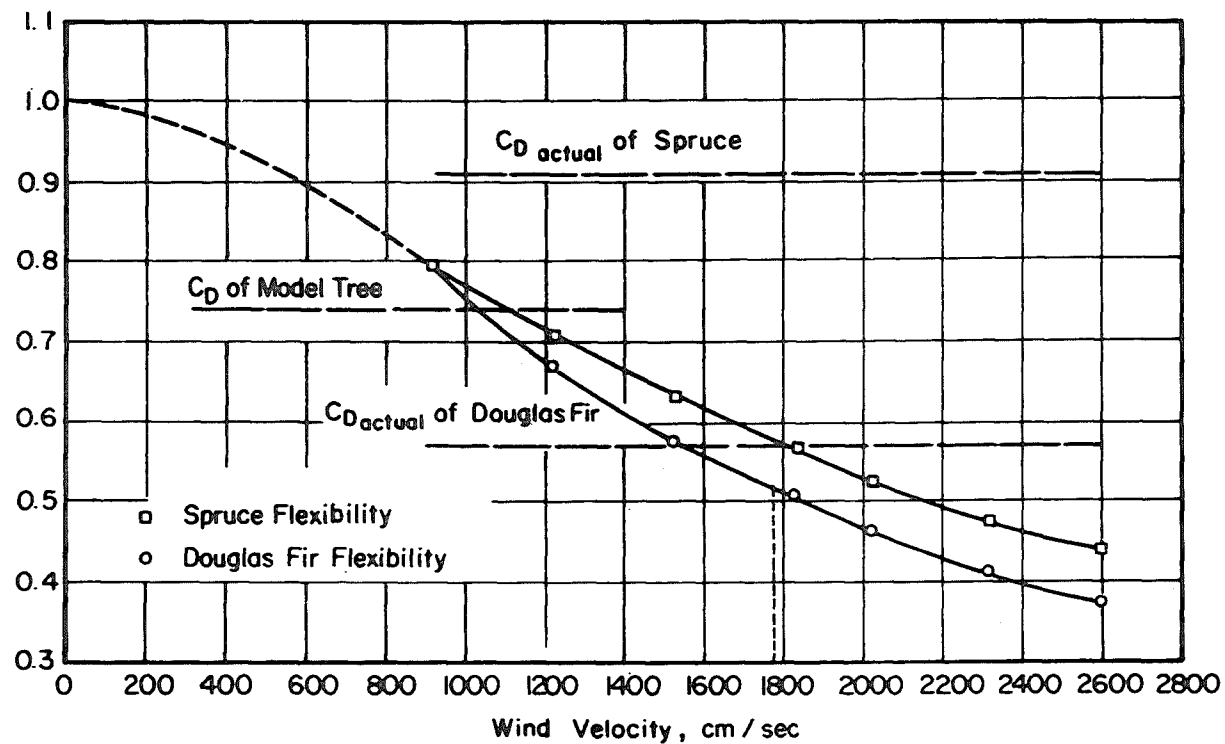
Figure 4.1.2   Tree flexibility and actual tree drag coefficient of spruce and
Douglas fir
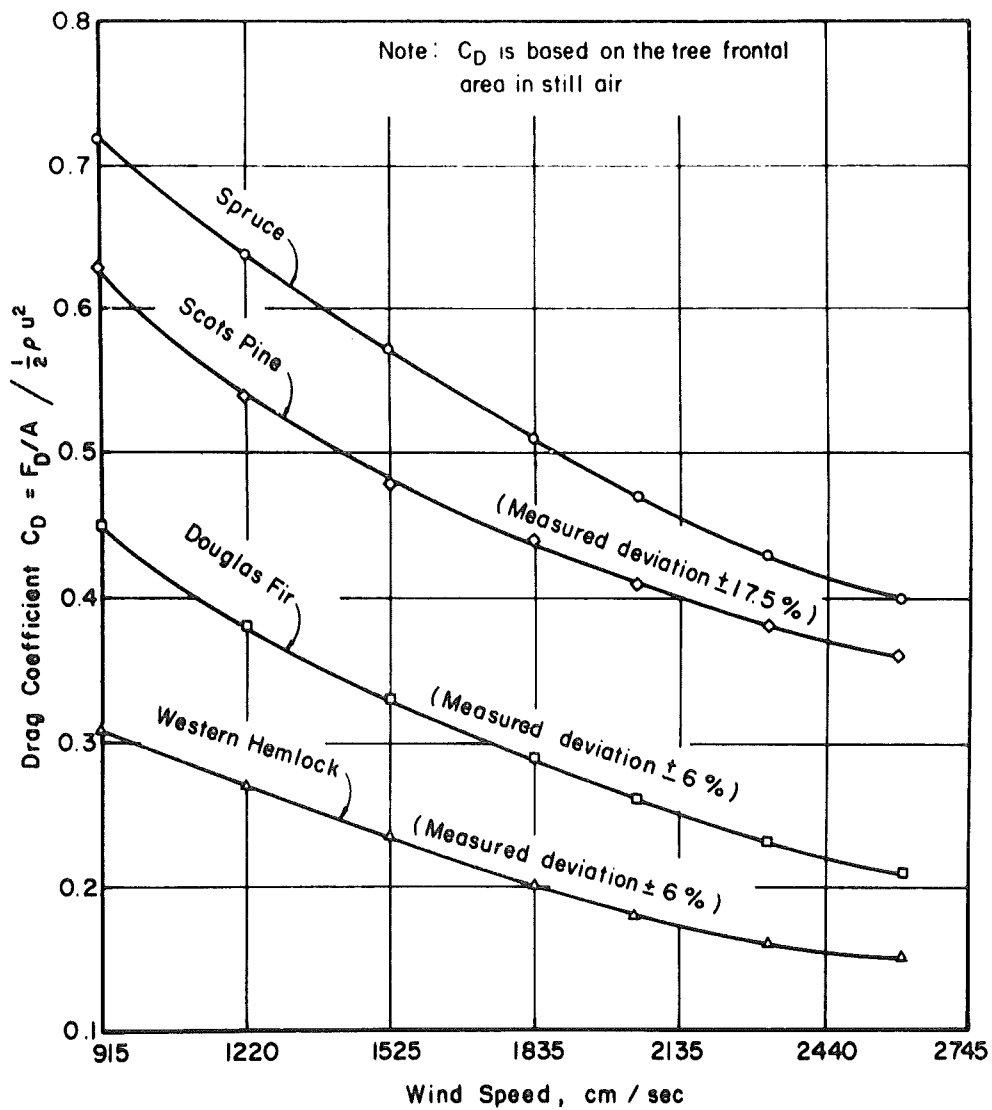
Fig. 4.1.3 Drag coefficient of prototype conifer trees,
after Raymer (1962)

Spruce   Douglas Fir
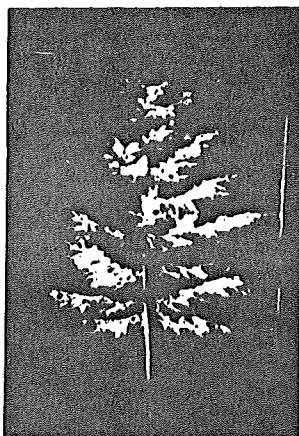
Scots Pine   Western Hemlock

Figure 4.1.4 Real conifer sample trees
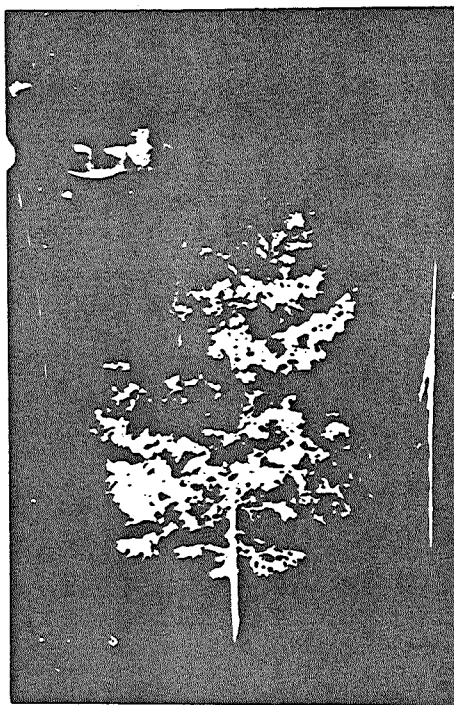
Tree No 3 (Spruce)
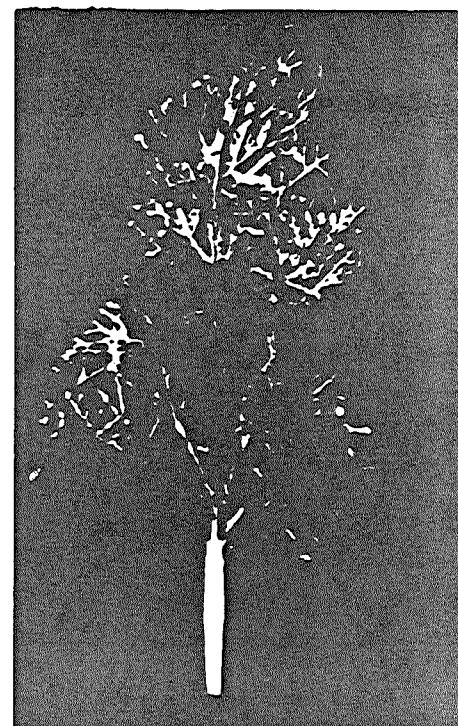
Figure 4.1.5 The comparison of the model tree with the spruce sample tree
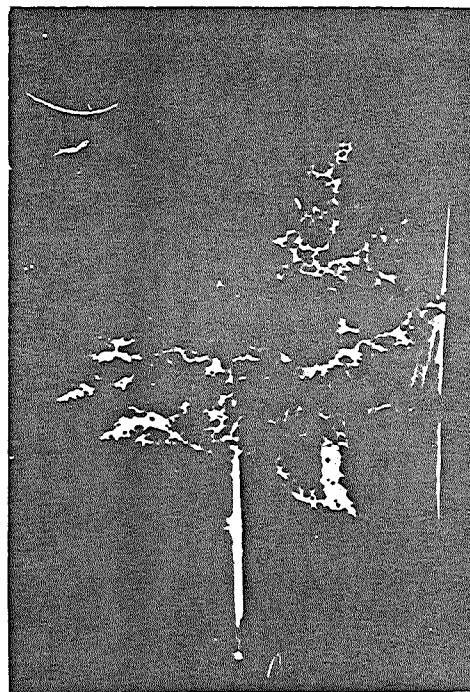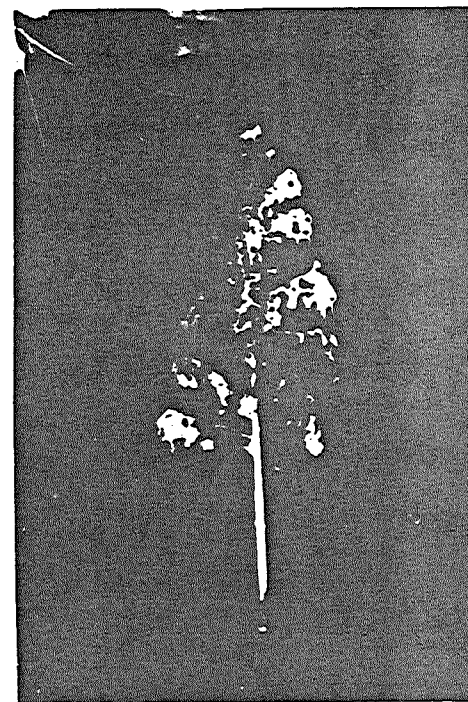
Tree No 8 (Douglas Fir)   Tree No 8 (Douglas Fir) in wind at 50 knots

Figure 4.1.1.1 The Douglas fir in still air and under 1750 cm/sec.

36 Artificial Tree Drag Samples

$U_a = 610$ cm/sec

Std. Dev. $\sigma = 1.14$ grams

Mean $= 10.7$ grams

Artificial Tree Drag Force (grams)

Cumulative Distribution
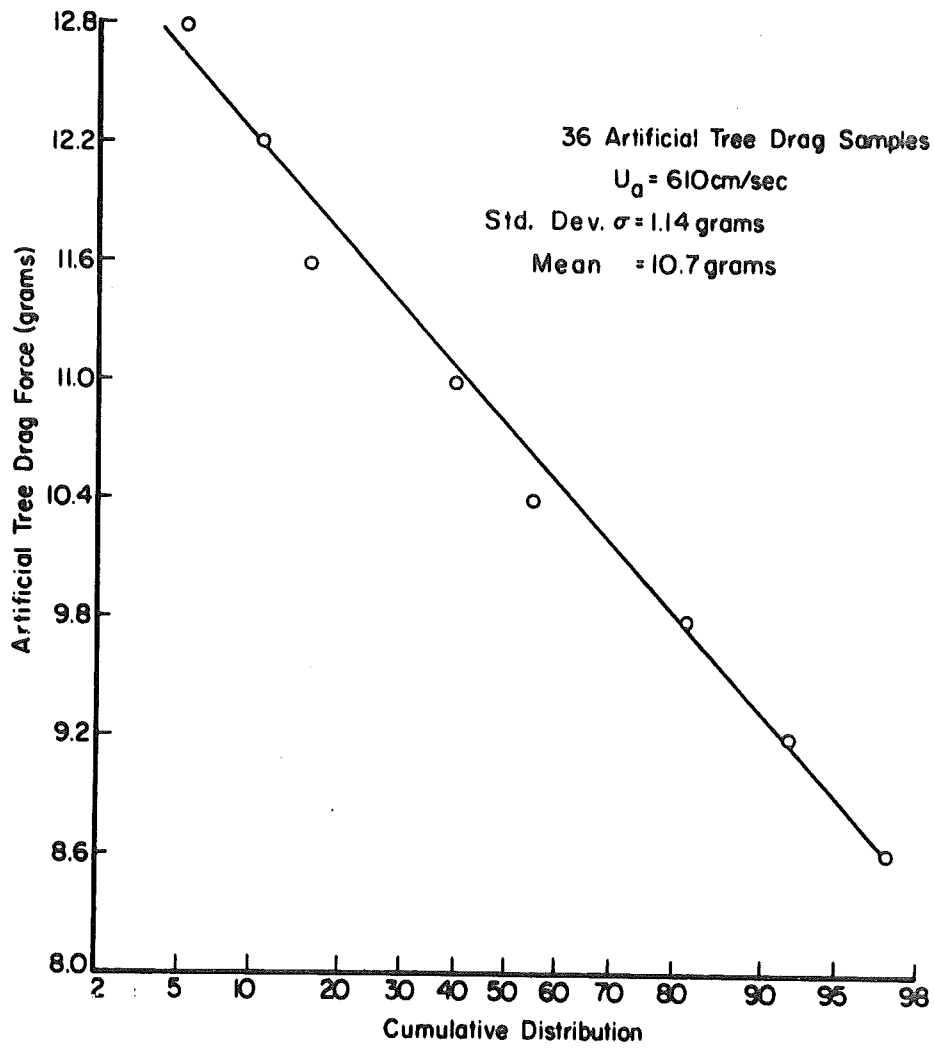
Fig. 4.1.2.1 The probability density distribution of a single
model tree drag force, U_a : 610 cm/sec
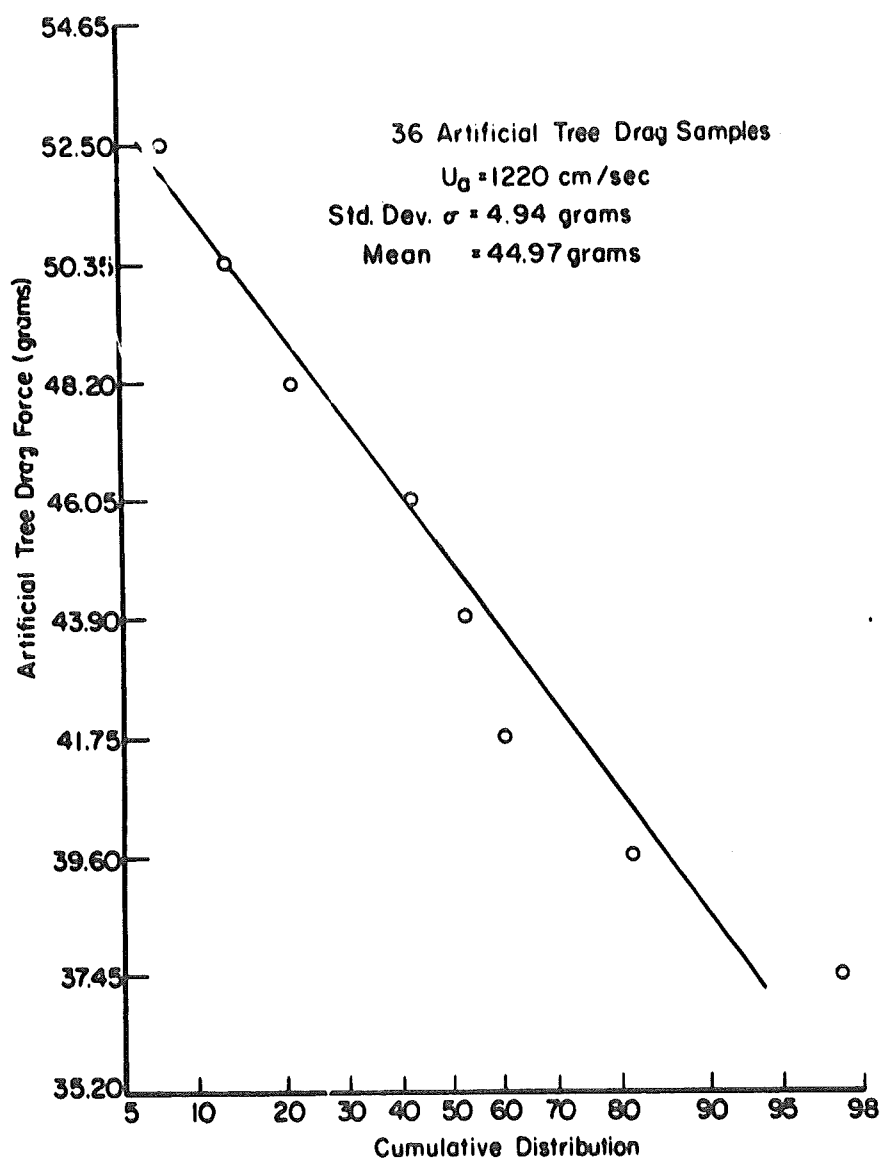
Fig. 4.1.2.2   The probability density distribution of a single
model tree Jrag force, U_a : 1220 cm/sec

Fig. 4.1.1 Velocity profiles at various stations on a smooth boundary, U_a : 1680 cm/sec
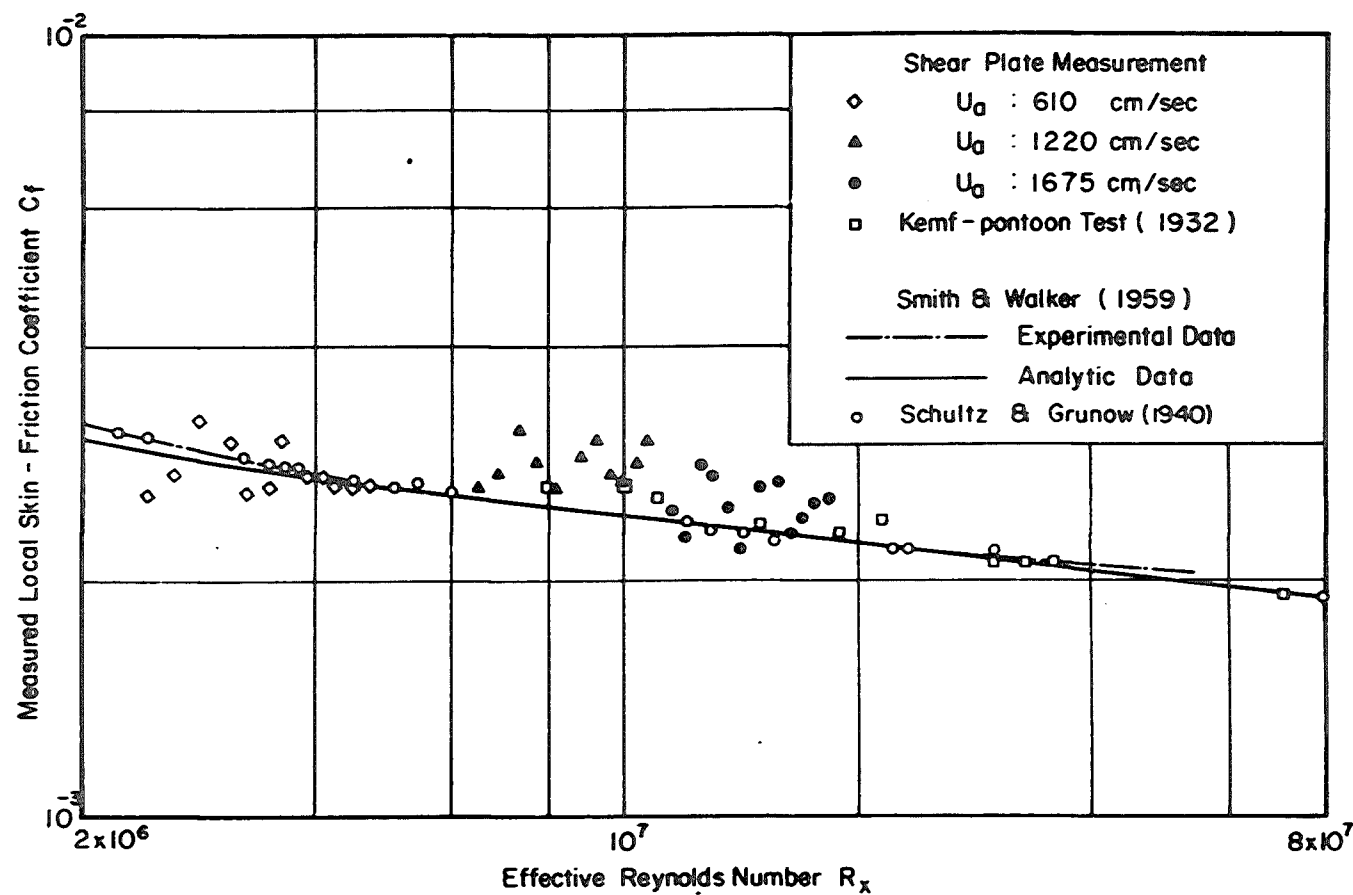
Fig. 4.2.2   Measured local skin-friction coefficient versus
effective Reynolds number; shear plate technique,
smooth boundary surface
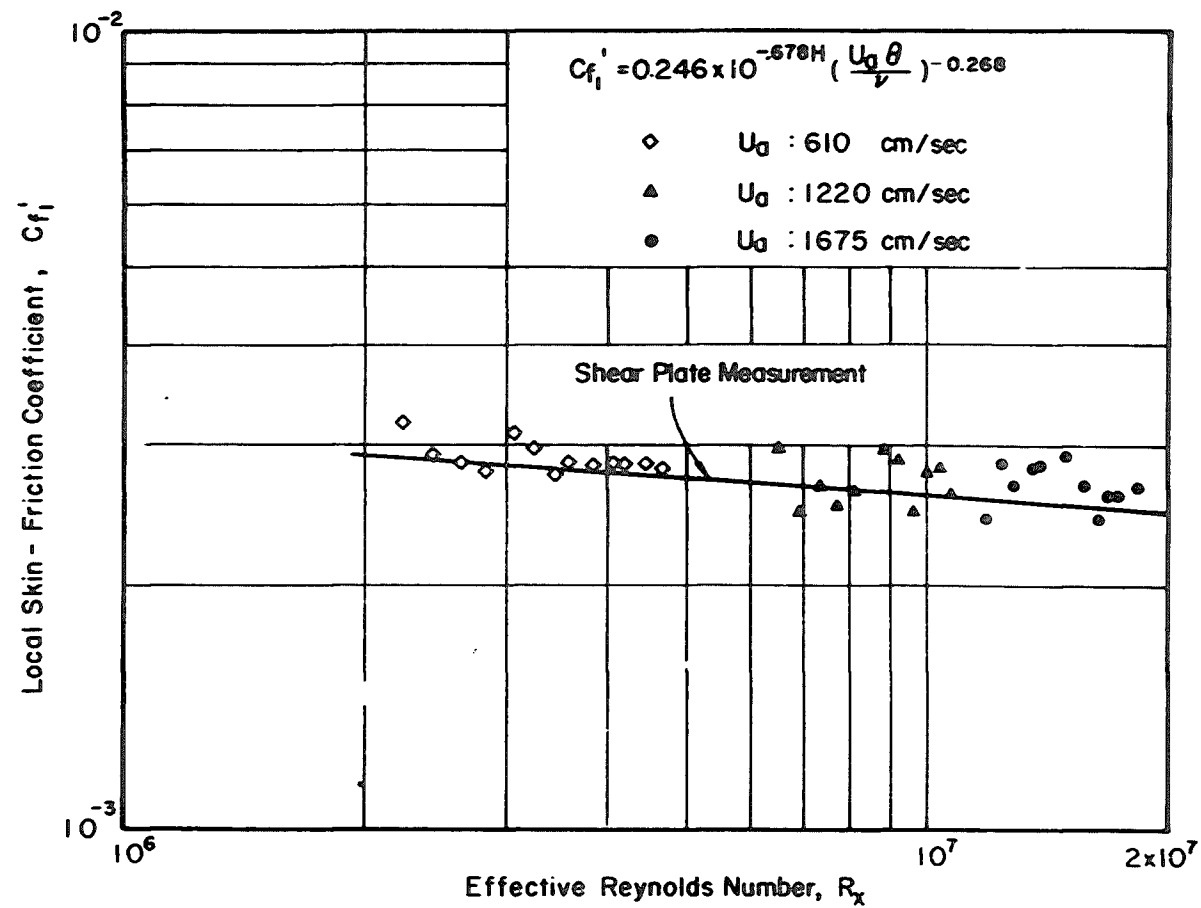
Fig. 4.2.3 Analytic skin-friction coefficient versus
effective Reynolds number, smooth boundary
surface
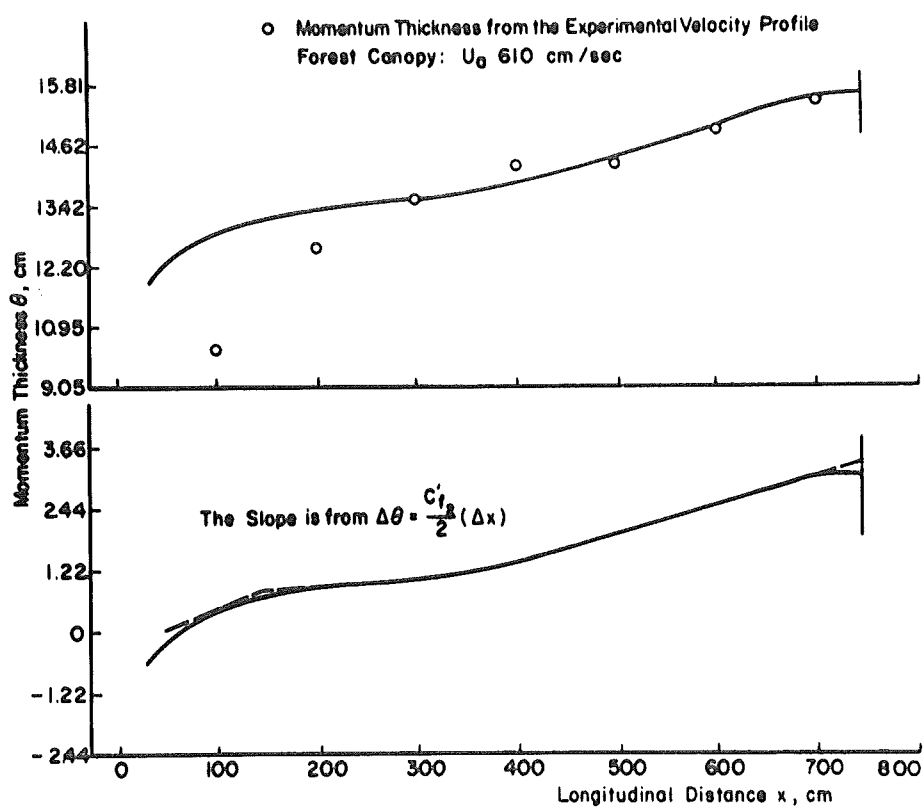
Fig. 4.3.1 Method of verifying the direct measured and analytic
momentum thickness θ .
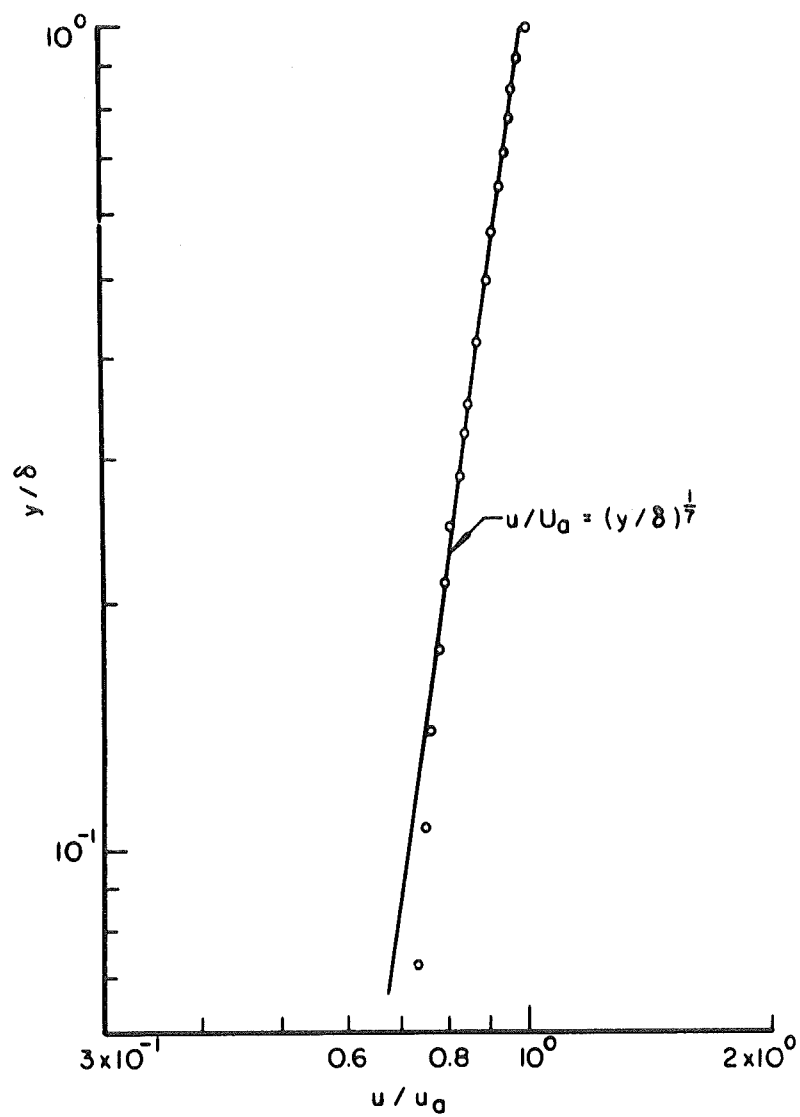
Fig. 4.3.1.1   Dimensionless velocity profile before the forest
canopy field, at station - 100 cm
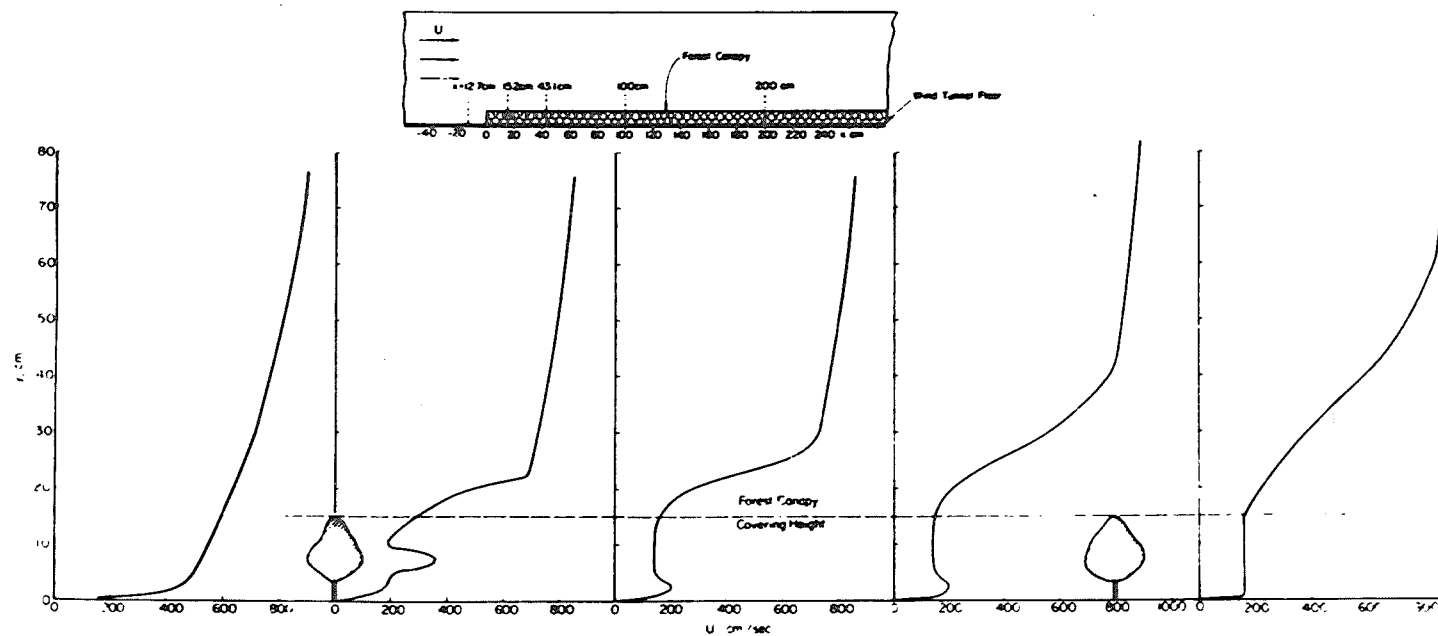
Figure 4.3.1.2 The velocity profile variation in the initial region of the
forest canopy field, U_a = 915 cm/sec.
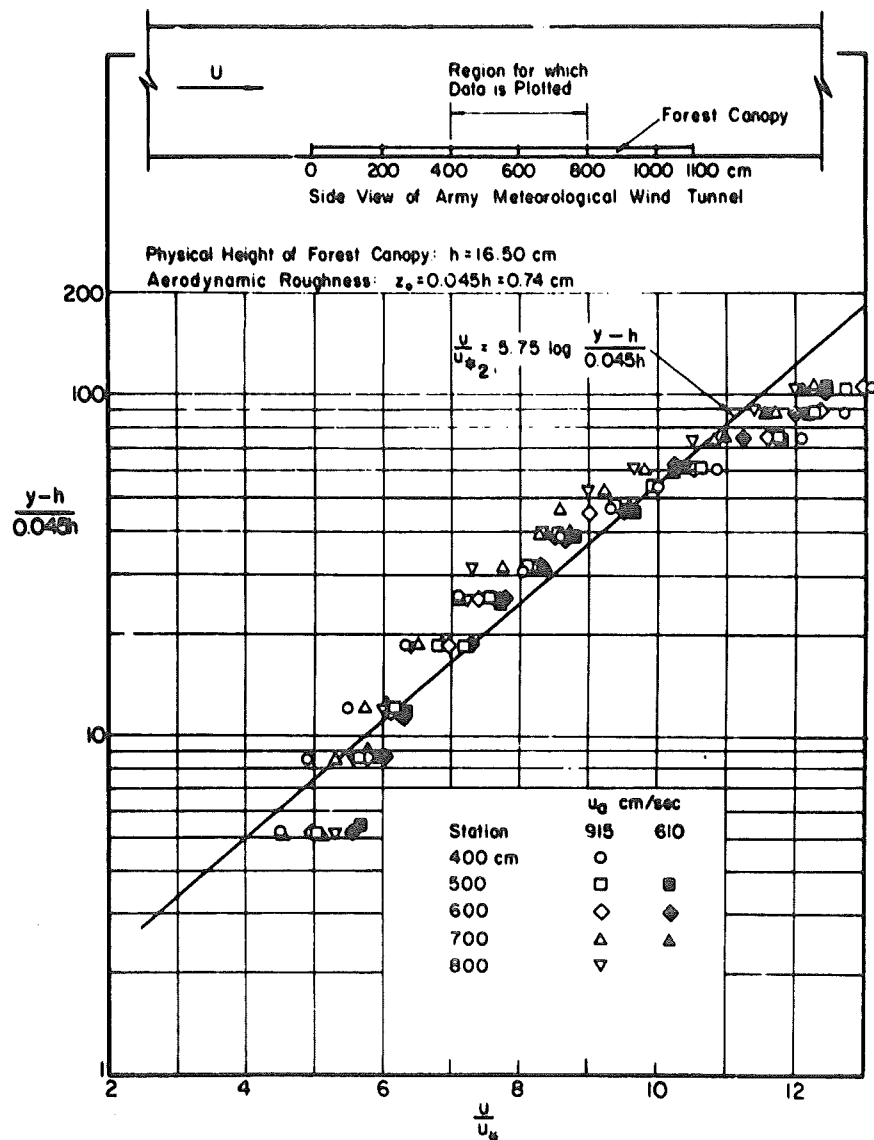
Fig. 4.3.1.3 Logarithmic velocity profile above the forest
canopy thick boundary layer
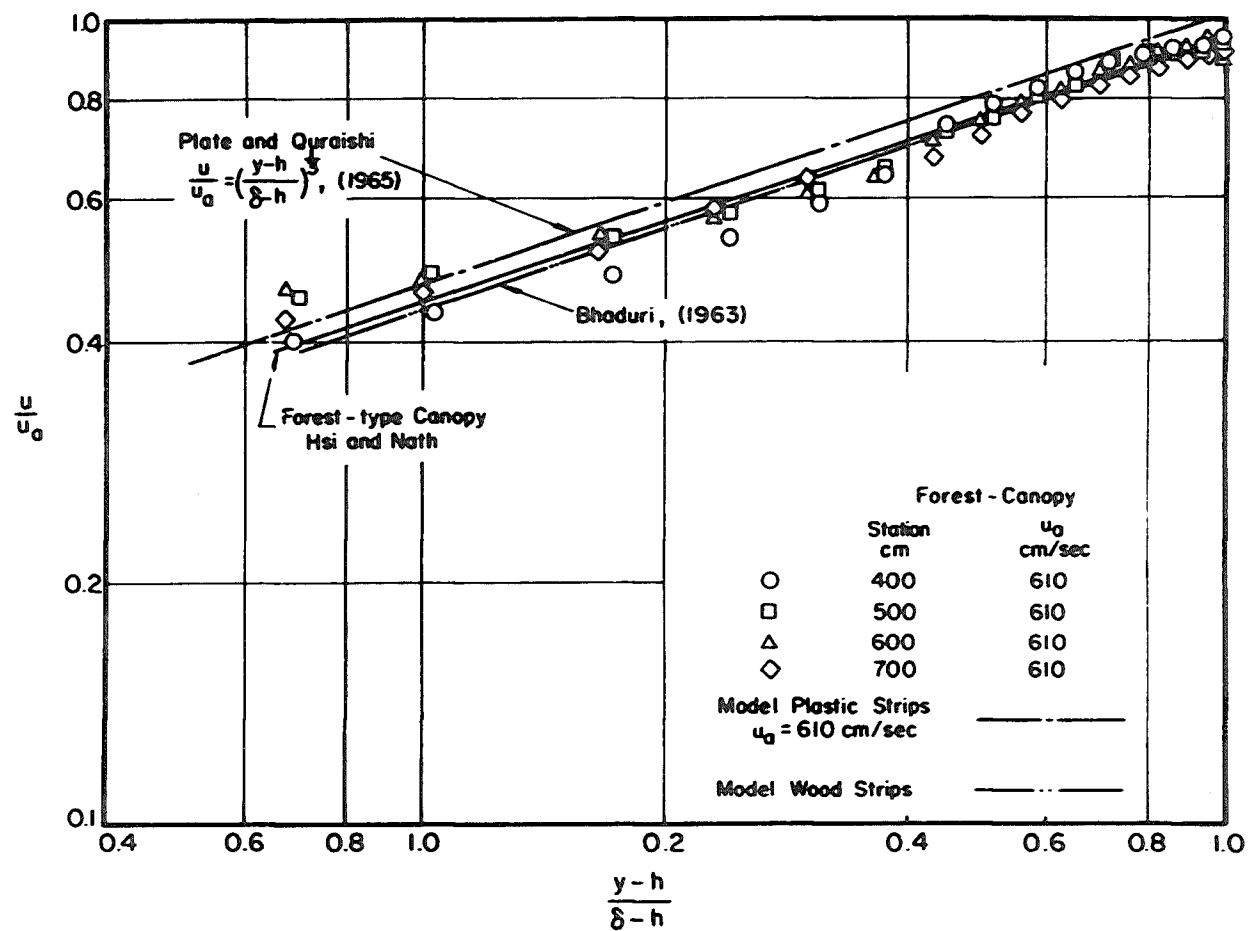
Figure 4.3.1.4 Non-dimensional velocity profiles above the center region of the model forest canopy

Fig. 4.3.1.5 The comparison of non-dimensional velocity profiles
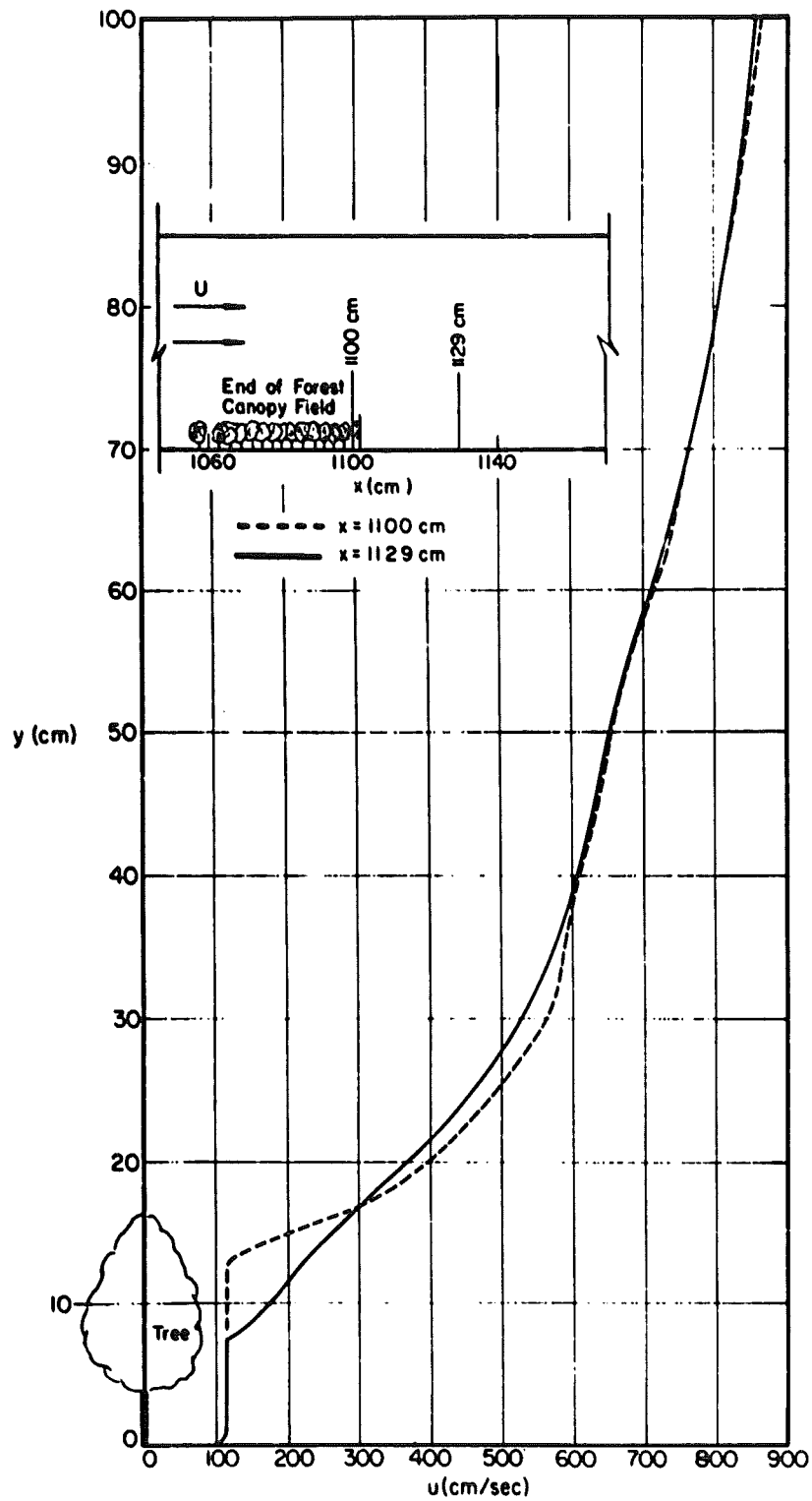within the canopies of the prototype and the model

Legend from figure:
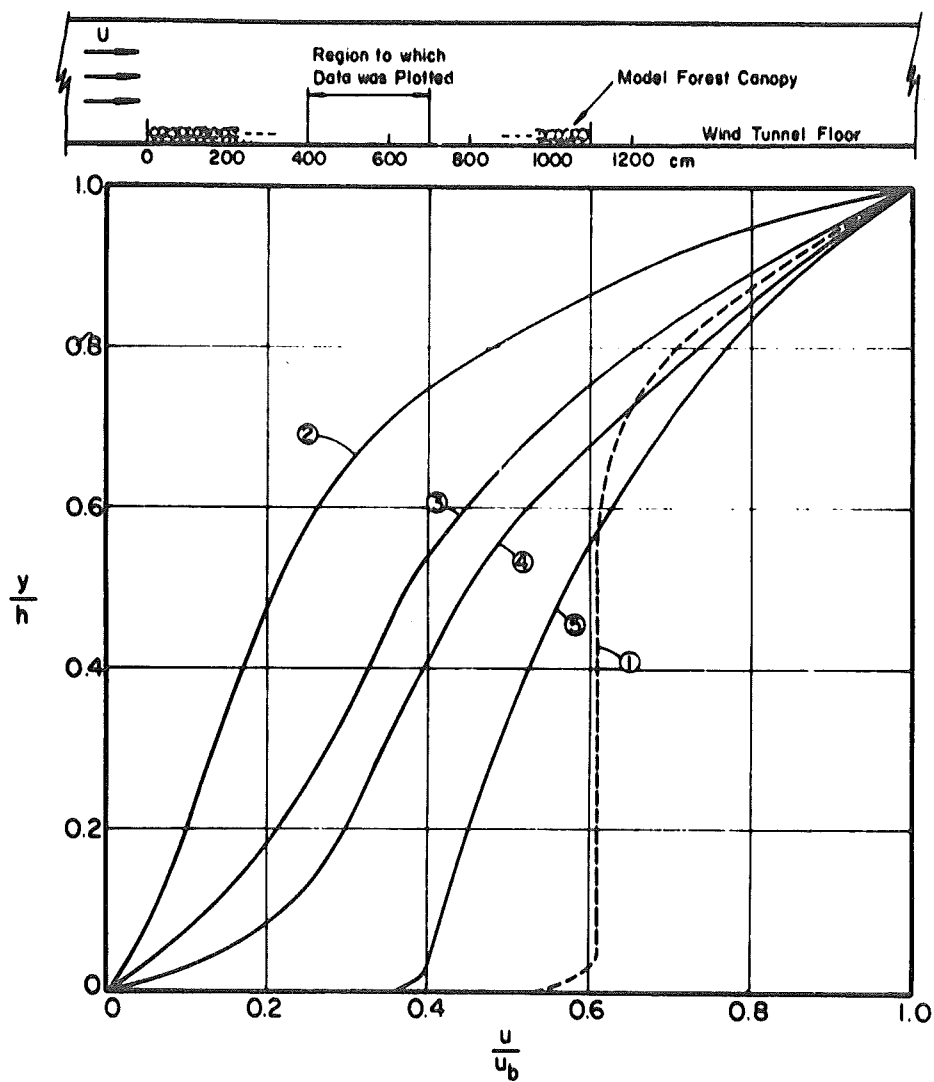
1 Model Forest Canopy, Hsi and Nath, Data at stations
          400, 500, 600, and 700 cm
2 Wheat Field, Stoller and Lemon (1963), Tan and
          Ling (1961), and Paechke (1937)
3 Corn Field, Tan and Ling (1961)
4 Plastic Strips, Plate and Quraishi (1965)
5 Pegs Canopy, Plate and Quraishi (1965)

Fig. 4.3.1.6 The comparison of wind velocity profiles at the end region of the experimental forest canopy field
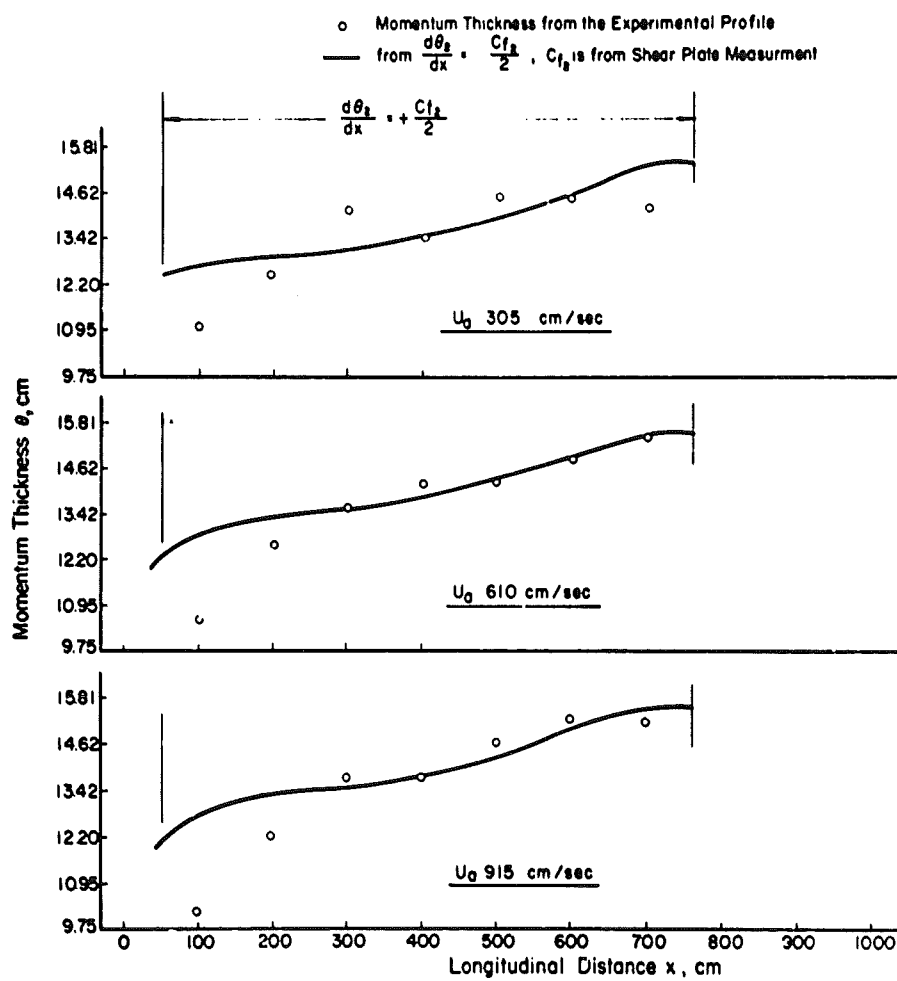
Figure 4.3.2 The comparison of momentum thickness θ between shear
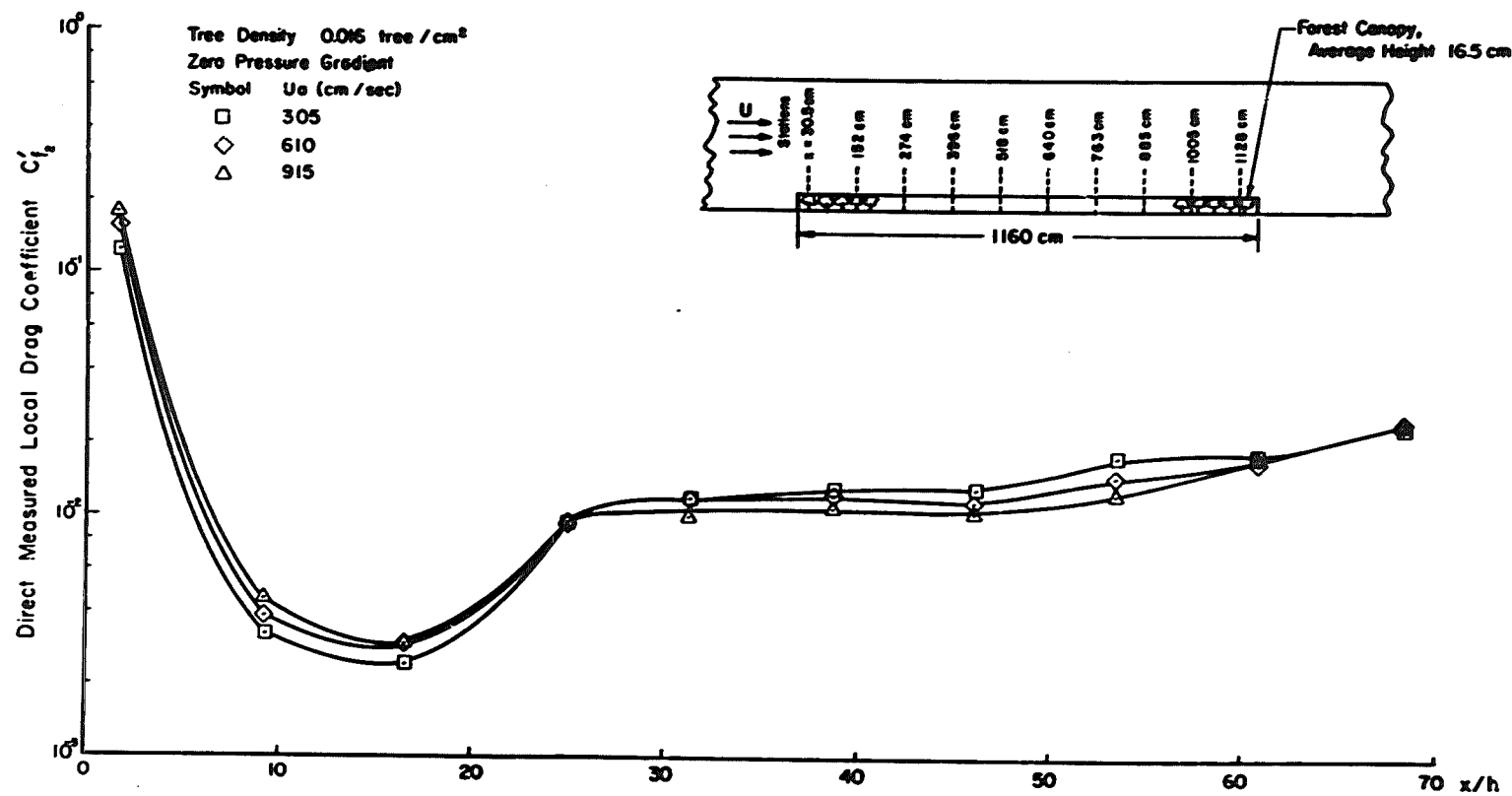plate data and experimental velocity profiles

Figure 4.3.2.1 Directly measured (shear plate) surface stress vs. longitudinal
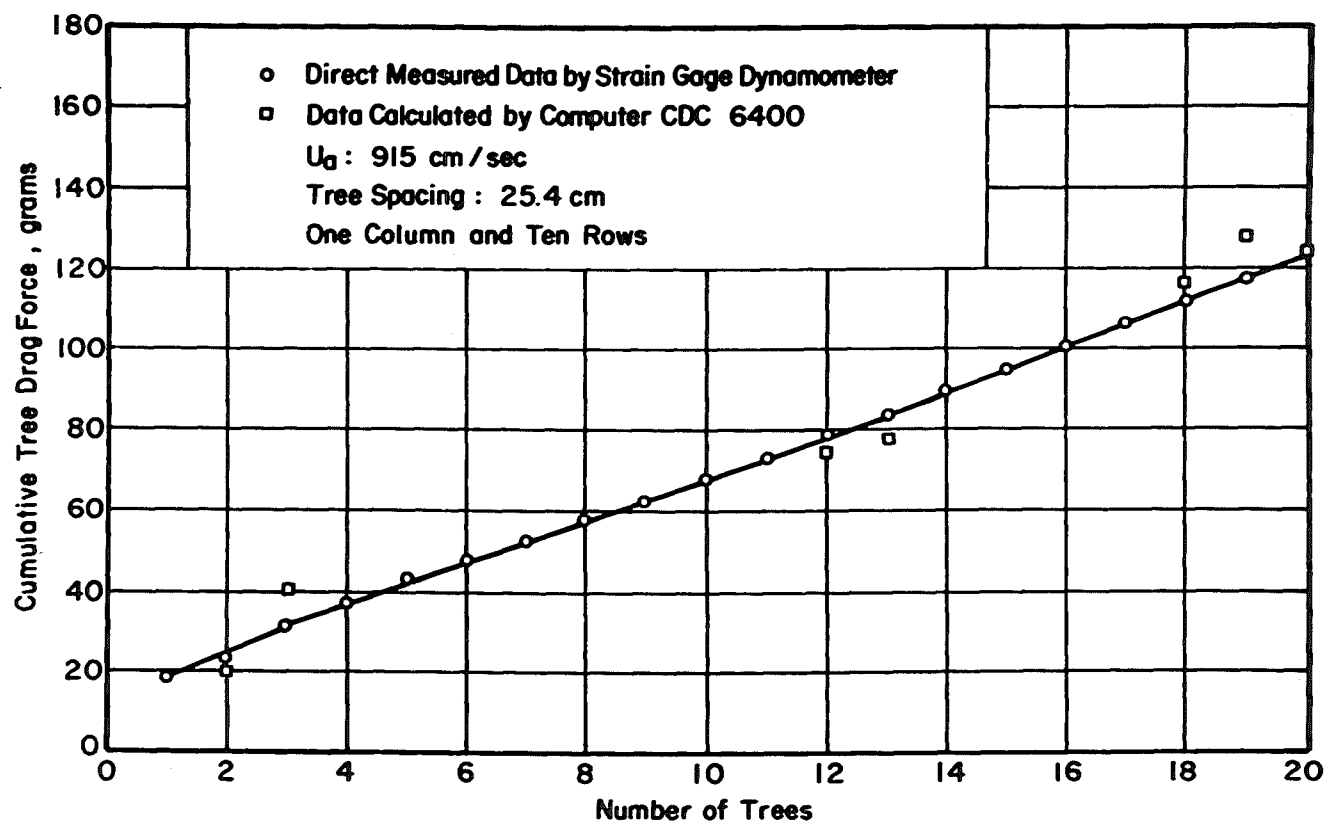distance, in dimensionless form, forest canopy, thick boundary
layer

Figure 4.4.1 Cumulative tree drag force from direct measurement and from computer calculation, orchard canopy, thick boundary layer
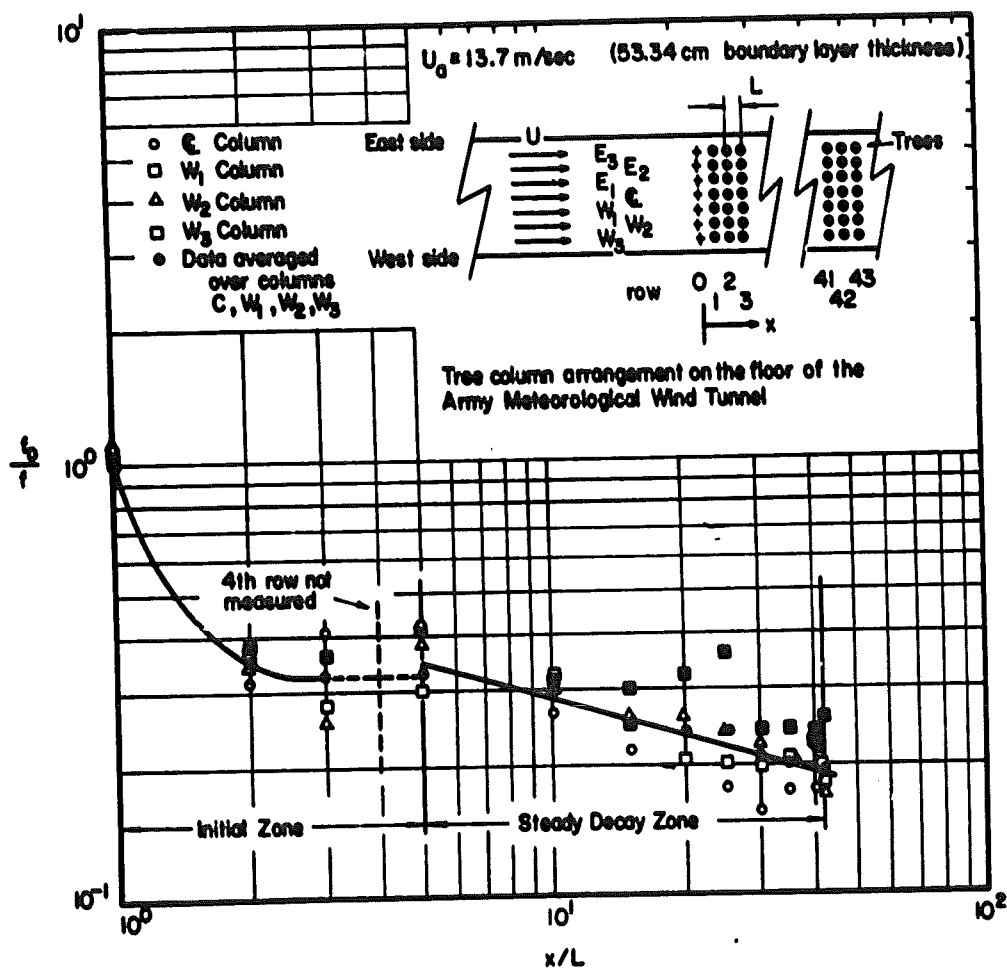
Fig. 4.4.2 Local drag force versus longitudinal distance in dimensionless form, orchard canopy, 25.4 cm tree spacing, thick boundary layer
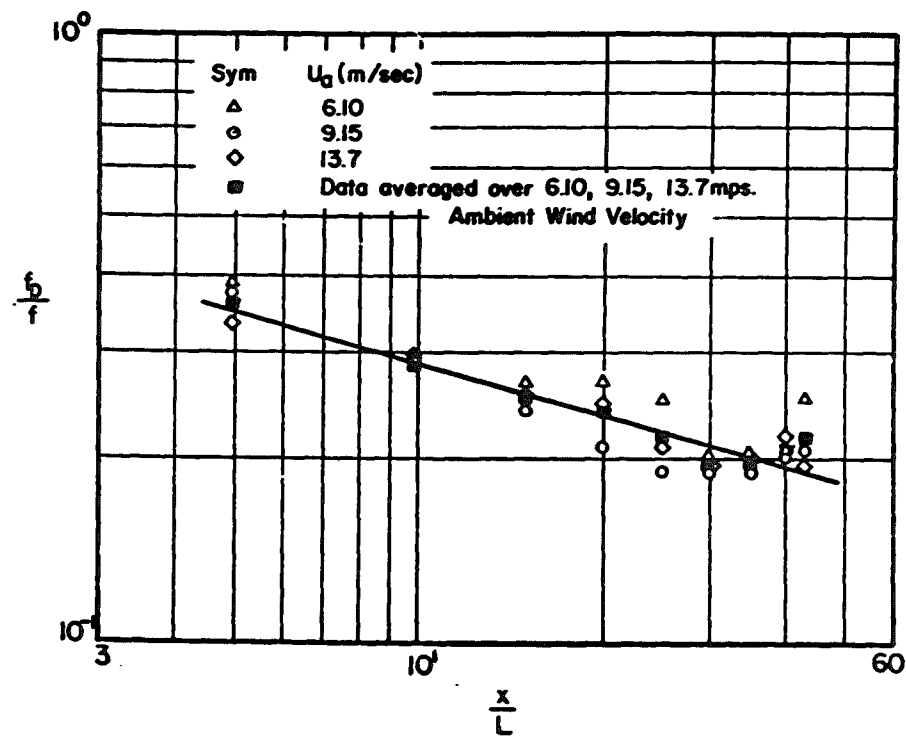
Fig. 4.4.3 Steady decay zone of orchard canopy, 25.4 cm
tree-spacing, thick boundary layer

$$\frac{u}{u_a} = \left(\frac{y}{\delta}\right)^{1/9}$$

$U_a = 915 \text{ cm/sec}$

$U_a = 1690 \text{ cm/sec}$

$$\frac{u}{u_a} = \left(\frac{y}{\delta}\right)^{1/7}$$

$U_a = 305 \text{ cm/sec}$

$U_a = 915 \text{ cm/sec}$

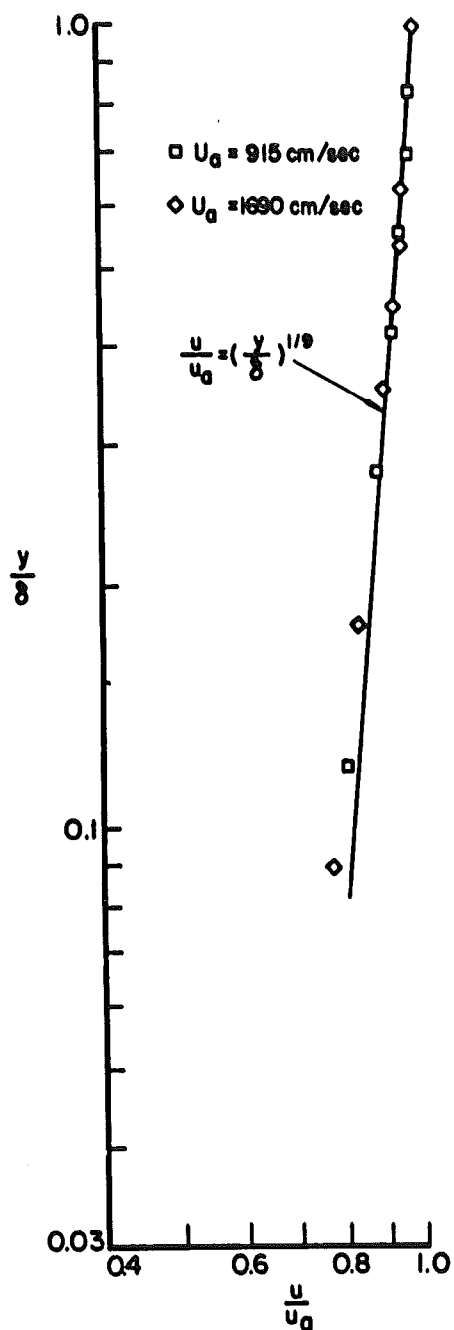$\frac{y}{\delta}$

$\frac{u}{u_a}$

$\frac{u}{u_a}$

Fig. 4.5.1.1 Dimensionless velocity profile before the brushy canopy field, at station - 12.7 cm, thin boundary layer
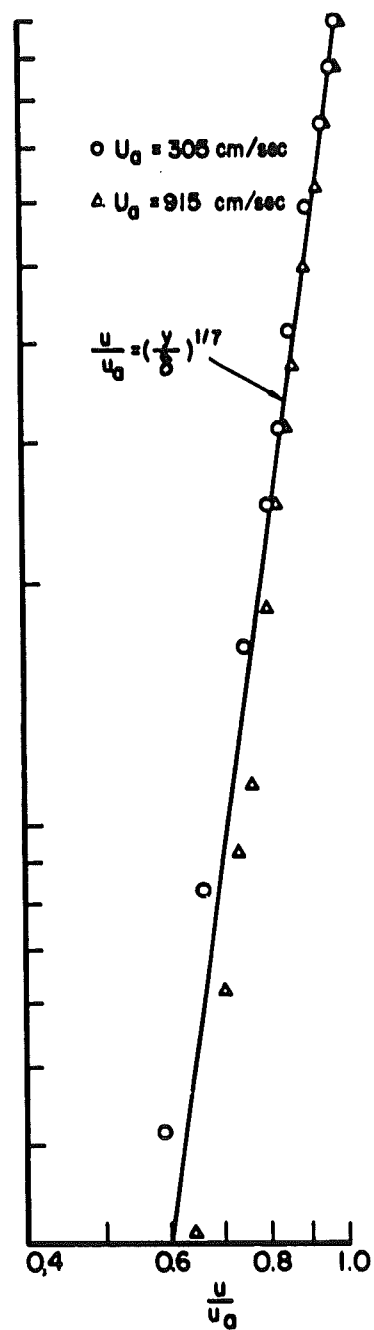
Fig. 4.5.1.2 Dimensionless velocity profile before the brushy canopy, at station - 12.7 cm, thick boundary layer
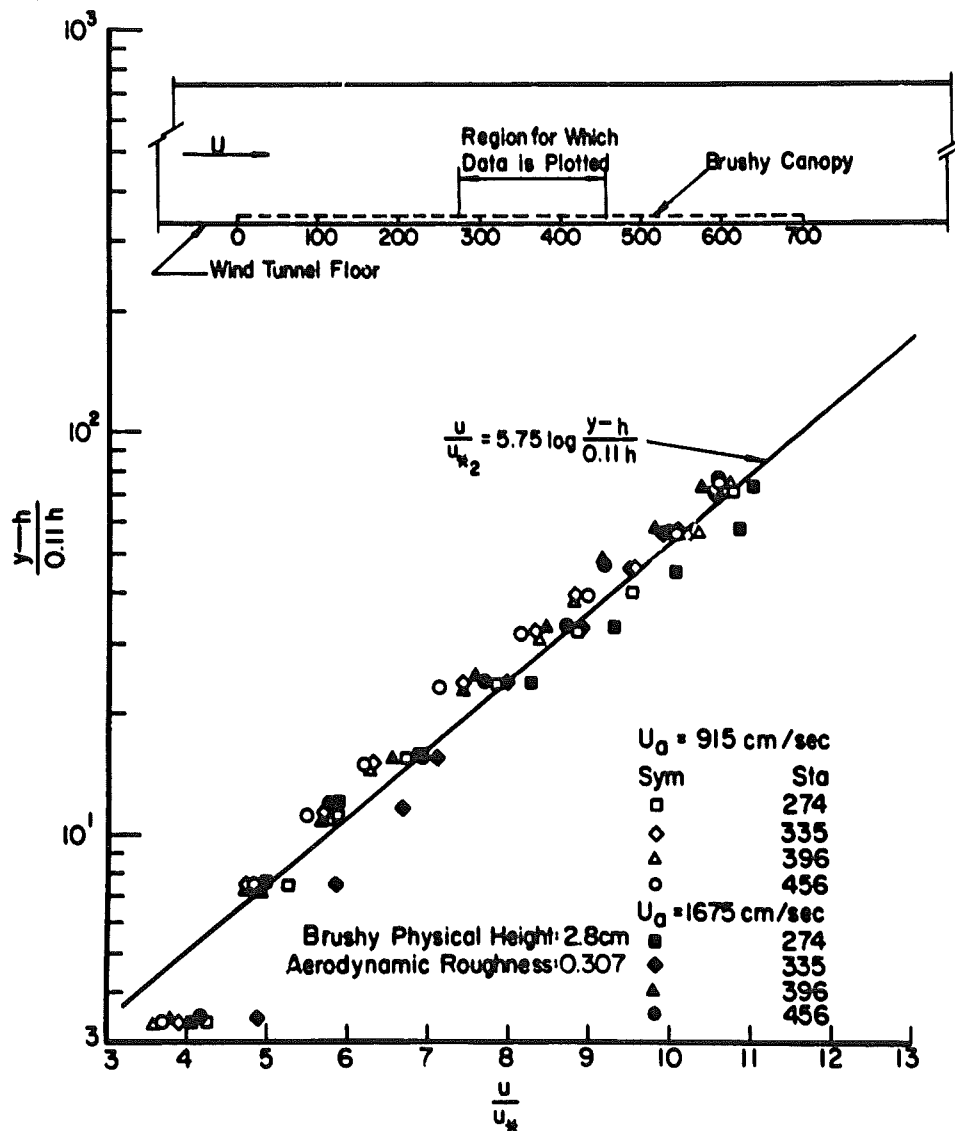
Figure 4.5.1.3 Non-dimensional logarithmic velocity profile,
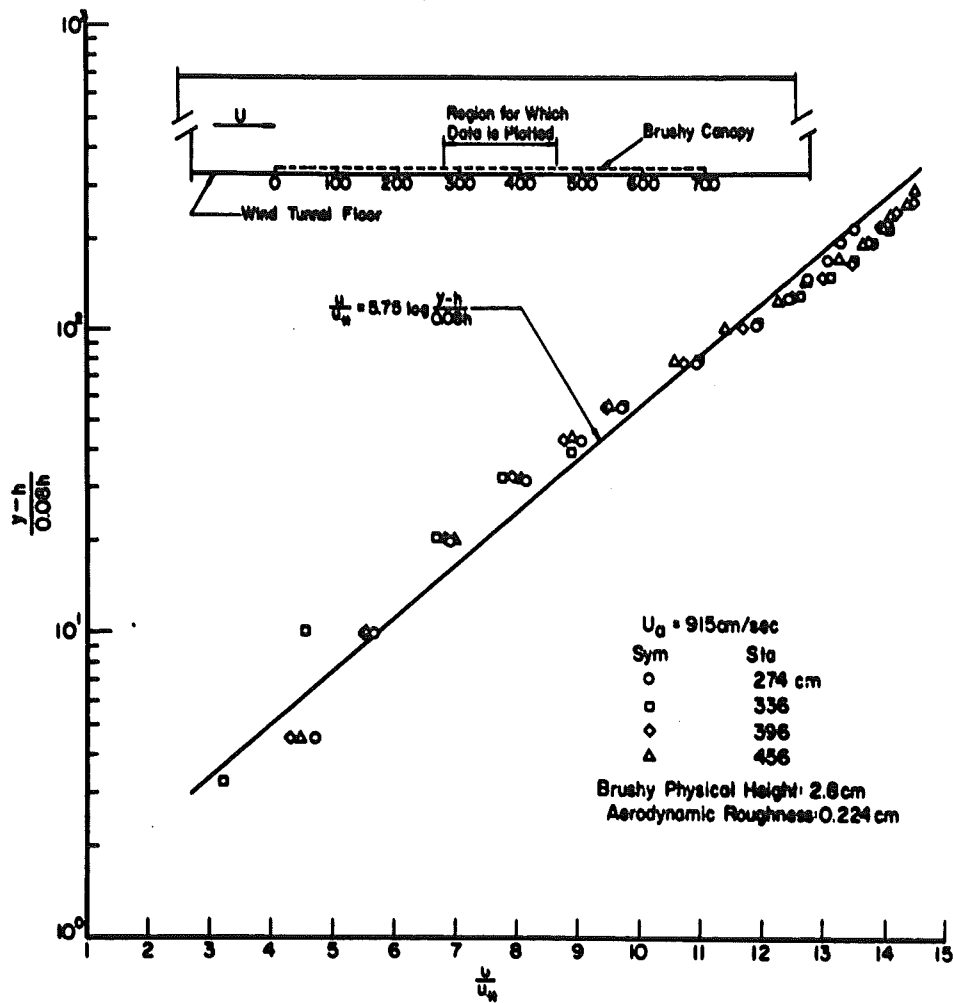brushy canopy, thin boundary layer

Fig. 4.5.1.4 Non-dimensional logarithmic velocity profile,
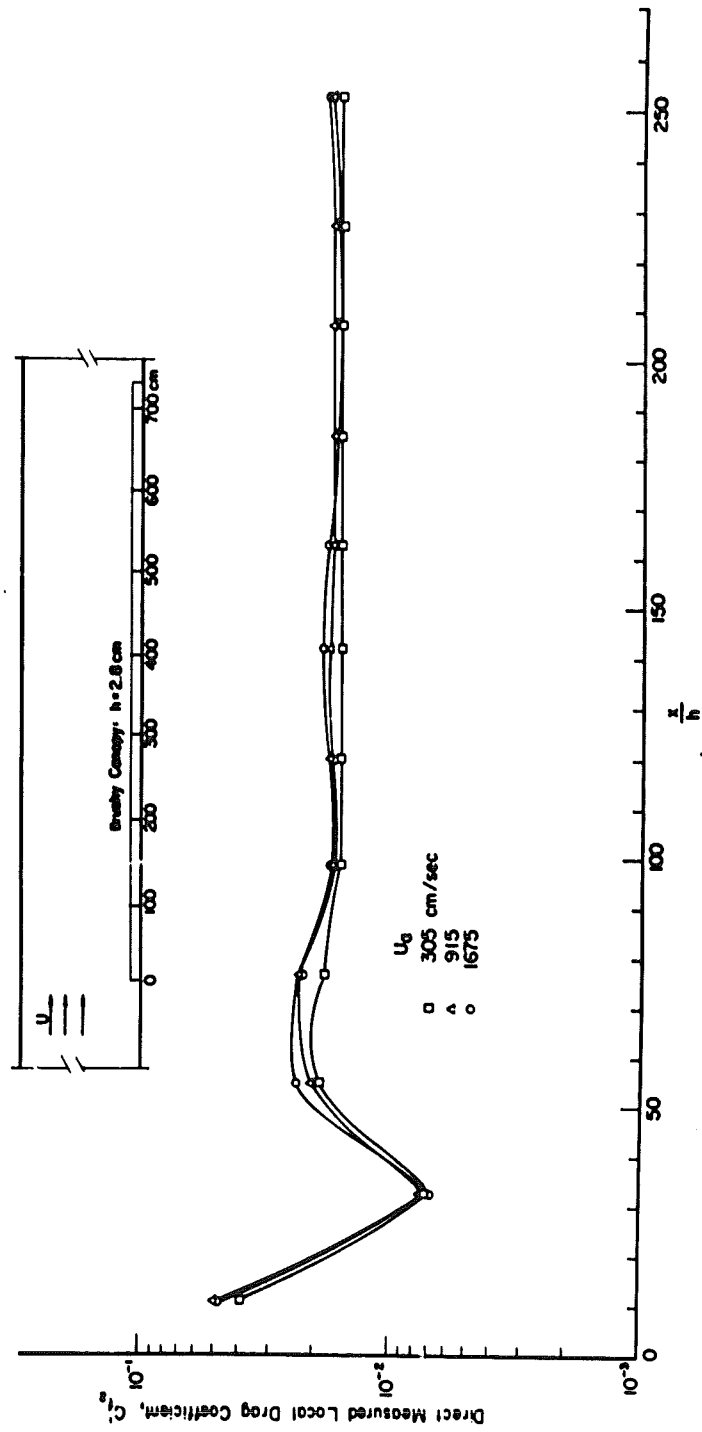brushy canopy, thick boundary layer.

121

Figure 4.5.2.1 Direct measured local drag coefficient vs. $\frac{x}{h}$, brushy canopy, thin boundary layer

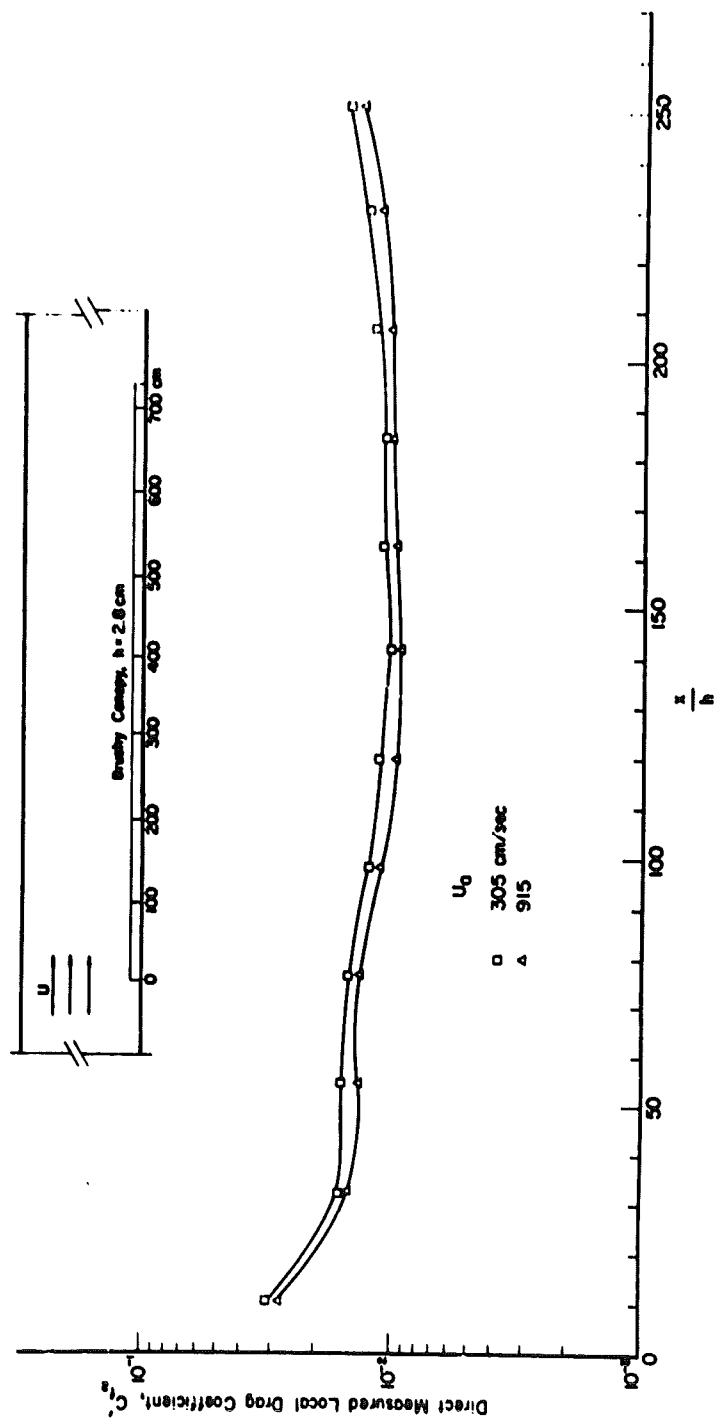Figure 4.5.2.2: Direct measured local drag coefficient vs. $\frac{x}{h}$, brushy canopy, thick boundary layer

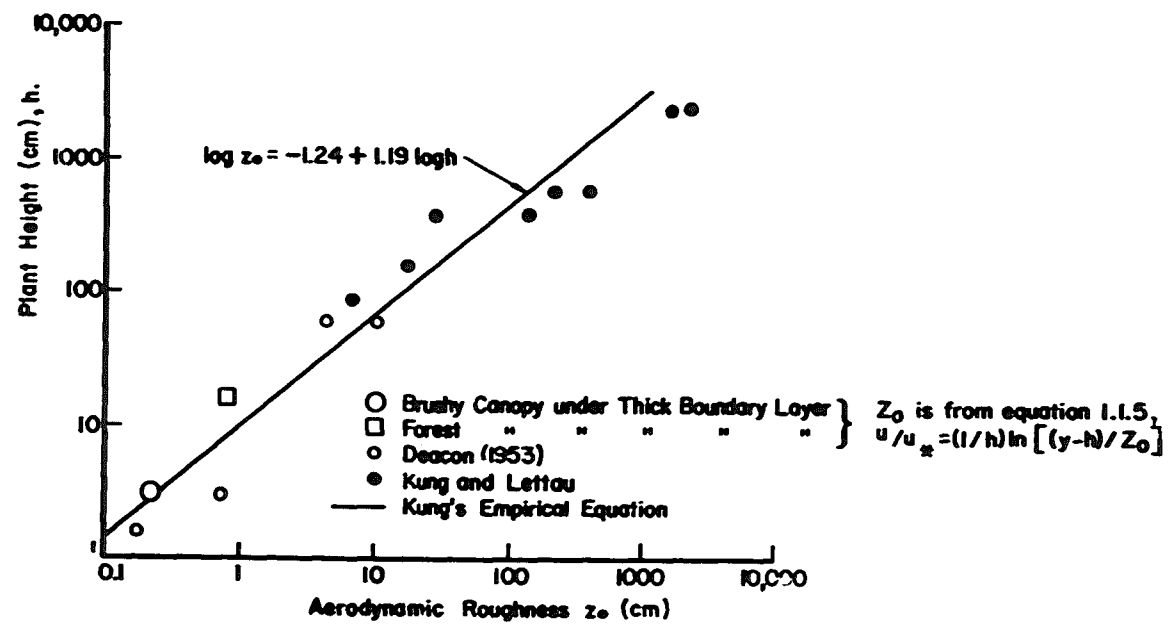Fig. 4.5.2.3 Aerodynamic roughnesses versus vegetation height
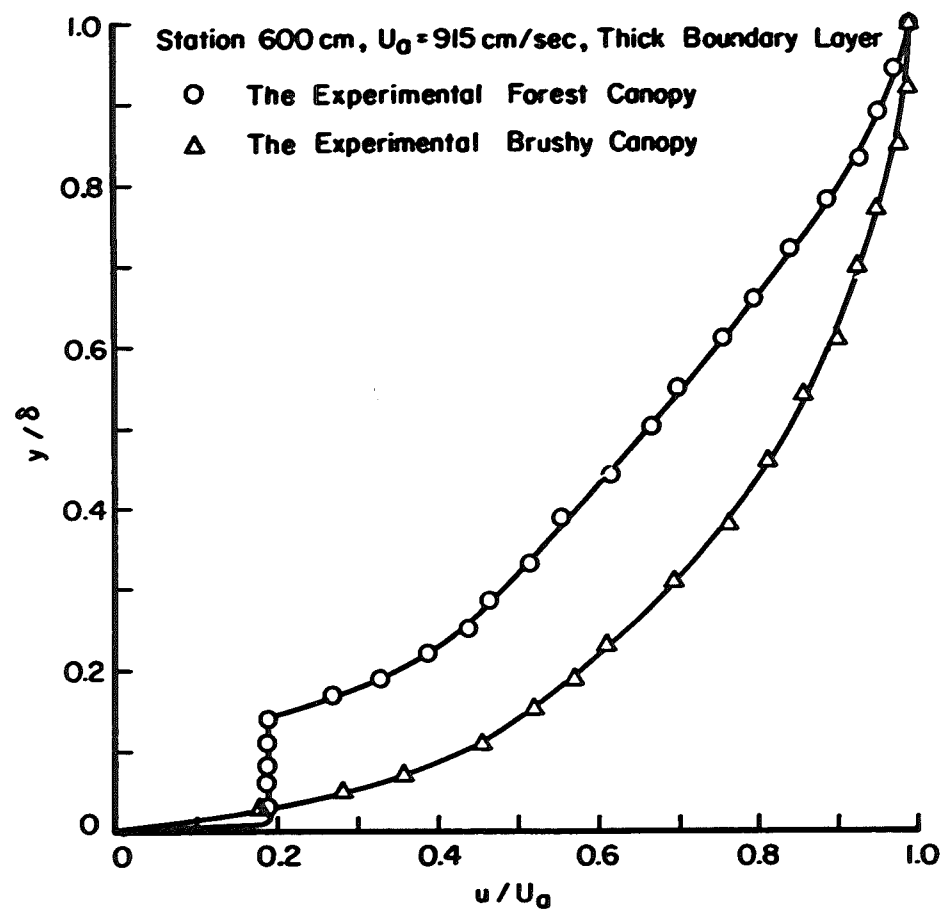
Fig. 4.5.3.1 The comparison of velocity profile in and above
the forest canopy with that of brushy canopy field
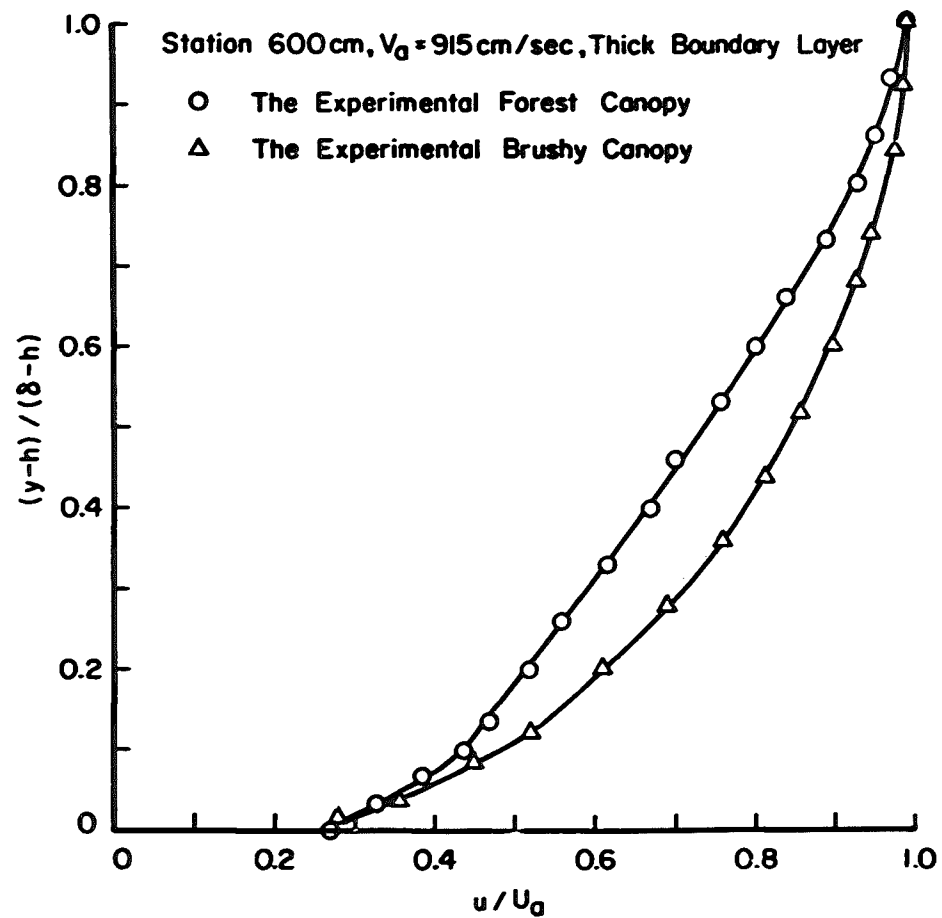
Fig. 4.5.3.2 The comparison of velocity profiles of the forest
canopy and the brushy canopy, above their fuzzy surface
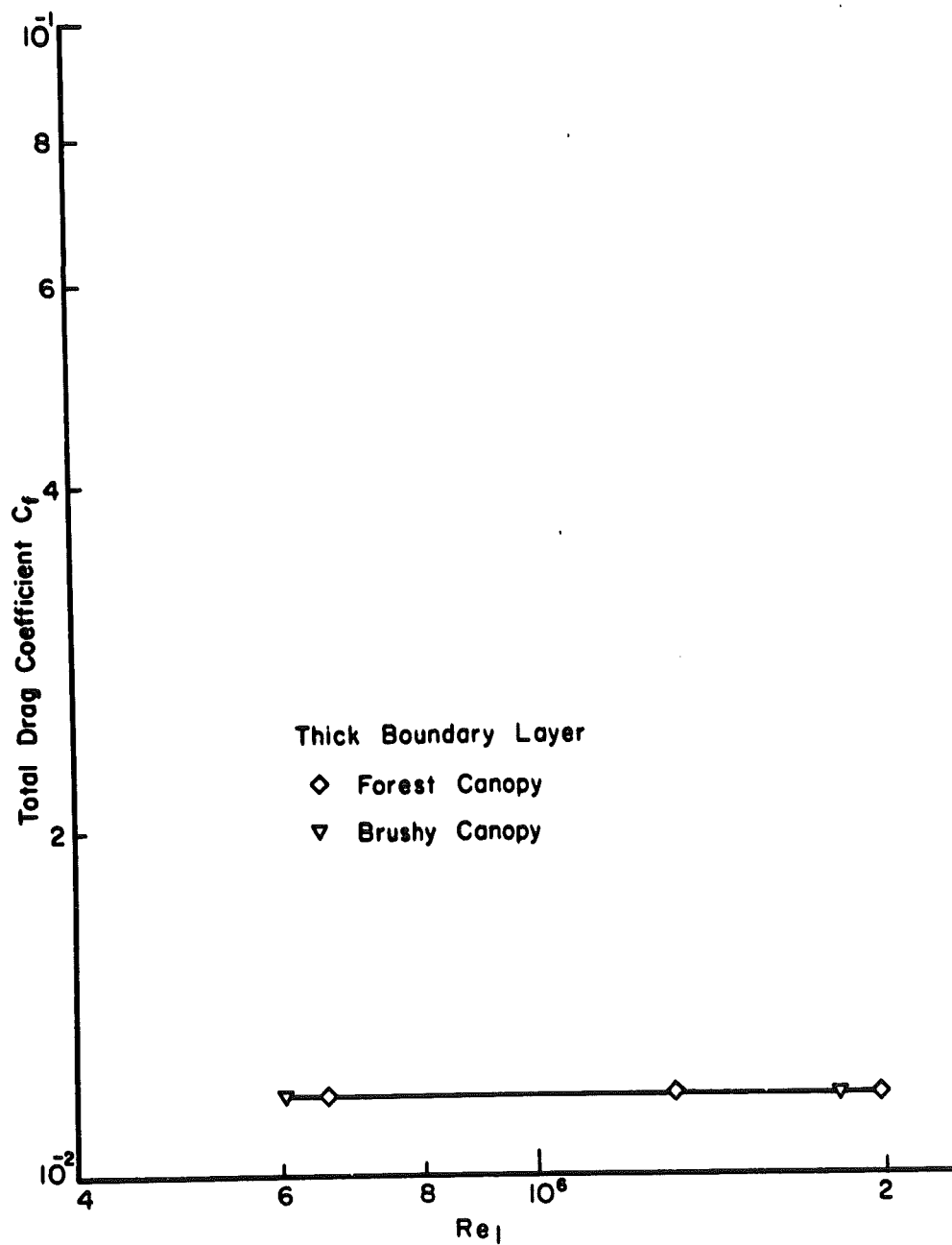
Fig. 5.1 Total drag coefficient of the experimental forest
and brushy canopy in the established region

$$\tau_w \sim (U_0)^{1.9}$$

Average Surface Stress, τ_w (gm/cm^2)

10^{-2}

10^{-3}

Brushy Canopy, Thin Boundary Layer, τ_w is 6.8 Times the Smooth Surface

Brushy and Forest Canopy, Thick Boundary Layer, τ_w is 4.3 Times the Smooth Surface

Smooth Boundary Surface

200   10^3 5000

Ambient Velocity, U_0 (cm/sec)

Figure 5.2   Direct measurement of surface stress for various canopies in fully developed region

DOCUMENT CONTROL DATA · R&D		
(Security classification of title, body of abstract and indexing annotation must be entered when the overall report is classified)		

1. ORIGINATING ACTIVITY (Corporate author)	2a. REPORT SECURITY CLASSIFICATION
Fluid Mechanics Program, College of Engineering Colorado State University, Ft. Collins, Colo.	Unclassified
	2b. GROUP

3. REPORT TITLE

WIND DRAG WITHIN A SIMULATED FOREST CANOPY FIELD

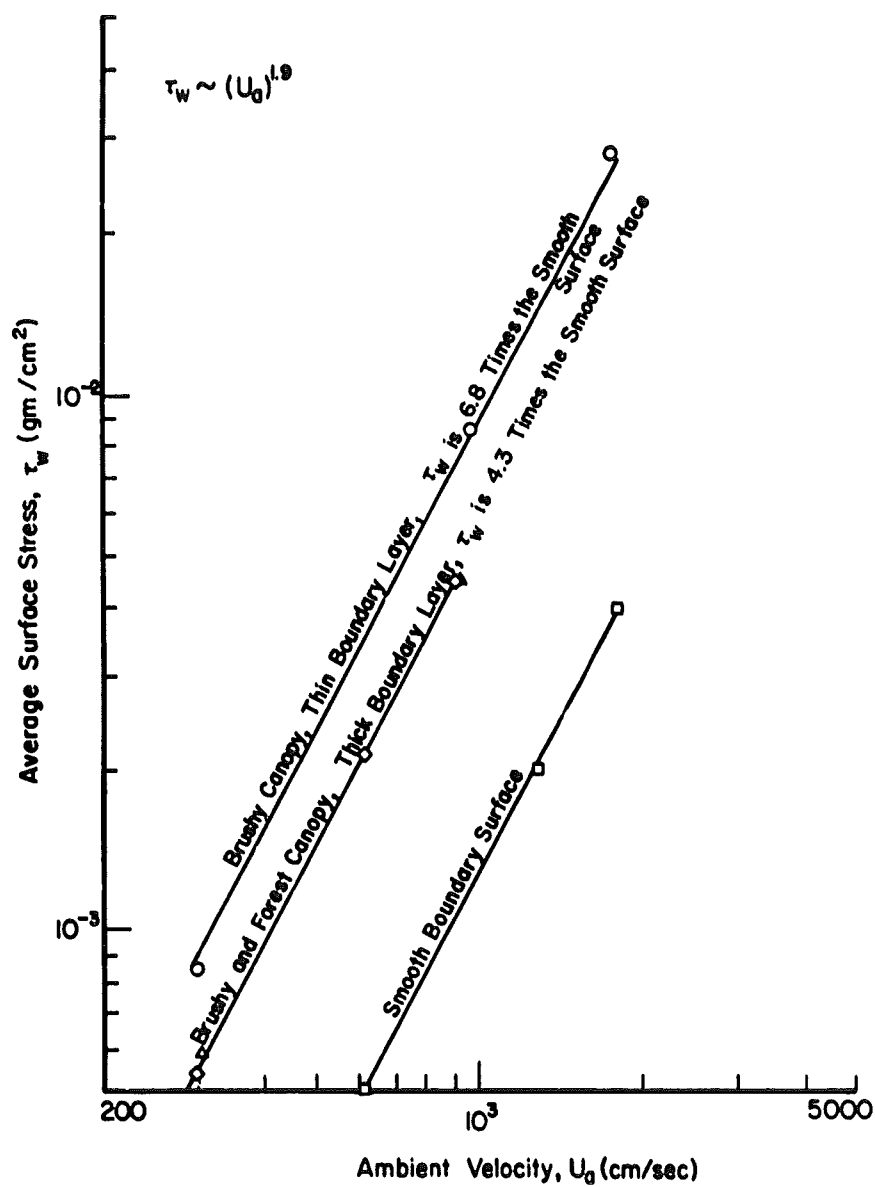**4. DESCRIPTIVE NOTES (Type of report and inclusive dates)**

Technical Report August 1968

5. AUTHOR(S) (Last name, first name, initial)

Hsi, George and
Nath, J. H.

6. REPORT DATE	7a. TOTAL NO. OF PAGES	7b. NO. OF REFS
August 1968	143	55

8a. CONTRACT OR GRANT NO.	9a. ORIGINATOR'S REPORT NUMBER(S)
DA-AMC-28-043-65-G-20	Technical Report
b. PROJECT NO.	
2273	9b. OTHER REPORT NO(S) (Any other numbers that may be assigned this report)
c.	
d.	CER68-69GH-JHN6

10. AVAILABILITY/LIMITATION NOTICES

Distribution of this report is unlimited

11. SUPPLEMENTARY NOTES	12. SPONSORING MILITARY ACTIVITY
	U.S. Army Materiel Command

13. ABSTRACT

This report presents an experimental and analysis study of wind drag within simulated forest canopy fields. The drag coefficients, aerodynamic roughness and wind velocity profiles are studied for various types of forest canopies. Furthermore, a brushy canopy field was studied which simulated the leafy portion of a forest without the tree trunks present. The wind drag force on a single experimental tree was also studied. This information is useful to those who are concerned with diffusion within a canopy in an atmospheric boundary layer.

In the course of this study a shear plate was developed which reliably measures a drag force from 0.1 gram to 2000 grams. The function of this plate was successfully validated by testing it in a turbulent flow over a smooth surface.

The drag coefficient of a single model tree, which was the same as those used in the simulated forest canopy fields, was compared with prototype conifers. The work found that a plastic model tree has drag coefficients between those for spruce and Douglas fir trees. The variation of the tree drag coefficient among trees of the same type is concluded by a statistical study on a number of plastic trees which have the same amount of foliage but which are different in the arrangement of the tree branches and the tree leaves.

DD FORM 1473 1 JAN 64

14	KEY WORDS	LINK A		LINK B		LINK C	
		ROLE	AT	ROLE	WT	ROLE	WT
	Simulated forest canopy field						
	Direct surface drag measurement						
	Turbulent boundary layer						
	Forest canopy simulation						
	Simulated single tree						
	Wind tunnel experimentation						

INSTRUCTIONS

1. **ORIGINATING ACTIVITY:** Enter the name and address of the contractor, subcontractor, grantee, Department of Defense activity or other organization *(corporate author)* issuing the report.

2a. **REPORT SECURITY CLASSIFICATION:** Enter the overall security classification of the report. Indicate whether "Restricted Data" is included. Marking is to be in accordance with appropriate security regulations.

2b. **GROUP:** Automatic downgrading is specified in DoD Directive 5200.10 and Armed Forces Industrial Manual. Enter the group number. Also, when applicable, show that optional markings have been used for Group 3 and Group 4 as authorized.

3. **REPORT TITLE:** Enter the complete report title in all capital letters. Titles in all cases should be unclassified. If a meaningful title cannot be selected without classification, show title classification in all capitals in parenthesis immediately following the title.

4. **DESCRIPTIVE NOTES:** If appropriate, enter the type of report, e.g., interim, progress, summary, annual, or final. Give the inclusive dates when a specific reporting period is covered.

5. **AUTHOR(S):** Enter the name(s) of author(s) as shown on or in the report. Enter last name, first name, middle initial. If military, show rank and branch of service. The name of the principal author is an absolute minimum requirement.

6. **REPORT DATE:** Enter the date of the report as day, month, year; or month, year. If more than one date appears on the report, use date of publication.

7a. **TOTAL NUMBER OF PAGES:** The total page count should follow normal pagination procedures, i.e., enter the number of pages containing information.

7b. **NUMBER OF REFERENCES:** Enter the total number of references cited in the report.

8a. **CONTRACT OR GRANT NUMBER:** If appropriate, enter the applicable number of the contract or grant under which the report was written.

8b, &c, & 8d. **PROJECT NUMBER:** Enter the appropriate military department identification, such as project number, subproject number, system numbers, task number, etc.

9a. **ORIGINATOR'S REPORT NUMBER(S):** Enter the official report number by which the document will be identified and controlled by the originating activity. This number must be unique to this report.

9b. **OTHER REPORT NUMBER(S):** If the report has been assigned any other report numbers *(either by the originator or by the sponsor),* also enter this number(s).

10. **AVAILABILITY/LIMITATION NOTICES:** Enter any limitations on further dissemination of the report, other than those imposed by security classification, using standard statements such as:

  (1) "Qualified requesters may obtain copies of this report from DDC."

  (2) "Foreign announcement and dissemination of this report by DDC is not authorized."

  (3) "U. S. Government agencies may obtain copies of this report directly from DDC. Other qualified DDC users shall request through

                              ."

  (4) "U. S. military agencies may obtain copies of this report directly from DDC. Other qualified users shall request through

                              ."

  (5) "All distribution of this report is controlled. Qualified DDC users shall request through

                              ."

If the report has been furnished to the Office of Technical Services, Department of Commerce, for sale to the public, indicate this fact and enter the price, if known.

11. **SUPPLEMENTARY NOTES:** Use for additional explanatory notes.

12. **SPONSORING MILITARY ACTIVITY:** Enter the name of the departmental project office or laboratory sponsoring *(paying for)* the research and development. Include address.

13. **ABSTRACT:** Enter an abstract giving a brief and factual summary of the document indicative of the report, even though it may also appear elsewhere in the body of the technical report. If additional space is required, a continuation sheet shall be attached.

It is highly desirable that the abstract of classified reports be unclassified. Each paragraph of the abstract shall end with an indication of the military security classification of the information in the paragraph, represented as *(TS), (S), (C),* or *(U).*

There is no limitation on the length of the abstract. However, the suggested length is from 150 to 225 words.

14. **KEY WORDS:** Key words are technically meaningful terms or short phrases that characterize a report and may be used as index entries for cataloging the report. Key words must be selected so that no security classification is required. Identifiers, such as equipment model designation, trade name, military project code name, geographic location, may be used as key words but will be followed by an indication of technical context. The assignment of links, rules, and weights is optional.